



Politecnico di Milano

Dipartimento di Scienze e Tecnologie Aerospaziali
Space Systems and Operations

Prof. **Lavagna Michèle Roberta**

Reverse Engineering
of the
Lunar Reconnaissance Orbiter

Final Delivery

TEAM 34

Restivo Silvio
Tamiozzo Davide
Verga Pietro
Viviani Mattia
Zambaldo Carlo
Zosi Andrea

Academic Year 2022/2023

Abstract

This document comprises the reverse engineering of the Lunar Reconnaissance Orbiter (LRO) mission. In the first chapters, the description of the whole mission, with particular focus on the main objectives, is followed by a functional analysis. Once the functionalities are identified, these are correlated with the mission timeline and ConOps, thus a mission analysis is performed. Particular attention is paid to the trajectory and Δv budget retrieval.

In the second part of the document, each of LRO's subsystems is analysed, described and reverse-sized, illustrating the rationale behind the choices made during the design phase. Specifically, the studied subsystems are: the Propulsion System (PS), Tracking, Telemetry and Telecommand (TTMTC), Attitude and Orbit Control System (AOCS), Thermal Control System (TCS), Electric Power System (EPS) and Command and Data Handling (C&DH). To conclude, a brief summary is given explaining the rationale behind the configuration of the subsystems and a general mass budget is presented.



Figure 1: Lunar Reconnaissance Orbiter rendering

This work is licensed under the Creative Commons Attribution-ShareAlike 4.0 International License.

To view a copy of this license, visit
<http://creativecommons.org/licenses/by-sa/4.0/>.

Contents

0 Notation	i
1 Mission Overview	1
1.1 Mission Objectives	1
1.2 Mission Drivers	1
1.3 Spacecraft Payload	2
2 Functional Analysis	3
3 Mission Timeline and Conceptual Operations	4
3.1 Mission Phases	4
3.1.1 Pre-Launch and Launch Readiness	4
3.1.2 Launch and Lunar Transfer	4
3.1.3 Orbiter Commissioning	5
3.1.4 Routine Operations	5
3.1.5 Extended Mission Operations	6
3.1.6 End-of-Mission Disposal	6
3.2 LRO primary modes	6
4 Mission Analysis	7
4.1 Mission Trajectory	7
4.1.1 Launch and Cruise	7
4.1.2 Lunar Orbit Insertion	7
4.1.3 Commissioning and Nominal Orbits	7
4.1.4 Extended Mission Orbit	8
4.2 Δv budget retrieval	8
4.3 Launcher Selection	8
5 Propulsion System	9
5.1 System Architecture	9
5.1.1 Thrusters	10
5.1.2 Propellant Tanks	10
5.1.3 Pressurising System and Feeding Lines	10
5.1.4 Integration of the Propulsion Unit	11
5.2 Propulsion System Configurations	11
5.3 System Preliminary Sizing	12
5.3.1 Mass Budget Retrieval	12
5.3.2 Pressure Cascade	13
5.3.3 Propellant Tanks	13
5.3.4 Pressurisation System	13
5.3.5 Modelling Considerations	14
5.4 System Review	14
6 Tracking, Telemetry and Telecommand System	16
6.1 Operational Scenario	16
6.2 Ground Stations	17
6.3 System Architecture	17
6.3.1 LRO Tracking - the Laser Ranging Subsystem	19
6.4 System Preliminary Sizing	19
6.4.1 Link Budget and SNR	19

6.4.2	Down-link in Ka-band with HGA (Scientific Data Transmission)	20
6.4.3	Down-link in S-band with HGA	20
6.4.4	Down-link in S-band with ODA	21
6.4.5	Up-link in S-band with HGA	21
6.4.6	Up-link in S-band with ODA	22
6.4.7	Sizing Considerations	22
6.5	System Review	22
7	Attitude and Orbit Control System	23
7.1	System Architecture	23
7.1.1	Sensors	23
7.1.2	Actuators	23
7.2	LRO primary modes	24
7.3	AOCS preliminary sizing	25
7.3.1	Pointing Budgets and Instruments Selection	25
7.3.2	Environmental Disturbances	26
7.3.3	Slew Manoeuvre	27
7.3.4	Momentum Unloading Operations	27
7.4	System Review	28
8	Thermal Control System	29
8.1	Lunar Thermal Environment	29
8.2	Architecture	30
8.2.1	Avionics Module, RW Assembly and Batteries	30
8.2.2	Propulsion module	31
8.2.3	Instrument Module	31
8.2.4	Deployable Devices	32
8.3	TCS Preliminary Sizing	32
8.3.1	LRO Thermal Properties	32
8.3.2	Hot Case Scenario	32
8.3.3	Cold Case Scenario	33
8.4	Bi-nodal Analysis and Thermal Decoupling	33
8.5	Sizing Considerations	34
8.6	System Review	35
9	Electrical Power System	36
9.1	Power Budget Required	36
9.2	System Architecture	36
9.2.1	Solar Array	37
9.2.2	Power Subsystem Electronics (PSE)	37
9.2.3	Lithium-Ion Battery	37
9.3	System Preliminary Sizing	38
9.3.1	Primary Source Selection	38
9.3.2	Secondary Source Selection	38
9.3.3	Bus Regulation Strategy Selection	38
9.3.4	Solar Array Sizing	39
9.3.5	Batteries Sizing	40
9.3.6	Sizing Considerations	41
9.4	System Review	41

10 On-Board Data Handling	42
10.1 Architecture	42
10.1.1 Components	43
10.1.2 Buses	44
10.2 System Preliminary Sizing	44
10.2.1 Sizing Considerations	45
10.3 System Review	45
11 Configurations	46
11.1 Launch Configuration	46
11.2 Propulsion System (PS)	46
11.3 Tracking, Telemetry and Telecommand (TTMTC)	47
11.4 Attitude and Orbit Control System (AOCS)	47
11.5 Thermal Control System (TCS)	47
11.6 Electric Power System (EPS)	48
11.7 Command and Data Handling (C&DH)	48
11.8 Scientific Payload	48
11.9 Mass Budget	49
12 References	50
13 Appendix	A-1
13.1 Mission Profile Overview	A-1
13.1.1 Launch	A-1
13.1.2 Lunar Orbit Insertion	A-2
13.1.3 Station Keeping Manoeuvre	A-2
13.2 Spacecraft Overview	A-3
13.3 Tracking, Telemetry and Telecommand System	A-3
13.3.1 Scientific Data Volume	A-3
13.3.2 Ka-band down-link usage	A-3
13.3.3 WS1 Ground Station Antenna Characteristics	A-4
13.3.4 System Integration	A-4
13.3.5 Thermal Control System	A-5
13.4 Electric Power System	A-6
13.5 Command and Data Handling	A-7
13.6 Configurations	A-9

List of Figures

1	Lunar Reconnaissance Orbiter rendering	2
2	Insertion Plane Relative to Earth and Target Plane	7
3	LRO's Propulsion System Diagram (source: [13])	9
4	LRO thrusters configuration	10
5	LRO's Propulsion System physical layout (source: [13])	11
6	PS operating pressure (source: [14])	14
7	LRO's contacts with ground stations (source: [6])	16
8	LRO communications system block diagram	18
9	LRO control modes	25
10	LRO Reaction Wheels (RWs) and Autonomous-Star Trackers (A-STRs)	28
a	RWs mounted to spacecraft structure	28
b	A-STRs mounted on Instrument Module	28
11	Lunar thermal flux with the β angle as seen from the Sun	29

a	$\beta = 0^\circ$	29
b	$\beta = 90^\circ$	29
c	Lunar heat flux	29
12	RWs Heat Dissipation	30
13	PS Shielding	31
14	Bi-nodal model of the LRO	34
15	LRO EPS block diagram	36
16	LRO Solar Array (SA) front and rear view	37
17	LRO battery [35]	38
18	LRO simplified system block diagram	42
19	LRO C&DH architecture (sources: [37][1]), a more complete schematic is reported in Figure 30	43
	a C&DH enclosure architecture	43
	b SBC software context diagram	43
20	LRO design overview showing modular construction [1]	46
21	LRO Launch configuration	46
22	Mission Profile	A-1
23	LRO Lunar Orbit Insertion	A-2
	a Insertion Plane Relative to Earth and Target Plane	A-2
	b Lunar Orbit Insertion (LOI) Sequence	A-2
24	Effects of perturbations on Mission Orbit [9]	A-2
25	Lunar Reconnaissance Orbiter	A-4
26	Avionics TCS (source: [14])	A-5
	a Avionics Panel Heat Pipe Network	A-5
	b Avionics Radiator	A-5
27	LRO Multi Layer Insulator (MLI)	A-5
28	SA containment canisters for the restraint bolts, shadowing 4 solar cells [14]	A-6
29	SA issue with Lunar Reconnaissance Orbiter Camera (LROC) Field of View (FOV)[14]	A-6
30	C&DH schematic	A-8
31	LRO design overview showing modular construction [1]	A-9

List of Tables

1	List of the primary (P) and secondary (S) LRO mission goals [4]	1
2	Correlation between scientific instruments and mission goals [5]	2
3	List of functionalities the system has to satisfy	3
4	First phase: ConOps and their relationships with functionalities	4
5	Second phase: ConOps and their relationships with functionalities	4
6	Third phase: ConOps and their relationships with functionalities	5
7	Fourth phase: ConOps and their relationships with functionalities	5
8	Fifth phase: ConOps and their relationships with functionalities	6
9	Last phase: ConOps and their relationships with functionalities	6
10	Δv retrieved from [9] and [10] vs computed. The additional 78 m/s come from margin standards.	8
11	Data for the Installed Thrusters (source: [15][16]) Note that the power consumption is referred to the one of the thruster's valves alone.	10
12	Thruster configurations (source: [10])	11
13	Comparison between computed and actual Hydrazine (N_2H_4) masses, from the corresponding Δv . m_{prop} are retrieved from [13] and the “Extra margin” accounts for ullage, residuals and loading uncertainty. “Extra manouvres” include momentum unloading and extended mission. Δv are retrieved from [9] and [10] and the additional 30+48m/s comes from margin standards.	12

14	Propellant Tank Sizing (values for one tank)	13
15	Helium Tank Sizing	14
16	Data for the antennas used in LRO communications ([21], [23])	18
17	TTMTC system characteristics (source: [1])	19
18	Expected losses in both down-link and up-link (if applicable).	20
19	Down-link in Ka-band with HGA - results	20
20	Down-link in S-band with HGA - results	21
21	Down-link in S-band with ODA - results	21
22	Up-link in S-band with HGA - results	21
23	Up-link in S-band with ODA	22
24	Attitude Control System (ACS) sensors characteristics (sources: [1], [26])	23
25	ACS actuators characteristics (sources: [1], [25], [16])	24
26	Minimum needed accuracy per each mode	26
27	Comparison between estimated and real data	28
28	Lunar thermal environment characterization [1][28]	29
29	Strictest temperature intervals to be satisfied [14]	30
30	Thermal fluxes and thermal absorbed powers	33
31	Main results of the thermal analysis	35
32	EPS budget (sources: [14][32][33])	36
33	Input parameters for the sizing of the SA	39
34	Results of the sizing of the SA	40
35	Input parameters for the sizing of the battery	40
36	Results of the battery sizing. Mass, volume and capacity refer to the entire battery pack, while number of cells in series and number of strings in parallel refer to the cells' arrangement in a single block.	41
37	C&DH memory sizing results	45
38	C&DH memory comparison with real data from [37][38][39]	45
39	Dry mass budget comparison between theoretical/computed and real data [14][1]. * the % of dry mass was retrieved from statistical data of satellites with similar mission to LRO	49
40	Δv computed through Tsiolkovsky equation knowing the masses of the launcher. All Δv are retrieved for a worst case scenario. [8]	A-1
41	Breakdown of LRO's daily data volume (source: [1])	A-3
42	Ka-band down-link utilization	A-3
43	WS1 characteristics	A-4
44	OBDH Throughput Computation	A-7
45	OBDH Memory Budget Computation (margined values use 400% margin)	A-8

0 Notation

Parameters

α	absorption coefficient	[\cdot]
δ	thickness	[mm]
Δv	variation of speed (referred to manoeuvre cost)	[m/s]
\dot{q}	heat flux	[W/m ²]
η	efficiency	[\cdot]
Γ	angular momentum	[N m s]
γ	heat capacity ratio	[\cdot]
λ	wave length	[m]
\mathfrak{R}	individual gas constant	[J/(kg K)]
E_b/N_0	energy per bit to noise power spectral density ratio	[\cdot]
σ_B	Stefan-Boltzmann's constant	[Wm ⁻² K ⁻⁴]
σ_y	yield strength	[MPa]
θ	angle	[deg]
ε	emissivity coefficient	[\cdot]
A	Area	[m ²]
B	bandwidth	[Hz]
C	capacity	[Wh]
E_d	energy density	[Wh/kg]
E_s	specific energy	[Wh/dm ³]
F	thrust	[N]
f	frequency	[Hz]
F_{\odot}	Sun irradiance	[W m ⁻²]
$F_{pl/sc}$	view factor	[\cdot]
h	height	[km]
I	moment of inertia	[kg m ²]
i	inclination of the orbit (Keplerian element)	[deg]
I_{degr}	inherent degradation	[\cdot]
I_{sp}	specific impulse	[s]
k	Boltzmann constant ($1.380649 \cdot 10^{-23}$)	[m ² kg s ⁻² K ⁻¹]
L	losses	[dB]
M	torque	[N · m]
m	mass	[kg]
N	number of	[\cdot]
P	power	[W]
p	pressure	[MPa]
Q	thermal power	[W]
q	average reflectivity coefficient	[\cdot]
R	data rate	[bps]
r	radius	[m]
T	temperature	[K]
t	time	[s]
V	volume / voltage	[m ³] / [V]
v	velocity	[m/s]
X	line efficiency	[\cdot]

Subscripts and Superscripts

0	initial
---	---------

\oplus	Earth
\odot	Moon
\odot	Sun
<i>c</i>	combustion chamber
<i>cable</i>	cable / transmission line
<i>day</i>	day-light
<i>des</i>	desaturation
<i>dry</i>	dry (no propellant is included)
<i>dyn</i>	dynamic
<i>ecl</i>	eclipse
<i>enc</i>	encoding
<i>f</i>	final
<i>feed</i>	feed / feeding
<i>inj</i>	injector / injection
<i>int</i>	internal
<i>IR</i>	infrared
<i>max</i>	maximum
<i>min</i>	minimum
<i>nom</i>	nominal
<i>press</i>	pressurant (Helium)
<i>prop</i>	propellant
<i>rad</i>	radiator
<i>RW</i>	reaction wheel
<i>s</i>	sampling
<i>sc</i>	spacecraft
<i>space</i>	free space
<i>tank</i>	referred to tank
<i>tot</i>	total
<i>typ</i>	typical

List of Acronyms

ACS	Attitude Control System	HGA	High Gain Antenna
AOCS	Attitude and Orbit Control System	HGF	High-pressure Gas Filter
AT	ACS Thruster	HK	House-Keeping
A-STR	Autonomous-Star Tracker	HLF	Hydrazine low-pressure filter top tank
BER	Bit Error Rate	HPLV	High Pressure Latch Valve
BOL	Beginning Of Life	HPR	High Pressure Regulator
BPSK	Bi-Phase Shift Keying	IMU	Inertial Measurement Unit
CCHP	Constant Conductance Heat Pipe	IR	Infrared
C&DH	Command and Data Handling	LAMP	Lyman-Alpha Mapping Project
CM	Center of Mass	LBLF	Hydrazine low-pressure filter bottom tank
COPV	Composite Overwrapped Pressure Vessel	LCROSS	Lunar Crater Observation and Sensing Satellite
CRaTER	Cosmic Ray Telescope for the Effects of Radiation	LEND	Lunar Exploration Neutron Detector
CSS	Coarse Sun Sensor	LET	Linear Energy Transfer
CTE	Coefficient of Thermal Expansion	LFDB	Liquid Fill and Drain valve Bottom tank
DET	Direct Energy Transfer	LFDT	Liquid Fill and Drain valve Top tank
DLRE	Diviner Lunar Radiometer Experiment	LHCP	Left Hand Circular Polarization
DoD	Depth of Discharge	LOI	Lunar Orbit Insertion
DSB	Data Storage Boards	LOLA	Lunar Orbiter Laser Altimeter
DSN	Deep Space Network	LR	Laser Ranging
ECI	Earth Centered Inertial	LRO	Lunar Reconnaissance Orbiter
EELV	Evolved Expendable Launch Vehicle	LROC	Lunar Reconnaissance Orbiter Camera
EEPROM	Electrically Erasable Programmable Read Only Memory	LRT	Laser Ranging Telescope
EOL	End Of Life	LTO	Lunar Transfer Orbit
EIRP	Effective Isotropic Radiated Power	LV	Launch Vehicle
EPC	Electronic Power Conditioner	LVLH	Local Vertical Local Horizontal
EPS	Electric Power System	LVPC	Low Voltage Power Converter
FDIR	Fault Detection, Isolation and Recovery	MAC	Multi-function Analog Card
FOV	Field of View	MCC	Mid-Course Correction
FSW	Flight Software	MIMU	Miniature Inertial Measurement Unit
GG	Gravity Gradient	Mini-RF	Miniature Radio Frequency instrument
GFDP	Gas Fill and Drain valve-Pyrovalve	MLI	Multi Layer Insulator
GFDR	Gas Fill and Drain valve-Regulator	MLV	Manifold Latch Valve
GFDT	Gas Fill and Drain valve-Tank	MOI	Mission Orbit Insertion
GS	Ground Station	NGSLR	Next Generation Satellite Laser Ranging

NT	Insertion Thruster	SA	Solar Array
N₂H₄	Hydrazine	SAR	Synthetic Aperture Radar
ODA	Omni-Directional Antenna	SBC	Single Board Computer
OQPSK	Offset Quadrature Phase Shift Keying	SK	Station-Keeping
OSR	Optical Solar Reflector	SOI	Sphere Of Influence
cPCI	Compact Peripheral Component Interconnect	SNR	Signal to Noise Ratio
PD	Proportional Derivative	SpW	SpaceWire
PDE	Propulsion-Deploy Electronics	SRAM	Static Random Access Memory
PID	Proportional Integral Derivative	SRP	Solar Radiation Pressure
PMC	Power Monitor Card	SSPC	Solid State Power Controllers
PPT	Peak Power Tracking	SUROM	Start-Up Read Only Memory
PS	Propulsion System	TCS	Thermal Control System
PSE	Power Subsystem Electronics	TLV	Tank Latch Valve
PSR	Permanently Shadowed Region	TRL	Technology Readiness Level
PV	Pyrovalve	TTMTC	Tracking, Telemetry and Telecommand
PWA	Printed Wiring Assembly	TWTA	Traveling Wave Tube Amplifier
RAM	Random Access Memory	TWT	Traveling Wave Tube
RF	Radio Frequency	USN	Universal Space Network
RHCP	Right Hand Circular Polarization	USO	Ultra-Stable Oscillator
RLG	Ring Laser Gyroscope	VDA	Vapour Deposited Aluminum
ROM	Read Only Memory	WS1	White Sands 1 - Ground Station Antenna
RW	Reaction Wheel		

1 Mission Overview

The Lunar Reconnaissance Orbiter (LRO) is the first mission of the *Vision for Space Exploration* program presented by NASA in 2004. It was launched, together with the LCROSS spacecraft, on 18 June 2009 from Cape Canaveral aboard the Atlas V rocket and begun its operative phase on 15 September 2009. The original mission was sized to withstand a 1-year exploration phase and a 3-years scientific one, with a possible extension of the latter. The robustness of the design allowed the LRO to continue the latter mission heretofore, until the moon impact that will decree the end of the mission.

1.1 Mission Objectives

The primary LRO mission objective was to collect the data necessary to support the design and development of the systems and missions which would return humans to the Moon [1] and eventually to Mars [2]. Therefore, the mission consisted in studying the lunar surface in order to identify safe landing sites, in locating and characterising potential resources and also in characterising the radiation levels experienced in a lunar environment. In addition, an *advanced technology demonstration package* was also included in the payload [3] to achieve a first in-space communication with laser technology. The discussed objectives have been summed up and reported in Table 1.

OBJ-ID	Main Objectives Description	
OBJ-01	(P)	Provide measurements to characterize possible human landing sites
OBJ-02	(P)	Identify and characterize potential lunar resources
OBJ-03	(P)	Characterize the Lunar Space Radiation Environment
OBJ-04	(P)	Acquire detailed maps of the lunar surface
OBJ-05	(P)	Study of moon polar regions in search for useful resources for future human mission or robotic sample return missions
OBJ-06	(S)	Prove new technologies

Table 1: List of the primary (P) and secondary (S) LRO mission goals [4]

1.2 Mission Drivers

The overall design of the mission and spacecraft was led by a set of driving requirements, these are:

- **“Discovery-Class” mission vs Accelerated Development Schedule:** the mission had to be developed from concept to launch within four years with about \$450M budget [1].
- **Orbit and Mission Duration:** to fulfill the mission requirements in terms of data resolution and to ensure a data collection across all the seasonal lunar lighting conditions. This led to the selection of a 50 km lunar orbit and set the duration of the primary mission to one year.
- **On-board Δv Capability:** a reasonable amount of fuel and large propulsion system were necessary to perform the LOI and all the subsequent orbit adjustments.
- **Near Continuous Nadir Pointed Operation:** this affected the communication methods and the solar array system, driving also the design of the TCS.
- **High Rate Data Downlink and Large On-board Data Storage:** high resolution imagery and data affected the on-board data storage capability and the downlink communications.
- **Capability for Extended Mission:** this led to a general over-sizing of the system, particularly the electrical and thermal subsystems.
- **Harsh Lunar Thermal Environment:** the spacecraft had to withstand a long-duration in a low-altitude lunar mission. Therefore, particular attention had to be paid in the design of the overall architecture.

1.3 Spacecraft Payload

The payload of the LRO is made up of seven different instruments, including the one for the new technology validation for space application. These are:

- **Cosmic Ray Telescope for the Effects of Radiation (CRaTER)**: dedicated to the measurement and characterization of galactic and solar cosmic rays through the Linear Energy Transfer (LET)¹ spectra to investigate the effects of different shields on radiation including tissue-equivalent plastics;
- **Diviner Lunar Radiometer Experiment (DLRE)**: charts the global day/night surface temperature, characterises the thermal environment at 300 km height, locates rock abundances globally and at landing sites, identifies potential polar ice reservoirs and maps the variations in silicate mineralogy;
- **Lyman-Alpha Mapping Project (LAMP)**: identifies Permanently Shadowed Regions (PSRs), assays the tenuous lunar atmosphere and its variability and searches for exposed ices and frosts near the lunar poles and in PSRs;
- **Lunar Exploration Neutron Detector (LEND)**: maps the flux of neutrons from the lunar surface to search for evidence of water by detecting hydrogen-rich spots and makes a global mapping of Lunar neutron emissions;
- **Lunar Orbiter Laser Altimeter (LOLA)**: provides the global geodetic lunar surface topography at high resolution, characterizes the illumination of polar regions and images PSRs and contributes to the assessment of meter-scale features such as landing site slope and surface roughness to facilitate landing site selection;
- **LROC**: assesses meter and smaller-scale features to ease the landing site localisation and certification, develops a meter-scale mapping of the polar regions to characterize the polar illumination environment In addition, it provides sub-meter imaging to characterise regolith properties and derive the meter scale topography, a multi wavelength mapping to find potential lunar resources and determines recent small impact rates;
- **Miniature Radio Frequency instrument (Mini-RF)**: allows the verification of an advanced lightweight Radio Frequency (RF) technology, the demonstration of a hybrid polarity Synthetic Aperture Radar (SAR), to obtain measurements of lunar surface as a function of radar band and resolution, to produce topographic data using interferometry and SAR stereo techniques and to map potential ice deposits in collaboration with Chandrayaan-1 satellite.

Table 2 reports the correlation between the instrument objectives with the mission high level goals.

Instrument	OBJ-01	OBJ-02	OBJ-03	OBJ-04	OBJ-05	OBJ-06
CRaTER			x			
DLRE	x	x	x		x	
LAMP		x		x	x	
LEND		x	x		x	
LOLA	x	x		x	x	
LROC	x	x		x	x	
Mini-RF		x		x		x

Table 2: Correlation between scientific instruments and mission goals [5]

¹LET is the amount of energy that an ionizing particle transfers to the material traversed per unit distance

2 Functional Analysis

To better understand the LRO mission, the macro-functionalities required to fulfil the high level goals have been extracted. Table 3 shows the actions that shall be performed throughout the mission.

First level	Second level	FUN-ID
Pre-Launch	Verification and Testing	FUN-01.01
	System Setup and Checks	FUN-01.02
Get to the Moon	Launch: escape from Earth gravity field	FUN-02.01
	Detach payload	FUN-02.02
	Insert in Lunar Transfer Orbit (LTO)	FUN-02.03
	Lunar Orbit Insertion (LOI)	FUN-02.04
Orbit the Moon	Arrival to Target orbit	FUN-03.01
	Transfer to Commissioning Orbit	FUN-03.02
	Transfer to extended mission orbit	FUN-03.03
Activate Orbiter	Detumbling	FUN-04.01
	Sun acquisition and panels deployment	FUN-04.02
	Instruments activation	FUN-04.03
	Subsystems checkup	FUN-04.04
	Spacecraft and Subsystems Calibration	FUN-04.05
Earth communications	Ground segment setup	FUN-05.01
	Ground segment acquisition and tracking	FUN-05.02
	Downlink and Uplink support	FUN-05.03
	Pointing Antennas	FUN-05.04
Withstand Environment	Provide thermal control	FUN-06.01
	Maintain ionisation effects within limits	FUN-06.02
	Withstand small meteorite impacts	FUN-06.03
	Cope with eclipses	FUN-06.04
Perform mission operations	Provide power supply	FUN-07.01
	Provide attitude determination and control	FUN-07.02
	Acquire Scientific Data	FUN-07.03
	Handle and Store Data	FUN-07.04
	Return Data to ground stations	FUN-07.05
Manage non nominalities	Ensure a suitable autonomy level	FUN-08.01
	Fault Detection, Isolation and Recovery (FDIR)	FUN-08.02
End of life disposal	Respect planetary protection standards	FUN-09.01
	Final Trajectory Prediction	FUN-09.02
	Finalisation Operations/Activities	FUN-09.03

Table 3: List of functionalities the system has to satisfy

3 Mission Timeline and Conceptual Operations

Once the main functionalities were identified, it was then possible to outline the timeline of the mission. This led to the distinction between six main phases and the modes, thus to the definition of the Conceptual Operations that were needed to fulfill the mission requirements. [6][7]

3.1 Mission Phases

3.1.1 Pre-Launch and Launch Readiness

This phase can be considered to have started when the first integration and test activities began, and continued until the start of the LV countdown sequence, for a total duration of approximately 1 year and a half. At this stage, two sub-phases could be identified: Space Segment Readiness and Ground Segment Readiness. Table 4 reports the most relevant ConOps involved for both segments.

Phase 1	Pre-Launch and Launch Readiness	Linked to
Space segment	Orbiter functional performance and environmental test	FUN-01
	Ship to launch site and launch site processing	
Ground segment	Ground system integration, validation and testing	FUN-01
	Flight procedures and operations development	
	Mission rehearsal and simulation	FUN-05.01

Table 4: First phase: ConOps and their relationships with functionalities

3.1.2 Launch and Lunar Transfer

This second phase started when the Launch Vehicle (LV) countdown sequence was initiated and it terminated when the last LOI manoeuvre was performed to capture into the commissioning orbit. Five sub-phases could be identified here: Launch and Ascent, Separation from LV, Deployment and Sun Acquisition, Lunar Cruise, Lunar Orbit Insertion. In Table 5 are shown the most relevant Conceptual Operations involved in this phase for both the Space Segment and Ground Segment.

Phase 2	Launch and Lunar Transfer	Linked to
Space segment	C&DH monitors the separation from Launch Vehicle	FUN-02.01 FUN-02.02 FUN-04.01
	Deployment of solar arrays and High Gain Antenna (HGA)	FUN-04.02
	Sun and Ground Station acquisitions	FUN-05.02
	Perform Mid-Course Correction (MCC) manoeuvre(s)	FUN-02.03
	Turn on CRaTER and LEND for calibration activities	FUN-04.03 FUN-04.05
	Perform the series of LOI manouevres	FUN-02.04 FUN-03.01
Ground segment	Configure orbiter to launch mode and monitor its status	FUN-02.01
	Perform initial acquisitions and check orbiter subsystems	FUN-05.03
	Plan and upload LOI burns	FUN-08.01

Table 5: Second phase: ConOps and their relationships with functionalities

3.1.3 Orbiter Commissioning

This third phase started once the LRO reached and inserted into the commissioning orbit. It lasted for approximately 60 days, until the insertion into the final mission orbit around the Moon. Two sub-phases could be identified here: Spacecraft Activation and Commissioning, Integrated Instruments Activation and Commissioning. Table 6 reports the most relevant ConOps involved in this phase.

Phase 3	Orbiter Commissioning	Linked to
Space segment	Test and calibrate solar array and HGA pointing	FUN-04.05 FUN-05.04
	Verify Ka-band and S-band downlink telemetry	FUN-04.04
	Configure and verify Thermal and Power subsystems	FUN-04.04 FUN-06.01
	Perform sensors and instruments calibration activities	FUN-04.05
	Configure the FDIR components	FUN-08.02
	Perform series of maneuvers to capture into Mission Orbit	FUN-03.01 FUN-03.02
Ground segment	Use primary ground network stations for support	FUN-05.03
	Verify whether frozen orbit exist at the 30x216 orbit	
	Generate and process tracking data	

Table 6: Third phase: ConOps and their relationships with functionalities

3.1.4 Routine Operations

Table 7 reports the most relevant ConOps involved in this phase for both Space and Ground Segments.

Phase 4	Routine Operations	Linked to
Space segment	LRO will be nominally nadir pointing	FUN-06.01
	Perform momentum management every 2 weeks	FUN-06.03
	Monthly SK maneuvers and instruments calibration	FUN-07.01
	Perform twice a year a 180° yaw rotation	FUN-07.02
	Twice a year LRO might be commanded to low power mode due to eclipses	FUN-06.04 FUN-07.01
	Perform monthly a mini-RF technology demonstration	FUN-05.04
	Collect, store and send data obtained from the scientific instruments payload	FUN-07.04 FUN-07.05
Ground segment	Use primary ground network stations for support	FUN-05.01
	Store and process data	FUN-07.04
	Perform orbit determination and attitude support to LRO	FUN-07.02
	Monitor orbiter health and safety	FUN-04.04
	Log and track of all possible ground and orbiter anomalies	FUN-08
	Provide control command sequences to the orbiter	FUN-05.03

Table 7: Fourth phase: ConOps and their relationships with functionalities

The so called “Routine Operations” begun once the LRO entered its final mission orbit and when all spacecraft and instruments commissioning activities were completed. It lasted for about 1 year, which was the minimum time required to fulfill the mission requirements related to lunar surface mapping. In this phase, seven sub-phases could be identified: Measurement Operations, Station Keeping, Momentum Management, Instruments Calibration, Lunar Eclipse, Yaw Manoeuvre, Safe Mode.

3.1.5 Extended Mission Operations

The “Extended Mission” phase started as soon as all main mission objectives for the main exploration phase were achieved. It is still active nowadays and it will last until all the available on-board fuel is exhausted. Since all LRO activities were planned from time to time based on the resources still available, no sub-phases were identified. In Table 8 are shown the most relevant Conceptual Operations involved in this phase for both Space and Ground Segments.

Phase 5	Extended Mission Operations	Linked to
Space segment	Adjustment of mission orbit to the extended mission orbit	FUN-03.03
	Continue measurement operations in agreement with established objectives and still available resources	FUN-07.03
	Send collected data to ground stations	FUN-07.04 FUN-07.05
Ground segment	Use primary ground network stations for support	FUN-05
	Store and process data	FUN-07.04

Table 8: Fifth phase: ConOps and their relationships with functionalities

3.1.6 End-of-Mission Disposal

This last phase will begin when the previous extended Scientific Mission phase will be declared concluded and the mission will eventually end when LRO will crash on the Moon surface. Also here, no sub-phases could be identified here, since no LRO activity was previously planned.

In Table 9 are shown the most relevant Conceptual Operations involved in this phase.

Phase 6	End-of-Mission Disposal	Linked to
Space segment	Continue measurements until all fuel is exhausted	FUN-07.03
	Impact with the Moon	FUN-09.01
Ground segment	Support end-of-mission activities	FUN-09.03
	Minimize the likelihood of an accidental impact	
	Track, if possible, the LRO trajectory as it impacts the Moon	FUN-09.02
	Respect requirements of planetary protection category II	FUN-09.01

Table 9: Last phase: ConOps and their relationships with functionalities

3.2 LRO primary modes

Throughout the mission lifetime multiple modes could be identified to provide regular activities [1]. These include the primary ACS modes (Sun Safe, Observing, Delta-V and Delta-H), but also modes such as Communication and Low Power. These modes will be thoroughly explained in the respective subsystems.

4 Mission Analysis

4.1 Mission Trajectory

4.1.1 Launch and Cruise

In this first phase, the LRO is set onto a geocentric orbit onboard the Atlas V 401 Evolved Expendable Launch Vehicle (EELV), along with the Lunar Crater Observation and Sensing Satellite (LCROSS), launching from Kennedy Space Center. After 45 minutes, the satellite separates from the LCROSS-Centaur stack to enter its transfer leg. Most of this phase is entirely defined by the launcher's supplier, which places the LRO onto an highly elliptical 35000x185 km parking orbit. From that, after a short coast, a second ignition of the upper stage inserts the spacecraft into the cruise path [8]. A minimum energy lunar transfer is chosen to bring the payload to the Moon Sphere Of Influence (SOI). The time window is limited by a science constraint: in order to fulfil OBJ-05, lunar polar regions have to be viewed in extreme lighting conditions. This can be possible if the LRO orbital plane is oriented such that it is near edge-on to the Sun, condition defined by a low beta-Sun angle at lunar solstice. At insertion, LRO orbit plane is fixed with respect to the Earth, as it can be seen in Figure 2. Therefore, to drive the target plane to a particular inertial orientation, the Earth departure must be within a few days of the point at which the insertion plane coincides with the target plane. As a result, a launch window of 2-3 days every 2 weeks can be found. During the cruise phase, a series of MCC manoeuvres is considered after the first 24h in order to correct 3- σ launch vehicle errors. During cruise Sun Safe mode followed by Delta-V mode are employed [9][10][11].

4.1.2 Lunar Orbit Insertion

Regardless the exact geometry at launch, the orbiter reaches the lunar SOI in 4-5 days and a sequence of 5 retrograde manoeuvres is performed to achieve the commissioning orbit. Before these ignitions, an engineering test is carried out to verify that all the systems are behaving nominally and to retrieve the precise attitude [10]. The first manoeuvre, denoted as LOI-1, lasts about 40 minutes and is the most expensive in terms of mass budget, since it provides the velocity decrease that allows the spacecraft to be captured by the lunar gravitational field and inserts directly at an 89.7 degrees inclination to avoid expensive manoeuvres. Its magnitude is a function of the launch date, due to variations of the Moon phase. To increase the robustness of the trajectory design and cope with an unforeseen failure of the propulsion system or of a processor, since this manoeuvre is critical, it was designed such that only half of the Δv performed is required to capture into orbit. LOI-2 and LOI-3 are designed as fixed duration manoeuvres to lower the orbit apocentre, the former providing also a correction to potential errors of the LOI-1. Once an intermediate 216x740 km orbit is reached, to circularise the latter, LOI-4 is performed at the pericentre height. Lastly, LOI-5 is executed over the lunar North Pole to lower the periapsis altitude to 30 km over the Moon's South Pole, reaching the commissioning orbit with ω equal to 270 degrees, thus avoiding an additional argument of pericentre rotation [9][10]. Being the intermediate orbits known, all the manoeuvres are deterministic[9].

4.1.3 Commissioning and Nominal Orbits

As anticipated before, the designed commissioning orbit is a 30x216 km stable polar orbit, with the pericentre above the lunar South Pole; however, the achieved orbit is a 31.5x199 km orbit. The latter is still quasi-frozen and it is also more efficient for the LOLA instrument, since it is designed to operate nominally at altitudes lower than 200 km [10]. The secular growth of both the argument of pericentre and the eccentricity are negligible, thus the station keeping budget is minimum (approximately 5 m/s

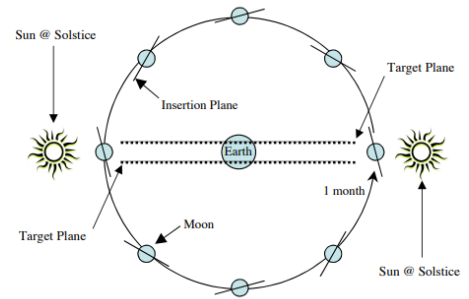


Figure 2: Insertion Plane Relative to Earth and Target Plane

per year). Due to the low maintenance and the high stability of the orbit, in this phase the instruments are activated and checked. This phase lasts for almost 60 days. Once all the subsystems are correctly operative the mission trajectory is moved to the exploration target orbit through a sequence of 3 Mission Orbit Insertion (MOI), spaced approximately 24 hours apart and performed at the pericentre [10]. If possible, the transfer is achieved in only one MOI exploiting the secular variation of the eccentricity to raise the periapsis altitude. The exploration mission nominal orbit is a 50 km quasi-circular polar orbit, in order to respect the mission drivers. However, the orbit is highly unstable and a sequence of Station-Keeping (SK) manoeuvres is required periodically. The nominal orbital parameters are maintained through an apse line rotation, obtained by 2 burns with a 24 hours separation: the first to circularise the orbit (SK#1), the second to get back to the nominal orbit (SK#2). The SK manoeuvre is performed once each lunar orbit period (27.4 days) and exploits the secular variation pattern of eccentricity and argument of periapsis to keep the altitude within 15 km of the target 50 km orbit, as it can be seen in Figure 24, reported in the Appendix. A momentum management manoeuvre is also required every two weeks to desaturate the RWs. [9][10]

4.1.4 Extended Mission Orbit

Once the nominal mission is complete, if no failure affects the LRO, it will likely have a significant amount of fuel left. Therefore, part of it can be used to transfer back to the 30x216 km quasi-frozen orbit to extend the mission into a scientific one. Thanks to the low maintenance of the trajectory, depending on the amount of fuel left, the LRO is likely to spend many years in this orbit.[9]

4.2 Δv budget retrieval

A simulation of the mission trajectory was performed and the obtained Δv values are compared with the real ones in Table 10. As a first approximation, the LOI-1 was considered as a Hohmann transfer between the parking orbit reached through the launcher and the Moon orbit around the Earth. Worst case scenarios are taken into account for the other manoeuvres.

Mission Plan	Δv [m/s] computed	Δv [m/s] from data
LOI-1	568.0	555.5
LOI-2 thru LOI-3	219.1	201.5
LOI-4	91.0	113.2
LOI-5	40.1	37.4
MOI	41.1	40.2
Station-Keeping (1 year)	162.0	162.0
Preliminary Total	1121.2	1109.8
Launch Dispersion Correction	30.0	30.0
Deterministic Margin	48.0	n/a
Corrected Total	1199.2	1139.8

Table 10: Δv retrieved from [9] and [10] vs computed. The additional 78 m/s come from margin standards.

4.3 Launcher Selection

A launch vehicle, in order to be suitable for a mission, must provide an energy at liftoff (C3) higher than the one required to reach the orbit of interest, which is a negative value for a lunar mission. The *Atlas V 401* chosen for the launch can provide a C3 of around $10 \text{ km}^2/\text{s}^2$, with a payload of 3000 kg. Thus, the vehicle is suitable for the mission [12]. In addition, a preliminary analysis of the Δv produced by the launcher was performed and it is shown in Table 40, reported in the Appendix.

5 Propulsion System

The LRO PS had to be capable of providing the Δv described in the previous sections, thus answering to functionalities FUN-02, FUN-03, FUN-07.02 and FUN-08.

As stated in [13], at a preliminary design phase a bi-propellant architecture was found to be the optimal solution in terms of mass savings. However, it was opted for the implementation a mono-propellant N₂H₄ system due to a higher simplicity and affordability, also allowing to re-use two already available tanks from the cancelled *NASA X-38* mission. This granted a reduction of the time required for the development of the propulsion unit while cutting the costs, at the expenses of a slightly greater dry mass of the system. In addition, since the PS was not only responsible for SK manoeuvres, but also for the LOI and MOI manoeuvres, the propellant mass loaded onboard was significant, as reported in Table 13. Indeed, at a preliminary design level, this turned out to be a reason of incompatibility with the original launcher selection (the *Delta II* rocket), hence the choice of the *ATLAS V*.

5.1 System Architecture

The PS of the LRO, according to [13], is based on eight 22 N ACS Thrusters (ATs) (Aerojet, MR106L) and four 90 N Insertion Thrusters (NTs) (AMPAC, MONARC-90) as it can be seen in Figure 3. The propellant is stored in two identical tanks, placed one above the other and pressure regulated. A third different tank is also installed, which contained 3.3 kg of Helium as pressurant

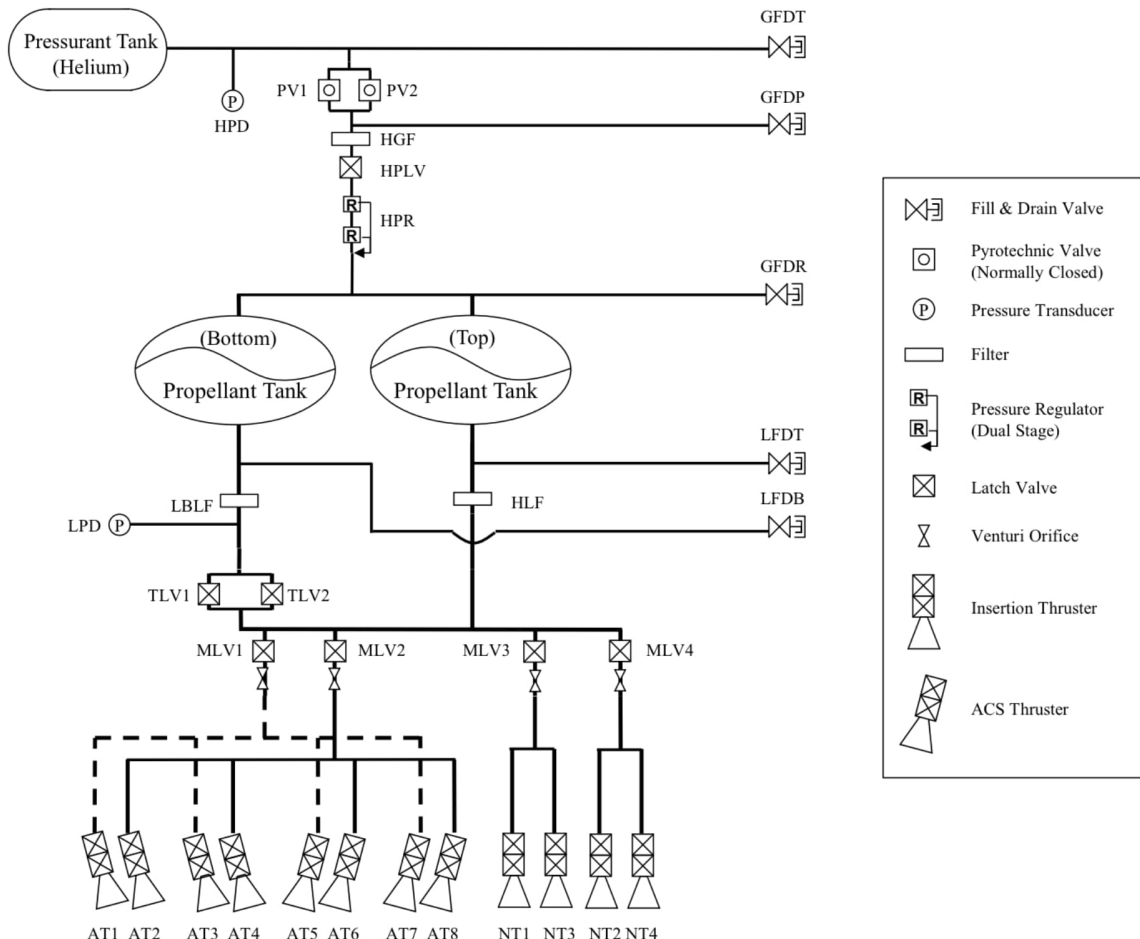


Figure 3: LRO's Propulsion System Diagram (source: [13])

5.1.1 Thrusters

The ATs operate in pulse mode and have the primary function of providing attitude control. They are located at the four corners of the spacecraft's aft face and are tilted of 15° towards the symmetry axis of the spacecraft. Whereas, the NTs operate in steady state, since they are required only during orbital manoeuvres, and are positioned in a diamond configuration on the same face as the ATs.

According to [13], the aim of the NTs arrangement is to minimise the torsional motion generated during the major manoeuvres. However, due to the internal disposition of instruments, the Center of Mass (CM) is misaligned with the symmetry axis of the orbiter, hence the selection of a 90° angle of installation for the NTs. For these reasons, the ATs contribution is required in every manoeuvre. During the early design phase, a two NTs thrusters configuration was also considered. However, the final choice fell on a four thrusters configuration, which allows to have shorter burn time, lower propellant mass and more operational flexibility [14], also ensuring a higher redundancy level. The key parameters for the two different types of thrusters implemented are reported in Table 11.

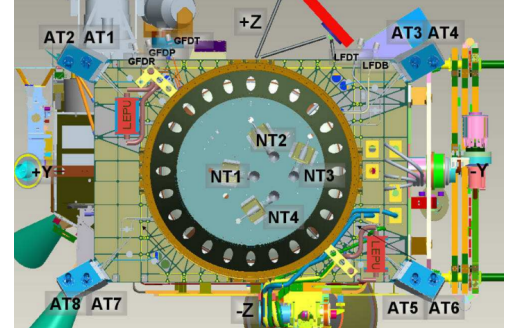


Figure 4: LRO thrusters configuration

Thruster ID	F [N]	I_{sp} [s]	p_c [bar]	m [kg]	P [W]
Insertion Thruster (NT)	90	232.1	5.5–27.6	1.12	72.00
ACS Thruster (AT)	22	228–235	3.8–13.4	0.59	36.16

Table 11: Data for the Installed Thrusters (source: [15][16]) Note that the power consumption is referred to the one of the thruster's valves alone.

A high level of redundancy is also guaranteed by the subdivision of the feeding system into four manifolds: indeed, even in case of latch valve or thruster failure, an effective Δv can still be provided. In addition, thanks to the Manifold Latch Valves (MLVs), each set of thrusters can be isolated from the rest of the system, particularly during launch and in fault contingency situations.

5.1.2 Propellant Tanks

The 895 kg of propellant onboard are stored at 1.875 MPa into two identical titanium oblate spheroid tanks, each one with an internal volume of 0.461 m^3 [13]. An elastomeric diaphragm is responsible for the separation of the pressurant gas from hydrazine. After each tank, the HLF and LBLF filters are implemented to prevent any particulate contaminants from entering the feeding system. In addition, two Tank Latch Valves (TLVs) are implemented downstream of the bottom tank to prevent propellant transfer from one tank to the other during launch. These valves are located in parallel to reduce the pressure drop before the thrusters. The pressure regulation of the propellant tanks is performed through a High Pressure Regulator (HPR), composed by two stages operating in series and implemented together with an High Pressure Latch Valve (HPLV). The choice of a pressure-regulated feed system with respect to a blow-down one was driven by the request of a constant thrust level for the entire duration of the mission, hence a constant tank pressure.

5.1.3 Pressurising System and Feeding Lines

The 3.3 kg of pressurant gas (Helium) are stored with an initial pressure of 26.738 MPa in a 0.082 m^3 Composite Overwrapped Pressure Vessel (COPV) tank. The latter is surrounded by a metal shell to allow dimensional changes of the COPV as the internal pressure decreases. The selection of Helium as pressurant was driven by its greater stability and reduced density compared with Nitrogen. Indeed, this can greatly reduce the weight of the pressurisation system and increase the payload capacity, thereby

ensuring reliability and safety [17]. The leakage of high pressure Helium towards the propellant tank is prevented by two redundant Pyrovalves (PVs) that are kept closed during ground operations until launch and are opened to perform the required maneuvers by on-orbit spacecraft commands. It has to be noted that COPV and PVs are a source of particulate contaminants too. To filter out these particles, a High-pressure Gas Filter (HGF) is located downstream of the pressurant Helium tank. Lastly, also five fill and drain valves (GFDP, GFDR, GFDT, LFDB, LFDT) were included for ground testing and loading of pressurant and propellant before launch.

5.1.4 Integration of the Propulsion Unit

The propulsion system was designed as a separate module [13], thus allowing an independent assembly and proof testing, granting also a simplified electrical-mechanical interfacing. As it can be seen from Figure 5, the two propellant tanks are integrated one over the other at the centre of the spacecraft's aft deck. This was done to have the propulsion system as compact as possible, while reducing the effects of the propellant on the inertia proprieties of the orbiter. Eventually, the COPV is mounted above the top propellant tank on a truss support structure, which is offset from the center of the tank. On the outside surface of the cylindrical structure surrounding the tanks are assembled and welded together the component panels, as shown in Figure 5. These include: a low-pressure panel containing the tank and manifold latch valves; a high-pressure panel with the regulator, high pressure latch valve, PVs and gas filter; two filter panels.

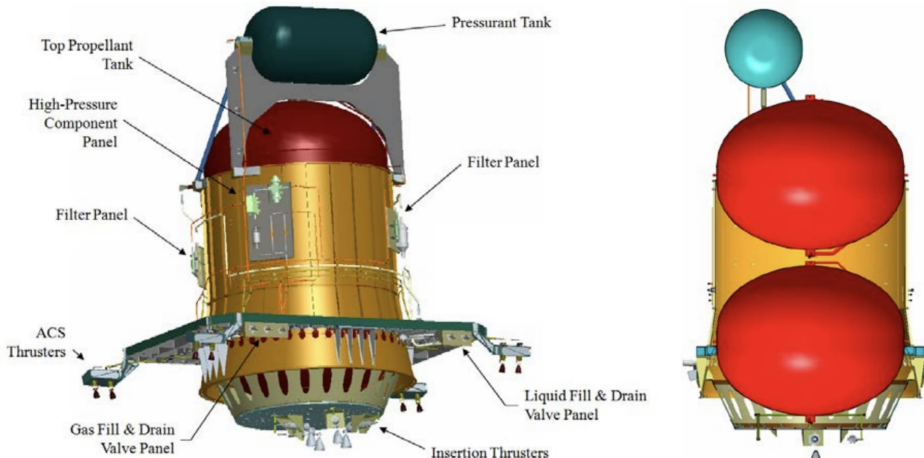


Figure 5: LRO's Propulsion System physical layout (source: [13])

5.2 Propulsion System Configurations

The various configurations of thrusters used for each manoeuvre are listed in Table 12.

Manoeuvre	Thruster Configuration (NT x AT)	Mode
MCCs	0 x 4	blow-down
LOI-E + LOI-1	4 x 8	press. regul.
LOI-2 to LOI-5	2 x 8	press. regul.
MOIs	2 x 8	press. regul.
SKs	2 x 8	press. regul.

Table 12: Thruster configurations (source: [10])

As shown in this table, at the very beginning of the mission, a blow-down strategy was employed to perform the MCC manoeuvres. Indeed, during the transfer to the Moon, the PVs had not yet been opened, in order to avoid an over-pressure due to thermal effects [13]. Subsequently, in preparation for LOI manoeuvres, the PV1 was opened, thus switching to a pressure regulated system. Since the MCC were considered as margins during the computation of the Δv and given that the mass allocated for these manoeuvres is minor with respect to the whole mission, the blow-down strategy was not modelled. In fact, as will be showed in Section 5.3, the whole Δv budget is used to size a pressure regulated system.

5.3 System Preliminary Sizing

5.3.1 Mass Budget Retrieval

In order to retrieve the preliminary sizes of the propulsion system, the dry mass of the LRO was set to 1018 kg [1][18]. The mass budget was then computed by applying Tsiolkovsky Rocket equation and the results are reported in Table 13. In more detail, as a first step, the mass ratio was retrieved, since the Δv breakdown was known from the Mission Analysis, while the specific impulse provided by the thrusters for each manoeuvre could be quantified as 225 s for the LOI and MOI manoeuvres and as 224 s for the others [10]. Assuming then a 20% margin over the dry mass, according to ESA *R-M1-1* [19], the initial mass of the LRO was found, thus allowing to compute the wet mass. Note that an additional propellant margin was accounted as 5.5% of Hydrazine mass, subdivided as follows: a 3% of ullage margin, a 2% accounting for residuals² and a 0.5% for loading uncertainties.

Mission Plan	Δv [m/s]		m_{prop} [kg]	
	computed	actual	computed	actual
LOI-1	568.0	555.5	477.5	444.9
LOI-2 and LOI-3	219.1	201.5	153.7	
LOI-4	91.0	113.2	59.5	227.1
LOI-5	40.1	37.4	25.4	
MOI	41.1	40.2	25.6	28.7
SK (1 year)	162.0	162.0	96.8	84.1
Extra Manoeuvres	n/a	n/a	n/a	50.5
Partial Total	1121.3	1109.8	838.5	835.4
Launch Correction	30.0	30.0	17.2	26.4
Deterministic Margin	48.0	n/a	27.0	20.9
Extra Margin	n/a	n/a	48.5	12.0
Corrected Total	1199.3	1139.8	931.2	894.7

Table 13: Comparison between computed and actual N_2H_4 masses, from the corresponding Δv . m_{prop} are retrieved from [13] and the “Extra margin” accounts for ullage, residuals and loading uncertainty. “Extra manouevres” include momentum unloading and extended mission. Δv are retrieved from [9] and [10] and the additional 30+48 m/s comes from margin standards.

²as stated by ESA margin *R-M1-6* [19]

5.3.2 Pressure Cascade

A critical aspect in the PS design is the evaluation of the pressure cascade. The nominal chamber pressure (p_c) was quantified as 1.3 MPa, according to the ranges of operative pressures of ATs and NTs reported in Table 11. The pressure drop across the injectors (Δp_{inj}) was then estimated as 30% of p_c , while the one across the feeding line (Δp_{feed}) in the order of 50 kPa. The dynamic pressure drop (Δp_{dyn}) was instead obtained³ by assuming a velocity of 10 m/s inside the feeding lines and by knowing the density of N₂H₄. Eventually, from these values, it was possible to compute the pressure inside the N₂H₄ tanks as the sum of all pressure drops plus the nominal chamber pressure, as reported in Equation 1.

$$p_{tank} = p_c + \Delta p_{inj} + \Delta p_{feed} + \Delta p_{dyn} \quad (1)$$

5.3.3 Propellant Tanks

From the knowledge of the total propellant mass and density, the total volume was retrieved, as showed in Equation 2. An additional 10% margin was then taken, according to ESA *R-M1-10* margin [19].

$$V_{prop} = 1.1 \cdot \frac{m_{prop}}{\rho_{prop}} \quad (2)$$

Since the LRO is equipped with two pre-existing identical tanks, the estimated volume of each one was compared with the value found on the data-sheet of the producer [20]. Then, by knowing the N₂H₄ tank pressure, the Titanium properties⁴ and assuming a spherical geometry⁵, the tank radius and thickness were computed, using Equations 3.

$$V_{tank} = \frac{V_{prop}}{2}; \quad r_{tank} = \sqrt[3]{\frac{3}{4} \frac{V_{tank}}{\pi}}; \quad \delta_{tank} = \frac{p_{tank} r_{tank}}{2 \sigma_{y,tank}} \quad (3)$$

Eventually, the total mass of each tank was obtained, as reported in Table 14.

N ₂ H ₄ Tank Sizes (1 tank)		computed	from data [13]
Pressure	[MPa]	1.740	1.875
Volume	[m ³]	0.508	0.461
Thickness	[mm]	0.453	n/a
Dry Mass	[kg]	3.89	n/a

Table 14: Propellant Tank Sizing (values for one tank)

It has to be pointed out that the evaluated δ_{tank} and m_{tank} are the minimum values required to withstand the operative pressure of 1.740 MPa. Whereas, from the data-sheet of the producer [20] the declared mass of 35.4 kg takes into account a higher proof pressure rating, of around 2.019 MPa, and a suitable margin.

5.3.4 Pressurisation System

To size the pressurisation system, the storage temperature of Helium was set to 25 °C, while its initial pressure to be 14.3 times the pressure in the combustion chamber [13] and the final one was considered equal to the one of the propellant tanks. Hence, the pressurant mass was computed, according to [21], from the conservation of energy, and the volume from the ideal gas law, as reported in Equation 4.

$$m_{press} = 1.2 \cdot \frac{p_{tank} V_{prop}}{\mathfrak{R}_{press} T_{press}} \cdot \frac{\gamma_{press}}{1 - \frac{p_{press,f}}{p_{press,0}}}; \quad V_{press} = \frac{m_{press} \mathfrak{R}_{press} T_{press}}{p_{press,0}} \quad (4)$$

³ $\Delta p_{dyn} = \frac{1}{2} \rho_{prop} v^2$

⁴density of 2780 kg/m³ and yield strength of 950 MPa

⁵note that this assumption is reasonable since the actual tanks are slightly oblate spheroids

However, this time it was not possible to perform an analysis on the thickness, as previously done for the Hydrazine tanks, due to the peculiar characteristics of the tank material. In fact, these are in composite and are covered with a metal shield, as described in Section 5.1.3. All the results are reported in Table 15.

Helium Tank Sizes (1 tank)		computed	from data [13]
Initial Pressure	[MPa]	24.888	26.738
Helium Mass	[kg]	6.15	3.3
Volume	[m ³]	0.153	0.081

Table 15: Helium Tank Sizing

5.3.5 Modelling Considerations

It can be noted from the previous tables that some estimated measures are slightly different from the actual ones. Since the approach for the thickness selection gives the minimum admissible value to achieve the desired function, a safety margin and manufacturing capabilities shall be considered to refine the estimation of the tanks' masses. Instead, the total propellant mass (Table 13) was over-estimated of about 4%. This was because of the Δv budget retrieval, which slightly differs from the actual mission data. In addition, also higher margins have been considered with respect to the one of the actual mission⁶.

Then, as shown in Table 15, the preliminary design of the pressurising subsystem results to be oversized. The blow-down strategy was not included in the numerical modelling since the allocated mass for the MCCs is minor with respect to the whole mission; thus, the modelled pressure-fed system has to manage those additional manoeuvres. The main effect on the volumes, when a blow-down is considered, is that at the beginning of the pressure fed phase the propellant tanks already contain a fraction of helium.

Moreover, a possible degradation of performances at End Of Life (EOL) was not taken into account. In fact, the system could in principle be used in blow-down also once the Helium reaches the propellant tanks pressure, as shown in Figure 6. This can explain the reason why the estimated pressurant mass in the helium tank is greater. For the same reason, the retrieved volumes of N₂H₄ tanks are the same as the installed ones, despite an additional mass of propellant at a slightly lower pressure. In addition to this, mild deviations in tank pressures and temperatures could also be the cause of propellant masses and volumes over-estimation.

Lastly, a cause of the differences between estimated and real data could be related to the formulation of the models used. Particularly, Equation 4 holds as long as the storage pressures are not too high, as stated in [21].

5.4 System Review

Aside from the preliminary sizing, a remarkable fact is that the LRO's propulsion system design met all the needs of the mission. Additionally, it accommodated as much existing hardware as possible

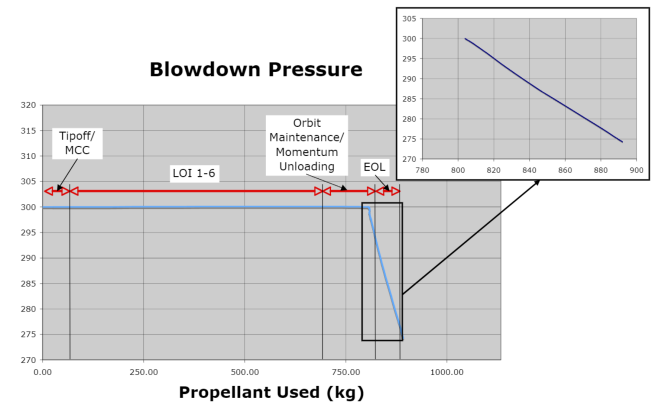


Figure 6: PS operating pressure (source: [14])

⁶especially the 20% applied to the dry mass, according to ESA R-M1-6 [19]

and was extremely fault-tolerant, given its design and high level of redundancy.

To summarise, the main choices and features that led to definition of its architecture are:

- The chemical propulsion system was designed in order to achieve the high Δv needed by the mission, thus answering one of the mission drivers.
- The use of Hydrazine simplified the system and increased its reliability with respect to a bi-propellant architecture, which is slightly more efficient but also more complex.
- The possibility of re-using existing propellant tanks, with a very high Technology Readiness Level (TRL), strongly reduced the cost and the development time, thus answering one of the mission drivers.
- A pressure regulated feeding strategy was selected to achieve a constant thrust level along all the mission, with the possibility of a short blow-down to compensate thermal effects during the Lunar transfer phase.
- Helium was chosen as pressurising gas thanks to its great stability and low density. Hence, it allowed to reduce the weight of the pressurisation system and possibly increase the payload.
- The stacked tank structure and flow control components are closely surrounded by the spacecraft structure and other spacecraft components, resulting in a very compact spacecraft configuration.
- An independent assembly and proof testing, which simplified also the electrical and mechanical interfacing, was made possible by having designed the system as a separated module. This was then placed at the centre of the spacecraft's aft deck to reduce the effects of the propellant on the inertia properties of the orbiter.
- To match the need of both SK and insertion manoeuvres, different thrusters (in terms of number and provided thrust) was employed. The ATs, used for SK and 3-axis attitude control, are located at the four corners of the spacecraft's aft face and are tilted of 15° towards the symmetry axis of the spacecraft, increasing the thrusters' moment arm about the centre of mass. Instead, the NTs, included in the system to provide high thrust during orbit insertion manoeuvres, are positioned in a diamond configuration on the same face and arranged to minimise the torsional motion generated during those manoeuvres.

6 Tracking, Telemetry and Telecommand System

The Tracking, Telemetry and Telecommand (TTMTC) system of LRO had to grant the transmission of scientific data to the ground and the exchange of telemetry to provide tracking and receive commands, needed by the LRO science and measurements. Hence, it satisfied several functionalities, more specifically FUN-05, FUN-07.05 and FUN-06.04.

6.1 Operational Scenario

Since the very preliminary phases, multiple Ground Stations (GSs) supported the communications with the LRO, in particular, the NASA Space Network, the Deep Space Network (DSN), and commercial S-band stations, in addition to White Sands 1 - Ground Station Antenna (WS1). Once the spacecraft safely reached its lunar orbit, primary support was achieved through WS1 and commercial S-band stations, with the DSN available for contingency support [22].

Several aspects had to be taken into account when LRO's TTMTC system was initially designed to provide the desired performances in the commissioning and nominal orbits.

Depending on the relative orientation between Earth and the LRO's orbital plane, the visibility periods of the spacecraft vary from continuous (when the Earth-Moon line is perpendicular to the orbital plane, which happens twice a month) to alternating visibility intervals. Moreover, temporary phenomena of interference may happen during the period in which the Sun is closer to the Moon, meaning that communications are no longer possible due to the intensity of solar radiation. In addition, specific instruments like the LROC and Mini-RF required daily tailored command timelines, like tracking schedules and antenna targets, in contrast to most of the other scientific instruments which operate autonomously over the course of a single orbit.

For what concerns the LRO data volume, as reported in Table 41 in the Appendix, during the operative phase about 462 Gbits of data were generated on-board the LRO every day. The majority of this data volume came from the scientific instruments (especially by the LROC, dedicated to capturing high resolution images) and therefore a high data down-link rate was required to guarantee its transmission to Earth. With this purpose, a Ka-band system was chosen for the high-speed transfers of telemetry and science data. In particular, this system had an on-orbit selectable return link, which ranged between 25 Mbps and 100 Mbps, and a signal frequency of about 25.6 GHz.

On the other hand, in order to transmit the data for tracking, telemetry, House-Keeping (HK) and command, an S-band system was implemented since a lower data rate was sufficient to fulfill these LRO demands. This frequency range was used both in up-link and down-link transfers, with a forward link data-rate of 4 kbps and a selectable return link data-rate between 125 bps and 1093 kbps [1].

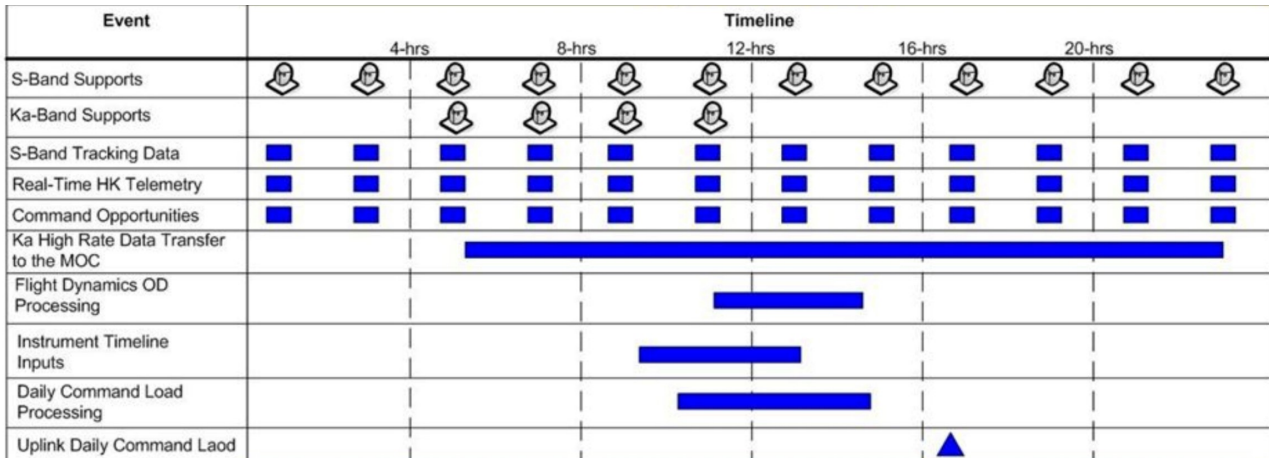


Figure 7: LRO's contacts with ground stations (source: [6])

It must be noted that the large amount of data collected from the scientific payload had to be down-linked toward a single Ka-band ground station, that is the WS1, described in Section 6.2. As reported

in Figure 7, 4 passes between the LRO and WS1 were guaranteed on average every day, each one lasting from a minimum of 45 min to a maximum of 56 min; the latter, independently from the visibility periods, is related to mechanical limitations on the pointing range of the High Gain Antenna (HGA). In reality, the actual number of passes fluctuated between 2 and 6, as the Moon moved through its entire declination range each month, but, even in the worst case, the amount of time available was enough to transfer the entire data volume collected in a single day. Particularly, Table 42 in the Appendix shows how each visibility window could be used in order to optimise the on-board memory usage per single day. Thanks to the specific orbit design, combined with an accurate selection of the most suitable S-band GSs, in a single day 12 S-band passes were guaranteed: one for each orbit and with a minimum duration of 30 minutes.

6.2 Ground Stations

To support the high data-rate as well as the high accuracy ranging, the telemetry and command requested, the WS1 was constructed at NASA White Sands Complex near Las Cruces, New Mexico (USA). This location was chosen because of its wide-open area and for the low humidity and precipitation presence, which are beneficial for the RF waves. The WS1 is a dual axis (azimuth/elevation) Cassegrain parabolic reflecting antenna, used for simultaneous transmission in S-band and reception in S-band and Ka-bands. Its main features are reported in Appendix in Table 43.

In addition to the WS1 antenna, four S-band-only stations, located worldwide, were selected in order to provide the minimum S-band coverage time of 30 minutes per orbit, as stated in Section 6.1. The selection of these antennas was based on S-band capabilities, the viewing coverage of the Moon and their availability. Eventually, the ground stations of Dongara (Australia), Kiruna (Sweden), Weilham (Germany) and South Point (Hawaii), that was also part of the commercial network Universal Space Network (USN), were chosen.

During nominal operations the ground support to LRO was provided by all the antennas previously mentioned, while in critical situations that are launch, early trajectory and in contingency operations, the DSN support was also used to communicate with the spacecraft, thanks to its peculiar properties such as the high Effective Isotropic Radiated Power (EIRP).

6.3 System Architecture

A schematic representation of the TTMT system architecture is shown in Figure 8. The main components of this system are:

- One High Gain Antenna (HGA): this parabolic antenna was chosen to transmit the scientific data, since its high gain allowed to direct a large amount of power to a specific target that is a GS on Earth. In addition, since a very accurate orientation for the antenna was needed, and given the almost continuous nadir-pointing operations, an articulated mechanism⁷ was required. This led to the selection of a deployable arm, folded during launch phase, on top of which the antenna dish was mounted.

The correct pointing of the main dish was guaranteed by two gimbals driven by two electric motors. Each of the two gimbals had a 180° range of motion, from -90° to 90° . This “working envelope” imposed mechanical limitations on the antenna pointing, which entailed a constraint for the visibility windows, as described in Section 6.1.

To guarantee the pointing toward the Earth, this has been integrated on the opposite side with respect to the face that points towards the lunar surface (nadir direction).

- Two Omni-Directional Antennas (ODAs): these were likely chosen to guarantee a contact with Earth while the HGA was not yet deployed and whenever the attitude of the spacecraft was unknown, but also in the case of a failure of one of the two HGA gimbal motors. Note that these two antennas have a low gain and are theoretically isoentropic radiators: therefore, the

⁷Indeed, this system allowed to de-couple the attitude of the LRO from the antenna pointing.

transmitted and received power are mild. These two antennas have been integrated in such a way to not have their field of view limited by the on-board instruments and sensors.

- One transponder: this component was integrated into the S-band system to determine the LRO in-orbit position and its distance from Earth.
- A Traveling Wave Tube Amplifier (TWTA): it consists of a Traveling Wave Tube (TWT), a Electronic Power Conditioner (EPC) and a High Power Insulator. It allows to amplify the Ka-band signal with a power of 40 W and a higher efficiency than a solid-state amplifier.
- Two modulators: the Ka-band modulator implemented a Offset Quadrature Phase Shift Keying (OQPSK) technique, which offers a good usage of the spectrum at the cost of being susceptible to phase disturbances. On the other hand, the Bi-Phase Shift Keying (BPSK) technique was used for the S-band communication to guarantee an excellent BER performance and to allow a reduced use of the spectrum, at the expense of a slightly more complex system.

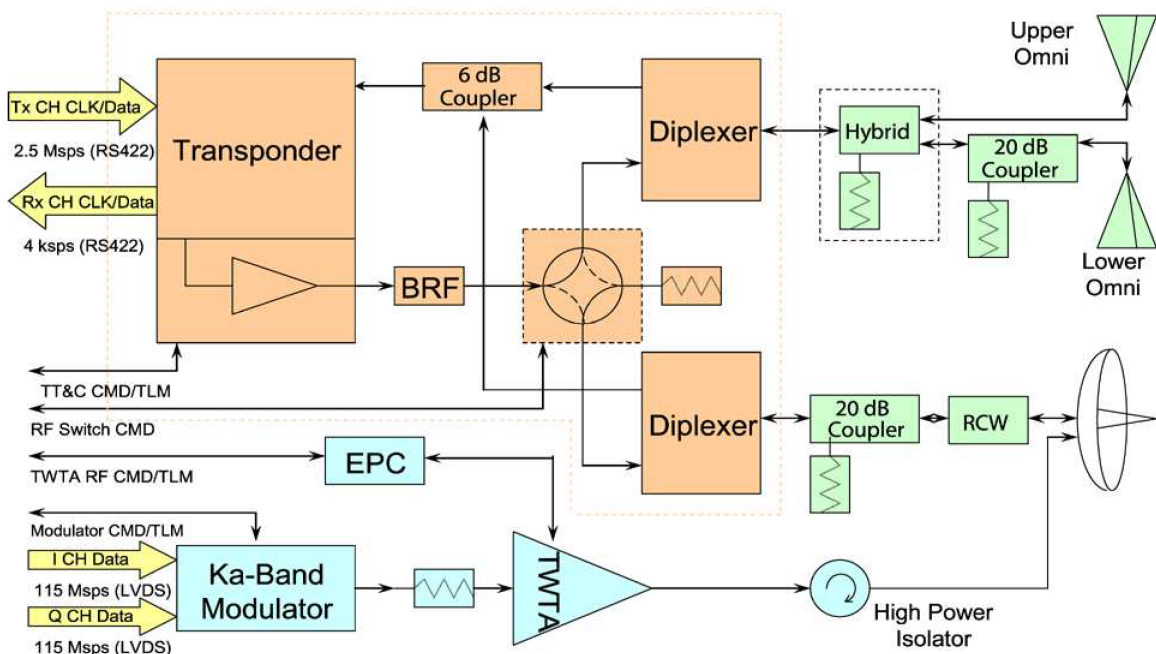


Figure 8: LRO communications system block diagram

The main characteristics of the antennas used to communicate with LRO are reported in Table 16; more information on the WS1 antenna are available in Table 43, reported in the Appendix.

Antenna	G [dBi]	d [m]	μ_{re}
HGA	44	0.75	0.55
ODA	1.64	n/a	n/a
WS1 GS	n/a	18.3	0.55

Table 16: Data for the antennas used in LRO communications ([21], [23])

Although the Ka-band system exploited only HGA to transmit the data toward ground, the S-band system could use either the ODAs or the HGA for the down-link transmission and always both antennas for receiving. For this reason, the two different antennas have an opposite polarisation, as reported in Table 17, thus allowing the selection of the up-link path from ground.

Parameter	S-Band System	Ka-Band System
Frequency (TX)	2271.2 ± 2.5 MHz	25.65 GHz ± 150 MHz
Frequency (RX)	2091.3967 ± 2.5 MHz	n/a
Polarisation	LHCP (Omni), RHCP (HGA)	LHCP (HGA)
RF TX Power	5.8 W (Diplexers)	41.9 W (TWTA Output)
Data Rate (TX)	from 125 bps to 1093 kbps	100 Mbps
Data Rate (RX)	4 kbps	n/a

Table 17: TTMT system characteristics (source: [1])

6.3.1 LRO Tracking - the Laser Ranging Subsystem

In order to improve the precision of orbit determination and tracking, as well as the accuracy of the measurements made by the instruments, a Laser Ranging (LR) system was implemented on-board. The LR makes one-way (up-link) range measurements of the laser pulse's time-of-flight from Earth to LRO, thus allowing to determine the position of the orbiter at sub-meter level. To transmit the laser pulse from Earth to the orbiter, an additional GS was used, that is the NASA's Next Generation Satellite Laser Ranging (NGSLR), located at Goddard Space Flight Center in Greenbelt (Maryland). The pulse is captured by the LRO through a Laser Ranging Telescope (LRT) mounted on the HGA and then is transmitted, through a fiber optic cable, to the detector assembly located within LOLA. This data, combined with the position of the spacecraft and LOLA data, allowed to improve the used lunar gravity model, which in turn helped to enhance the orbit determination. [1]

6.4 System Preliminary Sizing

In this section, a preliminary sizing of the TTMT subsystem will be performed: both down- and up-link communications will be considered, with the distinction between the S- and Ka-band cases. The considered GS was the WS1, as it represented the most used for both S-band and Ka-band communications.

6.4.1 Link Budget and SNR

To ensure that the receiver is capable of translating a signal (i.e. distinguishing it from noise) Equation 5 must be verified.

$$\frac{E_b}{N_0} > \left(\frac{E_b}{N_0} \right)_{min} + 3 \text{ dB} \quad (5)$$

This indicates that the actual E_b/N_0 value, obtainable by exploiting the link budget equation⁸ (6), must have a margin of at least 3 dB with respect to a certain $E_b/N_0|_{min}$, selected according to the chosen modulation, encoding techniques and Bit Error Rate (BER).

$$\frac{E_b}{N_0} = P_{RX} - 10 \log_{10} (N_0 R), \quad \text{where: } N_0 = k \cdot T_{noise} \quad (6)$$

$$P_{RX} = \text{EIRP} + G_{RX} + L_{atm} + L_{point} + L_{space}; \quad \text{where EIRP} = P_{TX} + G_{TX} + L_{cable}$$

As shown in Equation 6, in order to retrieve the received power P_{RX} , the antenna gains and the losses along the signal path are needed. The gains were either calculated using Equation 7 or retrieved by Table 16, while space and pointing losses were estimated using Equations 8. The atmospheric losses were then selected according to [21] (Fig.13.10 p.564), while the cable losses were set at -1 dB according to values used for similar applications.

$$G = 10 \log_{10} \frac{\pi^2 d_{RX}^2 \mu_{re}}{\lambda^2} \quad (7)$$

⁸note that in Equation 6 all terms are expressed in dB

$$L_{space} = 20 \log_{10} \left(\frac{\lambda}{4\pi r} \right); \quad L_{point} = -12 \left(\frac{\eta}{\theta_{RX}} \right), \quad \text{where: } \theta_{RX} = \frac{65.3 \cdot \lambda}{d_{RX}} \quad (8)$$

Results for the expected losses in both down-link and up-link are reported in Table 18.

	Atmosphere [dB]		Pointing [dB]		Free Space [dB]	
	Downlink	Uplink	Downlink	Uplink	Downlink	Uplink
Ka-band	-0.60	n/a	-0.6899	n/a	-232.910	n/a
S-band	-0.04	-0.04	-0.0050	~0	-211.853	-211.137

Table 18: Expected losses in both down-link and up-link (if applicable).

In a similar way to the procedure adopted before, to ensure that the receiver is capable of tracking the signal and distinguishing it from noise, Equation 9 must be verified.

$$\text{SNR}_{carrier} > \text{SNR}_{min} + 3 \text{ dB} \quad (9)$$

Here, the SNR_{min} was set to 10 dB (typical value for the DSN), while the $\text{SNR}_{carrier}$ was computed using Equations 10 once the data-rate and both the encoding and modulation coefficients⁹ were known.

$$B = R \frac{\alpha_{enc}}{\alpha_{mod}} \quad (10)$$

$$\text{SNR}_{carrier} = P_{carrier} - 10 \log_{10} (k \cdot T_{noise} \cdot B) \quad \text{where: } P_{carrier} = P_{RX} + 20 \log_{10}(\cos \beta_{mod})$$

The GS noise temperature for down-link transmissions (T_{noise}) was set to 21 K in order to match the G/T_{noise} value provided by [22], where the gain of the antenna was computed through Equation 7. On the other hand, the noise temperature for up-link transmissions was set to 614 K according to the general table presented in [21] (Tab.13-13 p.567). In addition, the modulation index β_{mod} was set, according to typical values, to 78° for every case except the down-link in S-band with ODA, where a value of 60° was chosen. Indeed, β_{mod} parameter strongly affects the Signal to Noise Ratio (SNR): lower values of it help improve the quality of the transmission.

6.4.2 Down-link in Ka-band with HGA (Scientific Data Transmission)

For the preliminary design of the link, the required BER was set to 10^{-5} , which is a typical value for down-link transmissions according to [21]. As a consequence, the $E_b/N_0|_{min}$ was retrieved to be 4.2 dB. A $P_{TX} = 16.22$ dBW was then considered, as well as a maximum data rate $R = 100$ Mbps and a corresponding bandwidth $B = 114.35$ MHz, according to Equation 10. Finally, G_{TX} was set to 44 dBi (see Table 16), while G_{RX} was calculated to be 71.24 dBi using Equation 7.

Substituting these values in the equations reported in Section 6.4.1, the results reported in Table 19 were obtained.

E_b/N_0 [dB]	$P_{carrier}$ [dB]	SNR [dB]	P_{RX} [dB]
31.64	-117.38	17.42	-103.74

Table 19: Down-link in Ka-band with HGA - results

It can be noted that both E_b/N_0 and SNR are respectful of the 3 dB margin with respect to their minimum acceptable value.

6.4.3 Down-link in S-band with HGA

In this case, the required BER was again set to 10^{-5} , which resulted in the same $E_b/N_0|_{min}$ value as before. A $P_{TX} = 7.63$ dBW was then considered (see Table 17), as well as a data rate $R = 32$ kbps

⁹ α_{mod} is equal to 2 when using QPSK modulation, while equal to 1 when using BPSK

and a corresponding bandwidth $B = 73.18 \text{ kHz}$, according to Equation 10. Finally, using Equation 7, G_{TX} and G_{RX} were calculated to be 22.43 dBi and 50.18 dBi respectively.

Substituting these values in the equations reported in Section 6.4.1, the results in Table 20 were obtained.

E_b/N_0 [dB]	$P_{carrier}$ [dB]	SNR [dB]	P_{RX} [dB]
37.68	-140.12	26.61	-132.64

Table 20: Down-link in S-band with HGA - results

Again, both E_b/N_0 and SNR are respectful of the 3 dB margin with respect to their minimum acceptable value.

6.4.4 Down-link in S-band with ODA

S-band communications with ODAs were the most onerous part of the TTMTTC subsystem to size due to the lack of data for the antennas. As reported in Section 6.1, the system can transmit with a selectable data rate within a wide interval. For this purpose, the highest value of E_b/N_0 was firstly considered in order to analyze the most conservative case. At such data rate, both the link budget and SNR resulted to be deeply below their lower limits. Hence, the nominal value for real time HK data transmission of 16 kbps was considered, which resulted in a bandwidth $B = 36.59 \text{ kHz}$. Then, G_{TX} was set to 1.64 dBi according to the value reported in Table 16. Using all these values and G_{RX} and P_{TX} from the previous paragraph, the results in Table 21 were obtained. Note also that in this case the modulation index β_{mod} was set to 60° for normal down-link data rate.

E_b/N_0 [dB]	$P_{carrier}$ [dB]	SNR [dB]	P_{RX} [dB]
19.90	-159.46	10.28	-153.44

Table 21: Down-link in S-band with ODA - results

As it can be seen, E_b/N_0 is way above the imposed minimum value of $(4.2 + 3)$ dB, while the same can't be said for the SNR: indeed, the obtained value is only 0.28 dB above the minimum value, thus not respecting the 3 dB margin.

6.4.5 Up-link in S-band with HGA

Earth to spacecraft communications were possible only in S-band at a frequency of $f = 2091.4 \text{ Hz}$ and at a fixed data rate $R = 4 \text{ kbps}$ to both the two kind of antennas. The selection of the HGA as the receiver was done through signal polarization, using RHCP, as reported in Table 17. As before, the GS antenna considered was the WS1, which had an S-band EIRP of 79 dBW [22], value that was directly inserted into Equation 6 since the P_{TX} was not available from literature. Then, since we're dealing with the S-band, the G_{RX} was calculated to be 22.44 dBi. A BER of 10^{-7} was finally selected, as it is a typical value for up-link communications according to [21] (Tab.13-13 p.567), resulting in a value of $E_b/N_0|_{min} = 5 \text{ dB}$. Using all the previous data, the results are those in Table 22.

E_b/N_0 [dB]	$P_{carrier}$ [dB]	SNR [dB]	P_{RX} [dB]
54.96	-123.38	37.72	-109.74

Table 22: Up-link in S-band with HGA - results

It can be noted that both E_b/N_0 and SNR are respectful of the 3 dB margin with respect to their minimum acceptable value.

6.4.6 Up-link in S-band with ODA

Repeating the same procedure as the previous paragraph, but now imposing $G_{RX} = 1.64$ dBi since we're dealing with the ODA, the results in Table 23 were obtained.

E_b/N_0 [dB]	$P_{carrier}$ [dB]	SNR [dB]	P_{RX} [dB]
34.16	-144.18	16.93	-130.54

Table 23: Up-link in S-band with ODA

It can be noted that the performances are lower using ODAs with respect to the previous case, due to the lower gain of the receiver. However, both E_b/N_0 and SNR respect the imposed margin with respect to their minimum acceptable value.

6.4.7 Sizing Considerations

The preliminary sizing of the subsystem may exhibit some poor results, particularly in terms of the SNR. Specifically, high data rate down-link transmissions in S-band frequency resulted to be the most problematic, while in up-link good performances were guaranteed by the GS. A cause of the former issue may be addressed to the total lack of data for the ODAs, whose gain and beamwidth were assumed from general tables. But also, as confirmed by literature, it has to be noted that ODAs were mostly used for low data rate transmissions and in emergency situations.

Moreover, the whole sizing was performed for a worst case scenario in order to be as conservative as possible. These conditions should occur rarely, thus the spacecraft may be designed to avoid transmitting with a high data rate in these situations. Beside all previous considerations, LRO TTMTTC system resulted to be capable of communicating the scientific data, also with a consistent margin with respect to the available time windows.

6.5 System Review

To sum up, the TTMTTC system was capable of transferring rather high amount of data in short periods with good margins, keeping information losses sufficiently below the required limits. The primary choices and features that led to definition of TTMTTC architecture are:

- The use of S-band for its efficiency as a conduit for real-time data and its high resilience to rain fade and other environmental interferences.
- The use of Ka-band for its capability to perform high-speed transfers of data.
- Convolutional and Reed-Solomon encoding were exploited due to their simplicity of implementation and reliability.
- OQPSK modulation for Ka-band optimised the use of the spectrum, enhancing the data rate, while BPSK modulation for S-band guaranteed an excellent BER with a reduced use of the spectrum.
- An HGA was chosen to transmit remarkable amount of data directing a large amount of power toward a specific target, while ODAs were necessary to guarantee a contact with Earth when out of range of the HGA.
- Two gimbals were built to guarantee an accurate orientation for the HGA despite the continuous nadir-pointing direction of the LRO.

7 Attitude and Orbit Control System

The LRO includes a wide selection of sensors and actuators to ensure the desired pointing accuracy throughout its mission profile. The control architecture ruling their employment is set by defining a series of modes to cover the whole mission duration. In particular, this system satisfies functionalities FUN-04.05, FUN-07.02 and FUN-09.02. The upper limit of the pointing accuracy required during the mission lifetime is about $60''$ per axis, while the knowledge error must be less than $30''$ [14].

7.1 System Architecture

7.1.1 Sensors

The LRO's AOCS consisted of the following sensors:

- 10 Coarse Sun Sensors (CSSs) to provide a first measurement of the location of the Sun in the Body frame of the spacecraft. They were manufactured by Adcole (now Redwire Space). The main advantages of these sensors are in their small dimensions and low cost [24]. The CSSs are placed on the solar panel, to provide its correct orientation towards the Sun, and on the corners of the spacecraft, to guarantee the measurement of at least 3 sensors to estimate the Sun relative position.
- 2 A-STR developed by Officine Galileo, which are capable of a robust and accurate 3-axis attitude determination in their reference frame with respect to the J2000 Earth Centered Inertial (ECI) with quaternion representation. If required, the processing of the A-STR output can provide the attitude rates, especially whenever the Inertial Measurement Unit (IMU) is unavailable; this ensures a high redundancy level for the system. The A-STR are aligned 60° apart to provide a measure even when one of the two is occulted by Earth, Sun or the Moon [24][25]. To minimise their exposure to high energy sources like the Sun or the Earth, the sensors are placed on the Instrument Module, the opposite side with respect to the solar panel, pointing outwards.
- 1 Honeywell Miniature Inertial Measurement Unit (MIMU) configured as IMU since three accelerometers are not included. 3 Ring Laser Gyroscopes (RLGs) with mutually orthogonal axes provide accurate rate measurements given their low noise and drift. Its values are used to propagate the attitude when A-STRs are updating, when the Kalman-filter is not active or if the quaternion data is not valid [25]. To increase accuracy and stability, the IMU is mounted on the LRO Avionics Panel: this face is the one to which the solar array is attached to and which is the closest to the centre of mass.

Sensor	Power [W]	Mass [kg]	qty	Performances
A-STR	11.2	4.2	2	accuracy of $20'', 90''$ about boresight, 16° of FOV
IMU	25.0	4.5	1	accuracy of $0.2''$, resolution up to $375^\circ/\text{s}$, 100 ppm linearity, 5 ppm stability
CSS	0	0.011	10	accuracy of 0.75° , 175° of FOV

Table 24: ACS sensors characteristics (sources: [1], [26])

7.1.2 Actuators

LRO is equipped with 4 RWs to provide control torque, manufactured directly at NASA/GSFC by the Component Hardware Systems Branch. They are arranged in a pyramid configuration (with the apex aligned with the $+X$ body axes of the spacecraft) and attached to the Avionics Panel to provide

very quiet, smooth changes in pointing of the spacecraft thanks to the proximity of the centre of mass. The geometry is driven by the momentum accumulation that is minimised with this solution so that desaturation manoeuvres can be done biweekly; ATs are the ones responsible for the latter. The system is designed with high redundancy: the desired control torque can be provided even in case of a single RW failure. However, in this unlikely situation, the interval between momentum unloading operations is reduced. [25]

In addition, LRO is equipped with 8 ACS Thrusters (ATs), these are used for SK and for 3-axis attitude control during momentum unloading operations. The ATs are located at the four corners of the spacecraft's aft face and are tilted of 15° towards the symmetry axis of the spacecraft, increasing the thrusters' momentum arm about the centre of mass. Lastly, 4 NT are used to provide Δv changes in order to follow the desired trajectory.

Actuator	Power [W]	Mass [kg]	qty	Performances
RW	16.6	11.9	4	$\Gamma_{max} = 80 \text{ Nms}$, $\Gamma_{max,nom} = 60 \text{ Nms}$, $M_{RW,max} = 0.16 \text{ Nm}$
AT	36.16	0.59	8	Thrust = 22 N, $I_{sp} = 224 \text{ s}$

Table 25: ACS actuators characteristics (sources: [1], [25], [16])

7.2 LRO primary modes

Throughout the entire mission lifetime, multiple control modes were adopted to ensure the desired orientation of the spacecraft [1]. These are:

- **Sun Safe:** is the spacecraft safe hold control mode and it exploits the CSSs to retrieve the Sun vector used for the initial attitude acquisition. This mode uses also the IMU and provides attitude control through RWs. Its main function is to retrieve the initial attitude and to provide Sun pointing in case of an anomaly onboard, without limitations on mode duration. Moreover, if a Sun vector is given from ground the Sun Safe mode is capable of keeping that attitude with a full sky reorientation if needed. In the event of an IMU failure, this mode uses only the data from CSSs, thus loosing control over the Sun-line but still being capable of providing an attitude. During eclipses, instead, an open loop control is provided, leaving the spacecraft free to rotate until Sun presence is detected again. In addition, the solar panels have a very specific configuration when entering this mode, since they are placed in the “default” position [1].

The Sun Safe mode was correctly activated immediately after separation from the LV to stabilise the spacecraft and place the LRO in a power positive orientation. During this period the deployables were extended. Two anomalous entries into Sun Safe mode were registered during the initial lifetime of the LRO. The first one happened during the initial transition into Observing Mode, caused by a lack of ephemerides data onboard, which ended up in a fault in attitude determination. The second one occurred during the first lunar orbit, after LOI-1, when both A-STR were occulted by the Moon for approximately 60 min. [25]

- **Observing:** is the primary Attitude Control mode and employs the A-STRs and IMU for attitude determination and the RWs for control. The two quaternions output of the A-STRs, combined with the spacecraft ephemerides [1] are processed by a six state Kalman filter to estimate the IMU bias and the inertial attitude of the spacecraft with a quaternion representation. A Proportional Integral Derivative (PID) control law is then used to provide the magnitude of the control actions required to the RWs. The attitude rate limits are set to $0.1^\circ/\text{s}$ to ensure wide margins over the momentum range that has a maximum of 80 Nms. This architecture provides a full-sky 3 axis attitude slewing and fine pointing both lunar nadir and off nadir. In addition, it is capable to point any given inertial target with fine pointing accuracy. Finally, this mode manages also the 2-axis gimbal of the SA and of the HGA.

The Observing Mode is activated during all nominal pointing and slew operations, calibration

activities included, and for attitude acquisition before activating Delta-V mode.

It was first engaged 5 min after the deployables were activated and the Sun Safe Mode had gathered an initial attitude and was the main responsible for the attitude determination and control in the commissioning and scientific phases, being able to keep the control error below the requirement of 15" and to provide an attitude accuracy of 30".

- **Delta-V:** is the mode designated for the manoeuvres that imply thrusters' firings. Since the accelerations, thus body rates, are high when the propulsion system is active, only the IMU measurements are included in the PID control. Indeed, A-STRs could lead to unreliable values. The thrusters torque command considered both the AT and NT with performances that depend on the event that the system was dealing with. This mode is used during cruise, MCC, LOIs and SK activities, with configuration of the ATs that is on-pulse for the sole LOIs, while for the rest is off-pulse. [1][24]
- **Delta-H:** is the mode responsible for RWs momentum unloading. The overall architecture is similar to the Delta-V mode, but some differences can be identified: the use of only the ATs and that the control law is only Proportional Derivative (PD). During this mode the ATs are used also to keep the attitude stability in place of the RWs. [1] and each RW has an actively constrained momentum level. The Delta-H Mode is performed whenever a targeted predicted momentum of 60 Nms is reached [27]: this is a conservative value with respect to the maximum allowable of 80 Nms. Once the momentum unloading operations end, the system returns to the previous mode that is either the Sun Safe or the Observing mode (generally the latter) [14]. Since the predictive models are over-conservative, the momentum unloading process is often triggered even before reaching 50 Nms. [27][24]

Figure 9 shows a flowchart briefly defining the control modes and the transition logic between them.

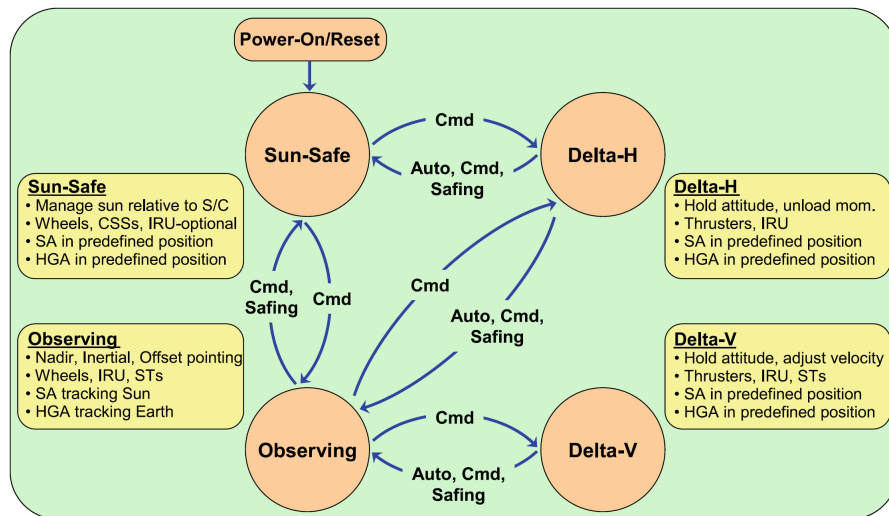


Figure 9: LRO control modes

7.3 AOCS preliminary sizing

7.3.1 Pointing Budgets and Instruments Selection

In order to retrieve the optimal choice in terms of sensors and actuators, all the control modes and their objectives shall be recalled; these are briefly summarised in Table 26.

Sun safe mode has to provide both an initial attitude and Sun pointing for an indefinite period of time while damping also all the body rates. For these reasons a coarse pointing is sufficient hence

the solution of CSSs, that can still ensure a good accuracy of 0.75° , below the 5° limit [21]. Since all the rates shall be damped, a 3-axis control is required; this can be provided by RWs that guarantee an accuracy way lower than $0.5^\circ/\text{s}$. The measurement of body rates is achieved through a MIMU.

Observing mode is instead responsible for the stabilisation and pointing of the satellite during the scientific and exploratory mission -hence a fine pointing (both nadir and inertial) shall be guaranteed. A-STRs provide the required accuracy of less than 0.1° [21] with the RWs that can guarantee also a fine control accuracy with drift rates below $0.1^\circ/\text{s}$. Once again, MIMU can provide the measurement of body rates.

Delta-V mode has the objective of providing velocity changes while preserving the attitude, in order to ensure the correct orientation during the firings. Therefore, a fine stabilisation is ensured by the RWs and the drift rates measured by the MIMU.

Delta-H is responsible for the desaturation of the RWs and has also the prerogative of maintaining the attitude of the spacecraft stable during the operation since RWs are temporarily unavailable. Thus, the ATs have the additional function of keeping the drift rates below $0.1^\circ/\text{s}$ [25].

Mode	Objective	Solution	Sensors and Actuators	Accuracy
Sun Safe	retrieve Sun vector	3-axis stabilisation and control	CSS, IMU, RW	$0.1^\circ \div 5^\circ$, drift $< 0.5^\circ/\text{s}$
Observing	nadir pointing	3-axis stabilisation and control	A-STR, IMU, RW	$<0.01^\circ$, drift $< 0.1^\circ/\text{s}$
Delta-V	provide velocity change	3-axis stabilization and control	IMU, AT, NT	$<0.1^\circ$, drift $< 0.1^\circ/\text{s}$
Delta-H	momentum unloading	3-axis stabilisation	IMU, AT	drift $< 0.1^\circ/\text{s}$

Table 26: Minimum needed accuracy per each mode

7.3.2 Environmental Disturbances

Due to the absence of both a magnetic field and an appreciable lunar atmosphere, the two environmental disturbances torques that mainly affect the LRO attitude are the Gravity Gradient (GG) and the Solar Radiation Pressure (SRP).

GG torque is always present during the entire LRO life cycle and cannot be neglected, given the spacecraft large size (especially when SAs are deployed).

A first estimation of its maximum value was carried out using Equation 11.

$$M_{GG} = \frac{3\mu}{2r^3} (I_{max} - I_{min}) \sin(2\theta) \approx 1.83 \cdot 10^{-6} \text{ N}\cdot\text{m} \quad (11)$$

where μ is the Moon's gravitational parameter, r is the distance between LRO's nominal 50 km orbit and the centre of the Moon, $I_{max} = 1478.3 \text{ kg m}^2$ and $I_{min} = 1071.3 \text{ kg m}^2$ are respectively the maximum and minimum moment of inertia and θ is the misalignment angle of the LRO body axes with respect to the LVLH frame. The two values of the inertia moments were retrieved from [14], while θ was originally set to 0.01° , because the nadir-axis of the LRO is the one associated with the maximum inertia momentum, thus its predicted misalignment with respect to the gravity-direction is rather low, in the order of the pointing accuracy around that axis. However, in a preliminary design, a 3-axis stabilised spacecraft has the accuracy requirement of $<0.1^\circ$ [21] (Tab.11-8 p.365). Keeping a conservative approach the limit value of 0.1 deg has been used to compute the first estimate of the disturbance torque due to the gravity gradient. As a final remark, GG can be assumed to be constant

across the whole LRO's nominal 50 km orbit since the satellite is always nadir-pointing and the orbit is circular.

SRP is the other main disturbance torque that affects LRO's attitude. It is present whenever the satellite is exposed to Sun and since the area of the SA is quite large, a non-negligible disturbing torque will therefore be present. A first estimation of the SRP maximum value was carried out using Equation 12.

$$M_{SRP} = \frac{F_\odot}{c} A_s (1 + q) \cos(\iota) (c_{sp} - c_g) \approx 3.79 \cdot 10^{-5} \text{ N}\cdot\text{m} \quad (12)$$

where $F_\odot = 1363.03 \text{ W/m}^2$ is the average solar irradiance at Moon distance, c is the speed of light in vacuum, $A_s = 14.87 \text{ m}^2$ is the satellite surface that sees the Sun, q is the average reflectivity coefficient (assumed to be 0.5), ι is the incidence angle (assumed 0 to have a worst case scenario) and $c_{sp} - c_g$, which value is around 0.37 m, is the difference between the satellite centre of pressure (assumed as the centre of the solar array) and the satellite centre of gravity (retrieved from [14]). The quantification of this disturbance torque was an order of magnitude higher than expected but this can be ascribed to the highly conservative choice of input variables.

7.3.3 Slew Manoeuvre

In this section, a “worst case scenario” slew manoeuvre (i.e. a rotation of $\theta_{max} = 180^\circ$ around the maximum inertia axis) was analysed to check whether the maximum imposed slew rate of $0.5^\circ/\text{s}$ was respected. To do so, recalling the main properties of the RWs listed in Table 25 and using Equation 13, the minimum time to perform this manoeuvre was computed as follows:

$$t_{min} = \sqrt{\frac{4\theta_{max} I_{max}}{M_{RW,max}}} = 340 \text{ s} \quad (13)$$

Then, knowing the value of $t_{min} = 340 \text{ s}$, the maximum slew rate of $\dot{\theta}_{max} = 0.5^\circ/\text{s}$ was retrieved as shown in Equation 14. This latter parameter is still respectful of the initial constraints, also considering that a worst case scenario was considered.

$$\dot{\theta}_{max} = \frac{\theta_{max}}{t_{min}} = 0.5^\circ/\text{s} \quad (14)$$

7.3.4 Momentum Unloading Operations

It is known from [14] that the momentum unloading operations are performed approximately every two weeks and also that the allocated propellant mass for the RWs desaturation is around 4.25 kg/year in LRO nominal mission orbit. A first preliminary estimation of those values is hereafter performed. Recalling that the period of LRO in its nominal orbit is around 113 minutes, it was possible to evaluate the accumulated angular momentum in the RWs during one full orbit: this was done using Equation 15, hence by multiplying the orbital period (with a correction factor of 3/4 applied to the SRP contribution to take eclipses into account) with the environmental disturbing torques acting on the satellite. Eventually, a margin of 100% was included to analyse a worst case scenario operation.

$$\Gamma_{1period} = 2 \cdot \left(M_{GG} \cdot t_{orbit} + M_{SRP} \cdot \frac{3}{4} t_{orbit} \right) \quad (15)$$

Then, recalling the nominal limit of RWs' angular momentum capacity, it was calculated the number of orbital periods before a momentum unloading manoeuvre was necessary. Knowing this value, it was eventually estimated, using Equations 16, the total propellant mass used to desaturate the RWs over a period of 1 year, i.e. the duration of the nominal mission phase.

$$m_{tot} = m_{prop}^1 \cdot N_{des,1year} \quad \text{where:} \quad m_{prop}^1 = N_{RW} \cdot \frac{t_{burn} F}{I_{sp} g_0} \quad (16)$$

The value of m_{prop}^1 represents the amount of propellant used for a single desaturation and it was obtained assuming a burning time $t_{burn} = 3.5 \text{ s}$ and that the thrusters were capable of providing only a constant thrust $F = 22 \text{ N}$. The results of all previous considerations are reported in Table 27.

	$\Gamma_{1\text{period}}$ [Nms]	$N_{des,1\text{year}}$ [-]	m_{prop}^1 [kg]	m_{tot} [kg]
estimated	0.39	32 (every ~ 11.5 days)	0.14	4.45
actual	n/a	26 (every ~ 14 days)	0.16	4.25

Table 27: Comparison between estimated and real data

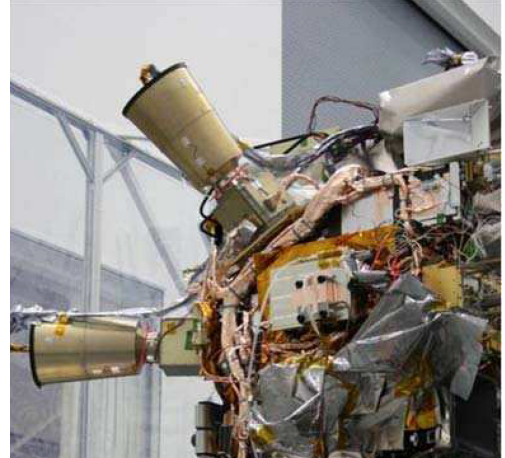
7.4 System Review

The AOCS is responsible of achieving and maintaining the desired orbit plus pointing and maintaining the desired attitude. This is made possible thanks to an articulated system of sensors and actuators with the help of an onboard control system. In particular:

- The sensors onboard are: 10 CSSs provide coarse measurement of the Sun's position in Body frame, 2 A-STRs give a fine attitude measure with respect to an inertial space, a IMU returns the body rates in a body frame. The actuators are: 4 RWs for attitude stabilisation and control outside the Δv manoeuvres, 8 ATs to provide momentum unloading and attitude stability during Δv manoeuvres and 4 NTs to provide velocity variations.
- Four modes can be used during the mission lifetime to successfully achieve the mission goals: Sun Safe that provides an initial attitude and a stable configuration in case of emergencies, Observing that ensures a fine pointing during the exploratory and scientific phases, Delta-V that is responsible for orbital maneuvers and Delta-H that provides momentum unloading.
- A reverse sizing was performed to ultimately retrieve the propellant mass required each year for momentum unloading that ended up being consistent with the effective mass allocated at launch. The mild overestimation is due to the highly conservative model of the disturbances acting upon the spacecraft throughout the mission. Also the maximum slew rate was obtained to verify it was under the allowable limit, condition that was respected. In addition, a preliminary analysis on the choices of sensors actuators and accuracy limits was performed.



(a) RWs mounted to spacecraft structure



(b) A-STRs mounted on Instrument Module

Figure 10: LRO RWs and A-STRs

8 Thermal Control System

The lunar thermal environment is one of the most demanding from a thermal control viewpoint, with heavy infrared loading from the Moon, lack of lunar atmosphere and low effective regolith conduction. Therefore, the sizing of the entire TCS was driven by these harsh conditions, together with the goal of having a system as simple as possible, minimizing radiator area and heaters power, still ensuring a high redundancy level. This led to a modular design, which minimises the number of radiators, the thermal interfaces and thermal blanketing.

In addition, the TCS had to take into account also that radiators have to be pointed to an optimal direction and their FOV must be clear. Moreover, they have to be thermally coupled with the internal components through a highly conductive path to optimise the dissipation of the generated heat. Particularly, thermal connections between components with similar operating-temperature ranges allow to increase the thermal capacitance, decreasing the sensitivity to temperature changes. This system is of fundamental importance and should satisfy functionalities FUN-06.01, FUN-06.03 and FUN-06.04.

8.1 Lunar Thermal Environment

The Lunar surface has a large temperature gradient due to the absence of an atmosphere, the rotational period and the thermo-physical properties of regolith. The diurnal temperature ranges between 100 K and 395 K in the equatorial region, while in permanently shadowed regions, near the poles, the temperature varies between 30 K and 100 K (see Table 28).

Parameters		Hot Case	Cold case
Surface temperature	[K]	395	100
Solar flux	[W/m ²]	1420	~ 0
Albedo coefficient	[–]	0.13	0.06
Max. Lunar IR flux	[W/m ²]	1335	5
Min. Lunar IR flux	[W/m ²]	1114	5

Table 28: Lunar thermal environment characterization [1][28]

The thermal flux on the LRO, resulting from Moon Infrared (IR) emissions, albedo effect and solar flux, vary within a wide range. Although the solar and albedo fluxes depend mostly on the exposure of the spacecraft to the Sun, the IR depends also on the angle β between the Sun-Moon and Moon-spacecraft lines. At high values of β , the IR flux is very low, reaching a minimum of about 5 W/m² for $\beta = 90^\circ$; whereas, for small angles, the IR flux increases, approaching a maximum value of 1335 W/m² for $\beta = 0^\circ$ (see Figure 11).

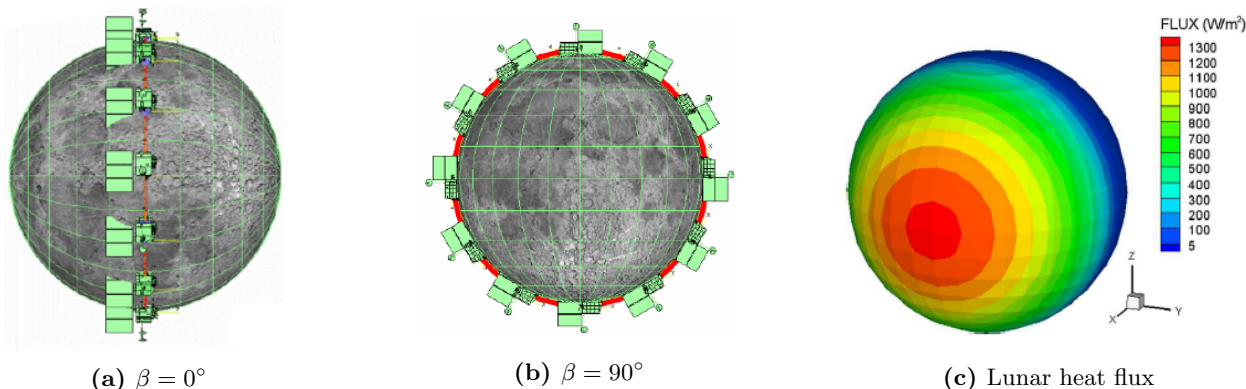


Figure 11: Lunar thermal flux with the β angle as seen from the Sun

8.2 Architecture

The LRO TCS accommodates four major elements: the spacecraft bus, which consist of the avionics, RWs assembly and a battery; the instruments module; the propulsion module and the deployable devices, such as the HGA and SA.

The TCS was designed and qualified to ensure the survival of the LRO in the most extreme lunar eclipse cold cases, which occur when the Moon is fully in the umbra.

The spacecraft was equipped with radiators to dissipate the internal heat generated, a high number of heat pipes to transfer the heat away from the critical components, heaters to avoid having too low temperatures and a lot of harness to create useful thermal paths. To provide the minimal exposure to the lunar environment, in particular to its surface, the radiators were integrated on the zenith face of the orbiter (pointing -Z). To avoid the absorption of high solar thermal power when exposed to the Sun, the radiators were covered with Optical Solar Reflectors (OSRs), allowing the reflection of most of the radiation in the visible band, still ensuring a strong emission in the IR band.

The LRO external structure was covered with a 15 layers MLI, made of Vapour Deposited Aluminum (VDA) onto a *Kapton* substrate [14] and the outer layer in *Kapton* too.

The MLI shields the spacecraft from the external environment, preventing thermal conduction and radiation to the internal components. While aluminium layers were chosen due to the high reflectivity, *Kapton* was selected for its low thermal conductivity and higher emissivity in the IR. On the zenith face (+Z) of the spacecraft this thermal blanket was not applied to provide a clear FOV to the radiators.

Components	Temperature Range [°C]	
	Operating	Survival
C&DH	-10 to +40	-20 to +50
Battery	+10 to +30	0 to +40
A-STRs	-30 to +50	-35 to +60
RWs	0 to +50	-30 to +60
Hydrazine tanks	+10 to +40	n/a
Pressurant tank	0 to +50	n/a
Structure	-50 to +50	-60 to +60
Mechanisms	-10 to +50	-20 to +60
Instrument module	-30 to +30	-40 to +40

Table 29: Strictest temperature intervals to be satisfied [14]

8.2.1 Avionics Module, RW Assembly and Batteries

Most of the LRO's avionics components have a very similar operative temperature range (Table 29). Indeed, these were thermally coupled into an embedded Constant Conductance Heat Pipes (CCHPs) aluminium honeycomb panel, which made the assembly light, highly conductive and with very good mechanical properties. This isothermal panel was linked to externally-mounted dual bore header heat pipes, which transfer the heat to a separate avionics radiator on the zenith face of the LRO.

The RWs assembly had a dedicated heat pipe system that coupled them with the avionics radiator (see Fig-

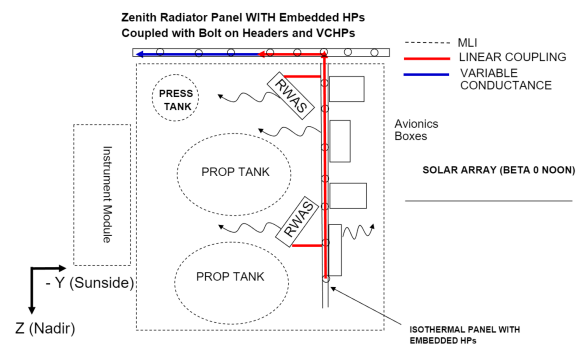


Figure 12: RWs Heat Dissipation

ure 12). To minimize the temperature variations during an orbit, the thermal mass was enlarged as much as possible by wrapping the avionics and the RWs around the propulsion system. Moreover, to guarantee the survival of the spacecraft during Lunar eclipses, this thermal mass is pre-heated, using software-controlled heaters: such procedure helps to minimize the heaters' power demand during this scenario, that otherwise would be very high.

The Lithium-Ions battery presents the tightest operational range of temperature (see Table 29), which was guaranteed by using a separate heat pipe network coupled with a dedicated radiator on the zenith face of the orbiter. To ensure a tight control of the battery temperature, the radiator was oversized and an heater was added.

8.2.2 Propulsion module

The propulsion module includes different components, which require specific thermal control design:

- Two propellant tanks: heaters were used to keep N₂H₄ temperature above the freezing point. While on the liquid hemisphere E-shaped heaters were placed in an array to provide a thorough coverage of the surface, on the gas hemisphere 4 strip heaters, tilted towards equator, provide the control of the heat losses from the liquid to the colder gas hemisphere. To spread the heat across the surfaces, the two tanks were over-taped with layers of aluminium tape. At the same time, to minimize the heat losses, the two tanks were covered with MLI.
- Pressurant tank: to keep the pressurant temperature as constant as possible, the tank was wrapped with MLI and 4 heaters were used. Each heater was integrated on an aluminum shell, attached to the COPV to limit its contraction due to the decrease of Helium pressure.
- Thrusters: all thrusters valves were individually blanketed with MLI and coupled with heaters. The structure near the nozzle was protected with an high-temperature blanketing material, which consist of *Kapton* layers covered with layers of stainless steel. To reduce the absorbance of the metal in the visible range, this surface was covered with Z-93 white paint.

As reported in the section regarding the propulsion unit integration, the two tanks were placed in a cylindrical structure on the side of which the component panels were located. Whether on the internal or on the external surfaces, some redundant heaters were used to create an internal warm cavity to keep the surface hot enough. A coating in *Aeroglase Z306* black paint helps the heat exchange between the warm cylinder, the propellant tanks and the lines near the cylinder. In addition, the overall structure, including the component panels, was covered with a MLI with the same characteristics of the external one. Also the pipe lines, which contained internally redundant spiral heaters, were wrapped in insulator material.



Figure 13: PS Shielding

8.2.3 Instrument Module

Since LOLA, LROC, LAMP and the A-STR require a very high pointing accuracy, they are integrated in a decoupled optical bench: the instrument module. The operative temperature range for these instruments resulted to be quite narrow as it can be seen in Table 29.

For this reason, the mechanical structure necessary to support the bench was built in *M55J* (High Modulus Carbon Fiber), which combines excellent mechanical properties with a thermal conductivity 7 times lower than the aluminium and a very low Coefficient of Thermal Expansion (CTE), allowing to withstand the most extreme thermal environment without losing too much in pointing accuracy. To keep the cold limit temperatures, this optical bench was also equipped with 25 low density heaters, small in size to avoid the generation of a temperature gradient due to uneven heating of the bench. To maintain the optical bench as isothermal as possible, it was fully blanketed with a 2-3 layers MLI with the same characteristics of the external one. Moreover, each of the instruments had a dedicated

radiator and, therefore, the thermal blanket has to provide a clear FOV to them.

On the other hand, CRaTER, Mini-RF, DLRE and LEND were integrated directly to the main LRO structure and were individually controlled through heaters and radiators.

8.2.4 Deployable Devices

As mentioned in Section 6, the HGA was implemented with a double gimbal axis. Due to the rotational joints, the various heat sources are not well coupled with the spacecraft structure, therefore, the antennas need to implement multiple radiators and heaters. Moreover, the entire hardware was wrapped with a 40 layers MLI, which was designed in order to prevent radiator blockage and provide a reliable rotation about the actuators axes. To dissipate the internal heat flux, the actuators were thermally coupled with coaxial cylindrical radiators by exploiting an aluminium tape, which has good thermal and mechanical properties.

Also the SA is double-gimbal driven and each actuator has its own heaters and dedicated radiators. In this case, the actuators were wrapped with about 20 blankets. To dissipate the heat power due to the part of the incident solar radiation that doesn't contribute to the photovoltaic effect, the side direct toward the deep space has been exploit as radiator.

8.3 TCS Preliminary Sizing

In order to get a rough estimate of the spacecraft needs in terms of cooling surfaces and electrical power required for heating, a mono-nodal thermal analysis was carried out.

The LRO was assumed as a $3.9\text{ m} \times 2.7\text{ m} \times 2.6\text{ m}$ cuboid, neglecting the presence of the SA and HGA, and was modeled as an equivalent sphere with the same external area of $A_{tot} = 55.4\text{ m}^2$.

An adequate interval of admissible temperatures was selected by choosing the highest minimum-temperature and the lowest maximum-temperature from Table 29 to satisfy most of the components' operative temperature ranges. For the choice of the two boundary temperatures, the battery and hydrazine tanks ranges were not considered due to their strict operative conditions that for sure require a dedicated thermal control. Such boundaries resulted to be 0°C and $+40^\circ\text{C}$ to which it was added a margin of $\pm 15^\circ$, leading to an admissible temperature range that goes from $+15^\circ\text{C}$ to $+25^\circ\text{C}$.

8.3.1 LRO Thermal Properties

The MLI coating that covers the spacecraft was modelled as 14 layers of *Kapton* covered by VDA with an emissivity $\varepsilon_{VDA} = 0.05$ plus one external layer in *Kapton* ($\varepsilon_{kap} = 0.82$). The equivalent emissivity of the coating was computed as shown in Equation 17, by evaluating firstly the emissivity of the 14 VDA layers and then adding in series a further thermal resistance with the *Kapton* emissivity.

$$\varepsilon_{MLI} = \frac{1}{\frac{1}{\varepsilon^*} + \frac{1}{\varepsilon_{kap}}} \quad \text{where:} \quad \varepsilon^* = \frac{1}{\frac{1}{\varepsilon_{VDA}} + \frac{1}{\varepsilon_{VDA}} - 1} \cdot \left(\frac{1}{14 + 1} \right) \quad (17)$$

The coating absorption coefficient in the visible range of the spectrum was considered to be half of the emissivity, as stated in [29].

8.3.2 Hot Case Scenario

In order to establish the necessity and possibly the required dimensions of a radiator, the spacecraft thermal exchange was analyzed when the thermal fluxes are at their maximum value, that is when LRO is directly exposed both to the Sun irradiance and to the illuminated surface of the Moon.

To evaluate the absorbed solar power, the equivalent sphere cross sectional area $A_{cross} = 13.8\text{ m}^2$ was considered, while for the infrared and albedo absorption, the view factor between the equivalent sphere and the Moon was computed considering the minimum possible altitude of 35 km. According to [28], the emissivity of the Moon was selected as $\varepsilon_{\mathbb{M}} = 0.97$, while the albedo coefficient as $a_{\mathbb{M}} = 0.13$.

Parameter	Solar	Albedo	Infrared
\dot{q} [W/m ²]	1420.00	167.78	1216.90
Q [W]	16.77	2.77	40.14

Table 30: Thermal fluxes and thermal absorbed powers

Table 30 summarises the thermal fluxes and absorbed powers computed.

In addition to these thermal fluxes coming from external heat sources, for the internal generation a maximum value of $Q_{int_{max}} = 684$ W was considered [14].

By applying the equation for the thermal balance of the spacecraft ($Q_{in} = Q_{out}$), it was possible to compute the temperature reached by the surfaces in absence of any radiator, that resulted to be 610.4 K. Since this value exceeds the upper temperature limit, a radiative surface (similar to the one of the real radiators) with an emissivity $\varepsilon_{rad} = 0.8$ (typical for an OSR radiator) was implemented. The minimum area of such radiator was computed according to Equation 18, imposing the spacecraft temperature to be equal to the upper boundary of the allowed range $T_{max} = 298$ K. Note that the radiator was supposed to be placed above one of the lateral surfaces of the spacecraft, so the effective area covered by the MLI coating was reduced to $A_e = A_{tot} - A_{rad}$.

$$A_{rad} = \frac{Q_{i_{max}} + Q_{Sun} + Q_{albedo} + Q_{IR} - \sigma_B \varepsilon_{sc} A_{tot} T_{max}^4}{\sigma_B \varepsilon_{rad} T_{max}^4 - \sigma_B \varepsilon_{sc} T_{max}^4} \quad (18)$$

The computed area was $A_{rad} = 1.965$ m², a value that allowed the radiator to be placed in any face of the spacecraft.

8.3.3 Cold Case Scenario

The evaluation of the electrical power needed to heat up LRO when its temperature goes below the lower limit $T_{min} = 288$ K was done for the worst cold case scenario. In such situation the spacecraft points to the dark side of the Moon and the Sun is shadowed by the Moon itself, so no thermal fluxes in the visible region of the spectrum reach the surface of LRO; instead, it is only subjected to the infrared thermal emission of the Moon, equal to $\dot{q}_{IR} = 4.838$ W/m², with a surface temperature of $T_{moon} = 100$ K. [28] Therefore, the heat power absorbed by the spacecraft was only in the infrared and it was computed considering that the radiator would never be pointed toward the surface of the Moon, resulting in 0.15 W of absorbed power. In this case, the view factor was computed considering an altitude of 65 km, which is the highest point that nominally LRO can reach during its mission. The minimum internal generation $Q_{int_{min}} = 407$ W was retrieved from [14].

Under these conditions, the spacecraft reached a minimum temperature of $T_{cold} = 256.3$ K (from Equation 19), way too low with respect the lower limit of T_{min} .

$$T_{cold} = \sqrt[4]{\frac{Q_{int_{min}} + Q_{IR}}{\sigma_B (\varepsilon_{sc} A_{eff} + \varepsilon_{rad} A_{rad})}} \quad (19)$$

To address this problem, heaters are needed in order to provide the thermal power that allows to remain inside the temperature range. Such power resulted to be $Q_{heaters} = 242.93$ W and it was computed according to Equation 20.

$$Q_{heaters} = \sigma_B (\varepsilon_{sc} A_{eff} + \varepsilon_{rad} A_{rad}) T_{min}^4 - Q_{int_{min}} - Q_{IR} \quad (20)$$

8.4 Bi-nodal Analysis and Thermal Decoupling

In order to have a global view about the thermal control that may be needed by LRO, another analysis was carried out by thermally decoupling the spacecraft envelope and the internal components, that were collapsed in a single iso-thermal point. Between the single iso-thermal point and the outer

space, a radiator was introduced to dissipate only the internal heat generation. In particular, the radiator is never directed towards the lunar surface, thus only the direct exposure to sun radiation was considered for its sizing. A schematic representation of the model used is reported in Figure 14. The external and internal heat fluxes are indicated as arrows and the coupling between internal components and the radiator is represented through a thermal resistance (named h_c hereafter). It may be noted also that the white space between radiator, internal components and the structure of the spacecraft (i.e. MLI in figure) implies the thermal insulation of these components, assumed as a first approximation. At this point, two adiabatic systems were analyzed: the first made of the external environment and the external surface of the spacecraft, while the second one composed of the internal components' node, a radiator and the external environment too. The solution of the thermal balance equation for the coating-environment system provided the needed optical properties of the coating, once having fixed at $+50^{\circ}\text{C}$ the surface temperature that guarantees the structure's survival [14].

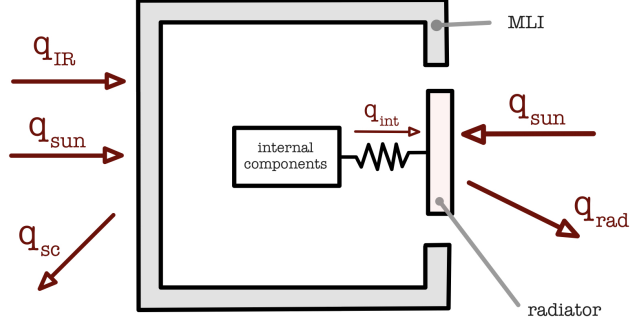


Figure 14: Bi-nodal model of the LRO

In particular, Equation 21 provided a value of $\alpha/\varepsilon = 0.487$, that is quite similar to the typical values for *Kapton* external layers [29][30]. Note that such value refers to the coating's external layer optical properties, since the system was assumed adiabatic on the other side, as MLI has the role to thermally insulate the spacecraft from the external environment. Indeed, MLI equivalent thermal resistance should be taken into account only if some heat flux flows through it.

For the radiator sizing, in order to simulate the heat pipes/harness that carry heat from the components to the radiator, a conductive resistance $h_c = \lambda/\delta$ was modeled considering the aluminum conductivity of $\lambda = 237 \text{ W m}^{-1} \text{ K}^{-1}$ and a typical thickness $\delta = 15 \text{ mm}$. Radiator's emissivity was assumed as before $\varepsilon_{rad} = 0.8$ [14][31], while the absorption coefficient as $\alpha = 0.08$ from literature [21]. The thermal balance of the radiator is a system of two equations in two unknowns (T_{rad} and A_{rad}) and was solved numerically.

$$Q_{int_{max}} = h_c A_{rad} (T_{rad} - T_{max}) \quad \text{and} \quad Q_{int_{max}} + Q_{Sun} = A_{rad} \sigma_b \varepsilon_{rad} (T_{rad}^4 - T_{max}^4) \quad (22)$$

The internal components' T_{max} resulted to be guaranteed with a radiator at $T_{rad} = 297.985 \text{ K}$ and with a surface of $A_{rad} = 2.803 \text{ m}^2$.

Neglecting the solar flux on the radiator and considering $Q_{int_{min}}$, it was possible to evaluate the lowest temperature reached by the internal components in absence of any heater. Such temperature resulted to be 237.866 K , lower with respect to the minimum operating temperature. To ensure T_{min} , the following system was solved in the unknowns Q_{int} and T_{rad} :

$$Q_{int_{min}} = h_c A_{rad} (T_{rad} - T_{min}) \quad \text{and} \quad Q_{int_{min}} = A_{rad} \sigma_b \varepsilon_{rad} (T_{rad}^4 - T_{min}^4) \quad (23)$$

This led to a power needed to be generated by the heaters equal to 408.263 W .

8.5 Sizing Considerations

LRO has several subsystem and components that require a dedicated TCS and different operating temperatures. Hence, both analysis cannot provide very accurate results due to the absence of multiple nodes. At the same time, the two preliminary models presented opposite hypothesis.

On the one hand, in the mono-nodal case, the internal heat was supposed to be transmitted equally across all the spacecraft, modelled as a sphere, neglecting the presence of any heat pipe, which would

increase the flux towards the radiator. Thus, only a minimum quantity of internal generated heat is dissipated through the latter, leading to a smaller radiator area, as shown in Table 31. As a consequence, the heat dispelled in the cold case is lower, hence a low power heater is required. On the other hand, in the thermal de-coupled case (i.e. the bi-nodal model) the radiator has to dissipate all the internal heat generated, as if the MLI could ideally insulate the spacecraft, resulting in a larger area. Thus, in the cold case a more powerful heater is needed to face higher heat dissipation. In any case a radiator and some heaters have to be adopted, whereas the investigated MLI has the optical properties similar to the VDA backed *Kapton*, as shown in both analysis.

Model	$A_{rad}[\text{m}^2]$	$Q_{heaters}[\text{W}]$	$(\alpha/\varepsilon)_{MLI}$
Mono-nodal	1.965	242.93	(assumed)
Bi-nodal	2.803	408.263	0.487

Table 31: Main results of the thermal analysis

8.6 System Review

The TCS design had to face several temperature ranges among the different components, as briefly shown in Table 29. In addition to a dedicated thermal regulation system, more general solutions were adopted to ensure the operating range, redundancy and simplicity, in particular:

- Thermal links between components with similar requirements, for a simpler architecture and enlarged thermal capacitance, reducing sensitivity to temperature variations;
- The use of highly conductive heat pipes, to minimize temperature losses and direct heat towards the optimally-directed radiators;
- MLI wrapped around the most sensitive components, enhancing insulation;
- Low CTE materials, to avoid losses in the instruments pointing accuracy.

9 Electrical Power System

The LRO EPS is designed to provide the required electrical power to all the subsystems throughout all operational modes and mission phases. In detail, the this subsystem satisfies functionality FUN-07.01 and the sizing was led by multiple requirements, as reported in Section 1.2.

9.1 Power Budget Required

In Table 32 is reported a breakdown of the power required by the LRO subsystems for each main phase/mode of the mission.

	Peak Power	Launch	Sun Safe	Delta-V	Observing		Delta-H	Eclipse
			Sun Acquisition	Lunar Transit.	S band	S+Ka band	manoeuvre	
Instruments	224.8	0	0	22	126.8	126.8	126.8	0
Comms	117.8	12	47	36	36	117.8	36	12
C&DH	123.4	127.1	127.1	124	120.4	120.4	120.4	114.3
Gimbals	50	0	40	0	50	50	50	0
PSE	50	50	50	50	50	50	50	50
PS	107.6	0	0	0	0	0	157.6	0
ACS	137	35	107	107	137	137	137	107
TCS	1001	0	155	n/a	0	100	n/a	235
Total [W]	1811.6	224.1	426.1	339	520.2	702	677.8	518.3

Table 32: EPS budget (sources: [14][32][33])

9.2 System Architecture

The LRO EPS was developed with a Direct Energy Transfer (DET) architecture, which means that the power is directly distributed from the main bus to all instruments and subsystems. This is ensured by 3 main components: a SA, a PSE and a Lithium-Ion secondary battery, as shown in Figure 15. The overall system performance required not to exceed 824 W average power capability per orbit with an unregulated 21 V ÷ 35 V bus, able to withstand peak loads up to 1849 W for a maximum of 5 min at EOL [1]. In addition, the system shall endure eclipse periods that vary seasonally between 0 and 40 min without exceeding a battery Depth of Discharge (DoD) of 30%. [34]

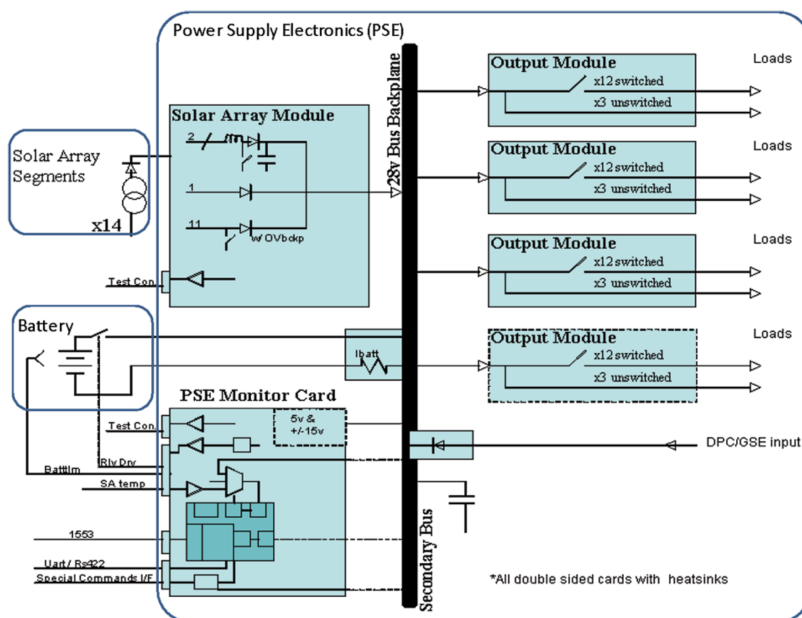


Figure 15: LRO EPS block diagram

9.2.1 Solar Array

A foldable SA is the primary energy source of the LRO. The Beginning Of Life (BOL) performances can be quantified in a peak power output below 2120 W at any β angle, with a maximum design voltage of 35 V. After 14 months, at a condition of $\beta = 0^\circ$, the same power output is reduced to 1849 W. The SA shall not only provide power supply to all the instruments onboard (scientific and operational) but also recharge the Li-ion battery. [34]

The SA is composed by 3 main foldable panel frames, for a total of 77 identical modules (44.9×28.4 cm) which are composed of 48 cells each. This results in a total of 3696 cells, grouped in configuration of 2 strings per module, 24 cells per string. Since the area of each cell is approximately 26.5 cm^2 , the resulting power-generating area of the SA is about 9.81 m^2 . Four of the 154 solar-cell strings could be potentially shadowed by containment canisters for the restraint bolts¹⁰ when $\beta = 70^\circ \div 75^\circ$, resulting in a reduction of 2.6% of the power generation. [14]

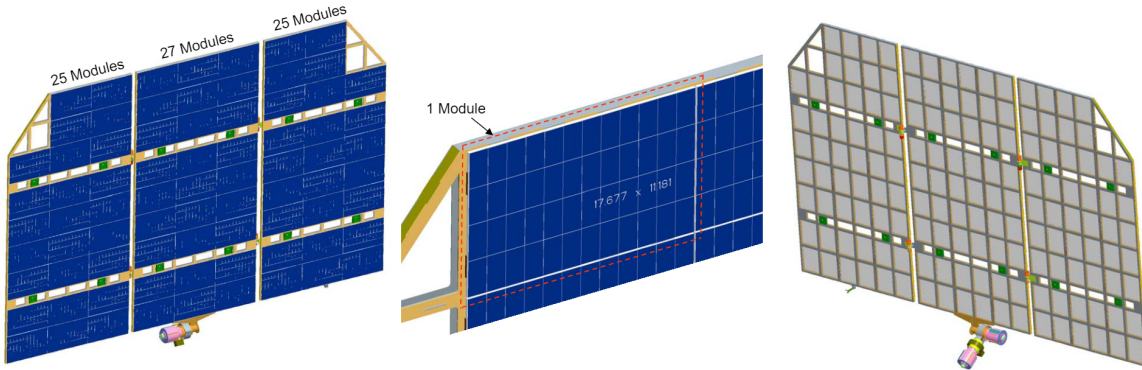


Figure 16: LRO Solar Array (SA) front and rear view

From Figure 16 it can be noted that the two external corners of the panels are not covered with cells: this was done to ensure a totally clear FOV to the wide angle camera mounted on-board in all the possible β angle conditions. During “orbit day”, the SA drive actuators are designed to rotate the panels at constant velocities (azimuth $\sim 3.2^\circ/\text{min}$, elevation $\sim 1^\circ/\text{day}$) in order to constantly maintain the correct pointing to the Sun as the LRO moves along its orbit. Then, just before the “orbit night”, these actuators are commanded to drive the SA in a configuration such that the panels are correctly oriented to the orbit dawn. The SA has a Sun tracking requirement accuracy of $\pm 2^\circ$ for all the β angle conditions. [14]

9.2.2 Power Subsystem Electronics (PSE)

The PSE is accountable for power distribution and battery charging. It is equipped with a fault detection system that provides bus protection by automatically shedding loads, through a Solid State Power Controllers (SSPC), with resettable circuit breaker capability. The PSE and the main bus, include also a Power Monitor Card (PMC), which monitors battery voltage, current and temperature to determine the power flow of the system in order to correctly activate the switches. Indeed, when the battery is fully charged (the limit is 30 A) during sunlight activities, the excess power produced is shunted back to the SA. [34]

9.2.3 Lithium-Ion Battery

As a secondary energy source, a single 36.4 kg Li-Ion battery is devoted to providing power to the spacecraft when the SA are not working, i.e. during eclipses. Lithium batteries were chosen due to their high energy density and low self-discharge rate. On the other hand, due to their poor robustness, a protection and battery management system was needed. In addition, their operational temperature

¹⁰these are components of the restraint devices required for SA stowage

range is one of the most demanding from the thermal control point of view; hence, a heat pipe assembly directly connected to a zenith-facing radiator keeps the temperature within this range. [1]

A maximum DoD of 30% is allowed during normal operations, enabling the battery to survive to the high number of cycles expected by the mission profile. The required EOL capacity is about 80 Ah, starting from a BOL storage capacity of 126 Ah [35]. Such capacity, together with the bus voltage, is provided by a total of 672 cells, partitioned in 7 blocks, composed of 12 strings of 8 cells each [1].

The architecture is integrated with a failure protection system, thus a cell malfunctioning can be accepted without resulting in a catastrophic loss. Indeed, open-circuit failures would result in a single string loss, while a short-circuit would activate an internal cell protection, leading again to an open-circuit failure. Capacity losses due to failures were estimated to be about 1% of the total capacity [1]. Capacity losses due to power converters losses are minimized by the direct connection of the battery to the electrical bus.

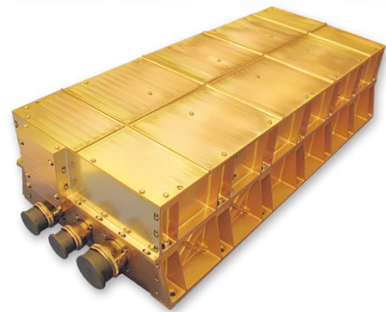


Figure 17: LRO battery [35]

9.3 System Preliminary Sizing

To perform a preliminary sizing of the EPS, LRO's orbit was considered to be the nominal 50 km one, in which the eclipse period is $t_{ecl} = 40$ min; mission lifetime was then assumed to be 72 months to be conservative with respect to the explorative, scientific and extended mission phases, according to [34].

9.3.1 Primary Source Selection

Since the solar total irradiance at the Moon is comparable to the one at the Earth and the power demand in Table 32 is within the range 0.2 kW \div 300 kW, a Solar Array (SA) is a feasible solution for the primary energy source selection, also according to [21].

On the one hand, this choice brings some drawbacks. Firstly, a medium degradation over life, but no catastrophic effects over performances, since the nominal mission includes a one year explorative plus a one year scientific phase. Secondly, as the SA shall point the Sun to generate power, the best location is the one facing it. Thus, the possibility of obstruction of the spacecraft (specifically the scientific payload) FOV must be taken into account, according to [21][14].

In addition, since the sensitivity to the solar incidence angle is high [21], an accurate pointing is required.

On the other hand, this configuration brings some advantages. These are a low IR signature, thus high compatibility with scientific instruments and an unlimited “fuel” availability, as long as the spacecraft is in sunlight.

9.3.2 Secondary Source Selection

Since the primary source selected is photovoltaic, a secondary energy source in the form of energy storage is required, capable of providing power during peak loads or when the primary is not working. A battery is the most common solution, with Li-Ion being the one with the best performance [21].

9.3.3 Bus Regulation Strategy Selection

Due to a longer exposure to sunlight rather than eclipse, the power generated once the battery is fully charged is more than the one required by the subsystems. Hence the need of a dissipating system, like a shunt in the SA. The most suitable power distribution architecture is a DET, since the most common alternative, the Peak Power Tracking (PPT), is non-dissipative (as reported in [21]), thus not suitable. In addition, the DET allows to have less mass onboard, fewer components, therefore lower risk of failures and higher total efficiency at EOL, according to [21]. The nominal bus voltage shall be the same as the battery nominal one, since it is a unregulated system and a common value is 28 V [21].

9.3.4 Solar Array Sizing

The SA was sized for the most demanding power request of $P_{day} = 1850$ W during day-light and an eclipse power request of $P_{ecl} = 518.3$ W, as stated in [14][33]. All input parameters used for the sizing are reported in Table 33.

Input Parameters			
A_{cell}	26.5 cm ²	F_{\odot}	1363.03 W/m ²
ρ_{cell}	4946.6 kg/m ³	V_{bus}	28 V
$\delta_{cellslayer}$	76 µm	ρ_{M55J}	1910 kg/m ³
V_{cell}	2.6 V	l_{beams}	30 cm
η_{conv}	0.3	δ_{beams}	1 cm
dpy	0.03	w_{beams}	2 cm
I_{degr}	0.77	N_{beams}	393

Table 33: Input parameters for the sizing of the SA

Firstly, the maximum power requested to the SA was computed using Equation 24.

$$P_{SA} = \frac{P_{ecl} \cdot t_{ecl}}{X_{ecl} \cdot t_{day}} + \frac{P_{day}}{X_{day}} \quad (24)$$

where $X_{day} = 0.85$ and $X_{ecl} = 0.65$ are the line efficiencies in daylight and in eclipse respectively, common values for a DET architecture as reported in [21]. The specific power of the SA at BOL was then computed using Equation 25, thus by multiplying the Sun irradiance (F_{\odot}) with the cells conversion efficiency (η_{conv}), with the inherent degradation (I_{degr}) and with the cosine of the misalignment angle between the SA and the Sun rays (θ). The latter can be quantified as 2° according to the SA pointing accuracy reported in [14].

$$P_{BOL} = F_{\odot} \cdot \eta_{conv} \cdot I_{degr} \cdot \cos(\theta) \quad (25)$$

The specific power of the SA at EOL was eventually computed by taking the product of P_{BOL} with L_{life} , that is a coefficient that takes into account the losses accumulated during the spacecraft's lifetime, hence its value depends on the degradation-per-year factor dpy , as reported in Equation 26.

$$P_{EOL} = P_{BOL} \cdot L_{life} \quad \text{where:} \quad L_{life} = (1 - dpy)^{t_{life}} \quad (26)$$

At this stage, it was possible to compute the minimum surface that shall be covered with solar cells: this was done by dividing P_{SA} by P_{EOL} . Then, knowing the area of a single solar cell, the preliminary number of cells was obtained from the ratio between the above-mentioned total photovoltaic area and the single solar cell area, whose value¹¹ was retrieved by looking at Figure 16.

Afterwards, it was retrieved the number of solar cells to be placed in series, to obtain the nominal bus voltage, dividing the latter by V_{cell} , whose value was retrieved from [36]. Since this number shall be an integer, it was rounded to the first greater integer. At this stage, the real voltage provided by the SA was computed multiplying the number of cells in series by their nominal voltage.

Finally, it was calculated the real number of cells, given by the ratio between the preliminary number of cells and the number of in-series-cells (rounded to the first greater integer) times the number of cells in series. From this value it was eventually possible to compute the real solar panel area by multiplying it by A_{cell} . This procedure is summarised hereafter by Equations 27.

$$N_{cells} = \left\lceil \frac{A_{SA}}{A_{cell}} \right\rceil \rightarrow N_{series} = \left\lceil \frac{V_{bus}}{V_{cell}} \right\rceil \rightarrow N_{cells}^{real} = \left\lceil \frac{N_{cells}}{N_{series}} \right\rceil \cdot N_{series} \rightarrow A_{SA}^{real} = N_{cells}^{real} \cdot A_{cell} \quad (27)$$

¹¹The value obtained with this procedure is 26.56 cm², similar to the actual 26.6 cm² of the GaInP/GaInAs/Ge triple-junction solar cell illustrated in [36], from this other parameters (e.g. cell's voltage and layer thickness) were retrieved

The mass of the overall array structure was obtained as the sum of the mass of the cells' layer and the mass of the reticular frame supporting it. The solar cells were assumed to be GaInP/GaInAs/Ge triple-junction solar cells, while the reticular frame composed of several beams (see Figure 16) made of *M55J*, a quasi-isotropic composite material with good mechanical properties and low density, as stated in [14]. All the useful characteristics of those two components are reported in Table 33 and were retrieved from [14] and [36].

For what concerns the cells' mass, it was considered a layer of cells with a thickness of 76 μm all over the computed total surface of the SA, as stated in [36]. Then, the supporting frame was estimated to be composed of approximately 393 beams¹², each one with dimensions of about $30 \times 1 \times 2 \text{ cm}$.

Hence, by knowing the average densities of both the triple-junction cells and the *M55J* composite beams, it was possible to compute their masses and eventually the mass of the overall SA structure. All the obtained results are reported in Table 34.

Sizing outputs			
A_{SA}	9.97 m^2	P_{SA}	2612.96 W
mass	48.79 kg	voltage	28.60 V
P_{EOL}	262.11 W/ m^2	P_{BOL}	314.67 W/ m^2
N_{series}	342	N_{cells}	3762

Table 34: Results of the sizing of the SA

9.3.5 Batteries Sizing

The battery capacity, dimensions and configuration could be estimated starting from the knowledge of P_{ecl} . The input values used for the sizing are reported in Table 35. The real battery is composed of a set of 7 identical blocks in parallel, while in the following sizing procedure a single block was studied.

Input Parameters			
DoD	30%	η_{line}	0.4
E_s	80 Wh/ dm^3	E_d	250 Wh/kg
V_{cell}	3.7 V	C_{cell}	1.5 Ah

Table 35: Input parameters for the sizing of the battery

The total capacity of a single block was computed from Equation 28, where the DoD comes from [1] and the line efficiency η_{line} from typical values.

$$C_{block} = \frac{T_{ecl} \cdot P_{ecl}}{N_{blocks} \cdot \eta_{line} \cdot \text{DoD}} \quad (28)$$

Then, from the specific energy E_s and the energy density E_d (typical values from [21]), it was possible to compute the mass and the volume of the single block, that must multiplied by 7 to find the quantities related to the entire battery pack. The number of cells in series was computed by rounding at the first greater integer the ratio between the nominal bus voltage (28 V) and the voltage of a single cell, value that comes from [35]. Because of the approximation, the real voltage provided by a string had to be recomputed by multiplying the number of cells in a string by their nominal voltage.

Finally, considering a battery pack efficiency of $\mu = 0.8$, the single string capacity was retrieved in order to compute both the number of string in parallel and the real capacity of the block. This procedure is summarised hereafter in Equations 29.

$$C_{string} = \mu \cdot C_{cell} \cdot V_{string} \rightarrow N_{par} = \left\lceil \frac{C_{block}}{C_{string}} \right\rceil \rightarrow C_{block}^{real} = N_{par} \cdot C_{string} \quad (29)$$

¹²This rough estimation was done according to the frame configuration shown in Figure 16

The total number of cells was then computed as the sum of all the cells in a string times the number of strings in a block and then multiplied by the number of blocks.

Sizing Outputs			
mass	35.98 kg	volume	11.55 dm ³
voltage	29.60 V	capacity	100.80 Ah
N_{series}	8	C_{string}	35.52 Wh
N_{par}	12	N_{tot}	672

Table 36: Results of the battery sizing. Mass, volume and capacity refer to the entire battery pack, while number of cells in series and number of strings in parallel refer to the cells' arrangement in a single block.

9.3.6 Sizing Considerations

Solar cells' conversion efficiency is strictly related to the operating temperature: high temperatures lead to a decrement of the efficiency, while low temperatures increase it. However, the sizing was performed without taking into account temperature variations nor transients that could occur in the early phases of solar exposure after an eclipse due to the SA thermal inertia.

Even so, the results are consistent with respect to the real subsystem: from the components' selection and both from the electrical and dimensional points of view. For instance, according to [14], the real mass of the SA (considering the cells and the frame only) is 49.1 kg, the photovoltaic surface 9.81 m² and the number of cells 3696. Indeed, very similar values were obtained from the preliminary sizing. The same can be said for the battery sizing: calculations provided a very accurate mass estimation (the actual one is 36.4 kg [1]) and a capacity estimation totally consistent with LRO requirements, as well as an exact arrangement of cells in a single block, that is 8s12p (i.e. 12 strings of 8 cells each), resulting in a total of 672 cells, if all 7 blocks are considered.

9.4 System Review

The EPS is able to provide power supply to both the spacecraft and its payload during any orbital condition for the whole transfer, exploration and scientific phases. The architecture chosen to achieve the multiple functionalities consisted in:

- DET distribution, chosen due to its higher efficiency, since it's a passive power control system, lower mass and less components onboard.
- 3-panel SA, active during sunlight, with the capability to shunt excess power. Chosen as best primary energy source because of its ability to fully supply the highest demanded power, also granting medium degradation over time. Its peculiar shape is given by the need to ensure the FOV of the wide angle camera. A low IR signature is achieved to enhance compatibility with instruments.
- SA gimbals, to maximise power generation. Due to high sensitivity to solar incidence angle of the primary energy source, they are characterised by high accuracy.
- PSE, to convey the energy to all the electric appliances and provide bus protection.
- Li-Ion Battery, charged by the SA, to provide power during eclipses and during peak power demands. It is characterised by high reliability and efficiency with low self discharge, at the expenses of a higher thermal control required.

10 On-Board Data Handling

LRO Command and Data Handling (C&DH) System is the heart of the control and data flow architecture. It is housed inside a single $41 \times 30 \times 29$ cm enclosure and its functions include [1][37]:

- Hosting ACS and Flight Software (FSW)
- Command acceptance and distribution, telemetry collection, internal bus scheduling, science data storage (384 Gbit) for the instruments
- Provide the interface for low rate telemetry and command/control of spacecraft subsystems
- Provide the interface to the spacecraft communications transmitter and transponder for high speed telemetry
- Provide a mission unique interface to the LAMP instrument as well as timing synchronization to all the instruments
- Science data formatting

Figure 18 depicts a schematic of the interconnections between the C&DH and all the subsystems.

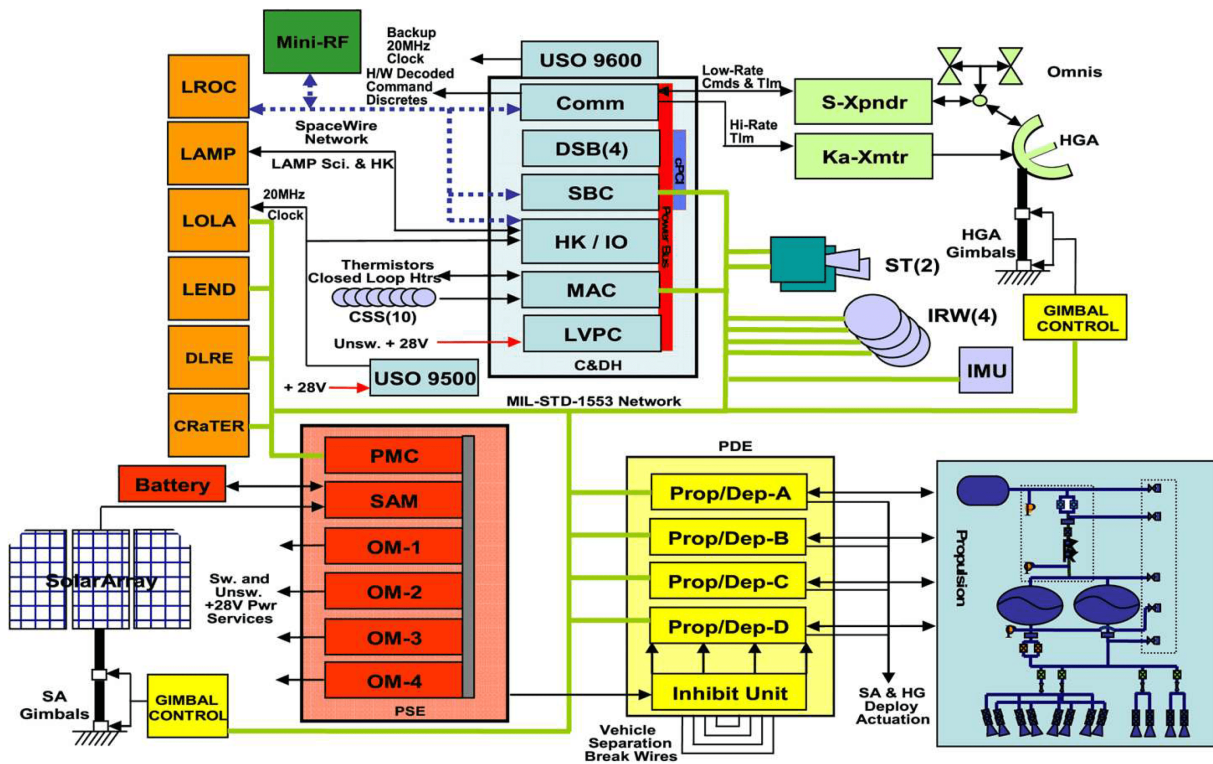
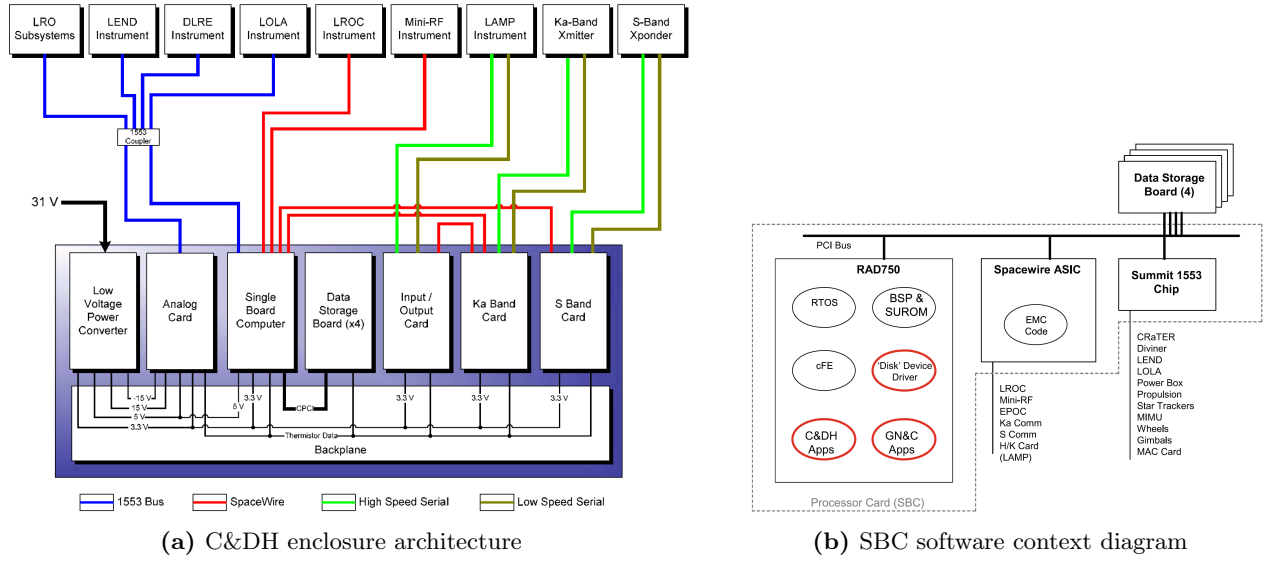


Figure 18: LRO simplified system block diagram

10.1 Architecture

As illustrated in Figures 18 and 19, LRO's C&DH system presents ten sub-assemblies, called Printed Wiring Assemblies (PWAs). In particular, Figure 19 illustrates a top-level block diagram of the C&DH with the LRO avionics and instrument interfaces, highlighting the interconnections between PWAs and other subsystems.

The LRO utilizes a single-string design architecture, except where safety and reliability concerns required additional protection. As a result, the C&DH was built with minimal hardware redundancy. To mitigate the risk associated with this design, autonomous failure detection and handling capabilities, including a low level watchdog hierarchy, were implemented in both hardware and software. [37]



(a) C&DH enclosure architecture

(b) SBC software context diagram

Figure 19: LRO C&DH architecture (sources: [37][1]), a more complete schematic is reported in Figure 30

10.1.1 Components

The C&DH enclosure contains the ten PWAs in a single housing, that are:

- A Low Voltage Power Converter (LVPC), which provides power to all the sub-assemblies except the Primary Ultra-Stable Oscillator (USO);
- A Multi-function Analog Card (MAC), which was custom-designed to manage the wide range of thermal environments in the lunar orbit;
- A Single Board Computer (SBC), the processing platform for the FSW. It utilizes the BAE RAD750 132 MHz 32-bit processor and carries 36 MB of Static Random Access Memory (SRAM) storage to store the executable code and provide backup data storage. In addition, it provides 64 KB of Start-Up Read Only Memory (SUROM) storage for Boot Code and 4 MB of Electrically Erasable Programmable Read Only Memory (EEPROM) of storage for Application Code. It supports performances of 260 MIPS when operating at 132 MHz and higher than 400 MIPS at 200 MHz; it also has a radiation hardness of 200 Krad and an overall TRL of 9 [37][38][39]. This SBC was selected because it was a BAE off-the-shelf product with a high TRL, with the addition of MIL-STD-1553 Bus Controller / Remote Terminal and 4-port SpaceWire (SpW) interfaces;
- Four Data Storage Boardss (DSBs), which operate as a mass storage system for the space- craft. The DSBs are designed to interface with the SBC via a Compact Peripheral Component Interconnect (cPCI) backplane interface;
- A Housekeeping / Input Output (HK/IO) card provides an interface to the LAMP instrument as well as providing synchronisation to all instruments on the spacecraft;
- A communications interface board, which includes S-Band Communication (SComm) and Ka- Band Communication (KaComm) cards, with two independent functions, allowing the addition or deletion of either without redesign;
- A backplane, providing inter-connectivity to all cards within C&DH enclosure.

In addition to these, also the primary and redundant USOs are components of the C&DH subsystem, even though they are externally mounted in separate assemblies. Note that the all the previous components had some level of heritage with previous NASA and/or DoD missions.

10.1.2 Buses

All C&DH components present electrical connections via the backplane for internal power distribution and cPCI bus data transfers.

Instead, the interconnection between C&DH, instruments and the avionics is granted through reliable standard data buses for data transfers and control; more in detail:

- A SpaceWire (SpW) network¹³ is used for high speed data transfers, specifically between the SBC and LROC, Mini-RF, the HK/IO card and the Communication cards;
- A MIL-STD-1553 bus is used for low data rate transfers;
- A combination of synchronous and asynchronous serial data transfers over RS-422 and LVDS electrical interfaces are used to interconnect the C&DH with some of spacecraft subsystems;
- A 32-bit 33 MHz Compact Peripheral Component Interconnect (cPCI) was implemented on the backplane to allow communication between SBC and DSB.

Indeed, this system is versatile and allows the C&DH to incorporate a hybrid implementation in which the SpW network, the 1553 bus, the legacy serial data connections and a cPCI bus are all utilized to interconnect the C&DH with the spacecraft subsystems and instruments.

In addition, the extensive use of SpW (ECSS-E-50-12A / ECSS-E-ST-50-12C) and MIL-STD-1553 allowed expandability and scalability, where late additions of more nodes could have been accommodated anywhere in the spacecraft and attached to the C&DH SpW network seamlessly [37].

Moreover, the use of these industry standard interfaces allowed access to relatively inexpensive and commercially available data simulators for ground support equipment [37].

10.2 System Preliminary Sizing

A preliminary sizing of the C&DH was carried out using an “estimation-by-similarity” approach.

Firstly, each of the LRO subsystems was broken down into its main components/functions; then, for each of them, the source code words, memory data as well as throughput, were estimated by similarity, as reported in Table 44 and 45 in the Appendix.

Secondly, for the most demanding modes of the mission the necessary Read Only Memory (ROM) and Random Access Memory (RAM) were estimated, respectively with Equation 30 and Equation 31.

$$\text{ROM [kB]} = \frac{\text{Code[words]} \cdot 32[\text{bit}/\text{word}]}{8[\text{bit}/\text{byte}] \cdot 1000[\text{byte}/\text{kbyte}]} \quad (30)$$

$$\text{RAM [kB]} = \frac{(\text{Code[words]} + \text{Data[words]}) \cdot 32[\text{bit}/\text{word}]}{8[\text{bit}/\text{byte}] \cdot 1000[\text{byte}/\text{kbyte}]} \quad (31)$$

Similarly, the throughput was computed for each component/function by scaling typical kIPS values found in the literature for an acquisition frequency f_s which depends on the specific component, as shown in Equation 32.

$$\text{throughput [kIPS]} = \frac{\text{kIPS}_{typ} f_s}{f_{typ}} \quad (32)$$

Note that before computing the ROM RAM and throughput required, a margin of 400% was applied to total Code, Data and throughput to take into account possible variability during the design and development process.

The overall results obtained from the analysis¹⁴ are reported in Table 37.

¹³LRO was the first mission in space to use the full network capability of SpaceWire (SpW). [37]

¹⁴The full tables from which the overall results were retrieved can be found in the Appendix.

Mission Mode	Code [kB]	Data [kB]	Throughput [MIPS]	ROM [MB]	RAM [MB]
Observing	3956.8	16192.2	41.6	3.96	20.15
Sun Safe	3764.8	4860.8	37.2	3.77	8.63
Delta-V	4187.2	5451.2	56.4	4.19	9.64
Delta-H	4187.2	5451.2	56.4	4.19	9.64

Table 37: C&DH memory sizing results

10.2.1 Sizing Considerations

The values obtained from the preliminary sizing are consistent with the RAD750 processor, both in terms of memory (ROM and RAM) and throughput, as shown in Table 38.

	Throughput [MIPS]	ROM (EEPROM) [MB]	RAM (SRAM) [MB]
Data	< 260	4	36
Estimated	56.4	3.96	20.15

Table 38: C&DH memory comparison with real data from [37][38][39]

In addition, it can be noted that the Observing mode was a driver for the memory selection, particularly RAM. Indeed, the processor has to handle the large data volume coming from the scientific payload, which then has to be transferred and saved to the DSB [40]. Hence, this justifies the selection for a 36 MB RAM, still granting a large margin for possible unplanned changes. Also, the selected 4 MB of ROM are greatly consistent with the largely-margined estimated value of 3.96 MB. To conclude, throughput was possibly underestimated in this preliminary analysis due to the lack of sufficient data on components working frequencies. Still, it was highly below the threshold of 260 MIPS, further validating the selection of RAD750 processor.

10.3 System Review

Despite its minimal hardware redundancy, the C&DH was capable of performing several sophisticated tasks with a wide margin of tolerance in a small and light structure, thanks to the versatile architecture and the use of industry standards. The modular structure made the system flexible, reduced the risks of design errors and simplified the test phase, also allowing a possible re-use of the architecture in other NASA missions with similar requirements[37]. The main components are summarised hereafter:

- SBC, the most suitable product on the market during the design phase with a very high TRL, used to process the information of all the systems with extended capability.
- Four DSBs, to store the instruments data between successive down-links.
- the PWAs, dedicated to Voltage regulation, I/O, communications and multiple other functions, allowing for a modular architecture.
- the busses, especially SpW and MIL-STD-1553, intensively used to allow expandability, scalability as well as to provide a standard interface between subsystems.
- Different interface boards, to provide synchronisation and compatibility between each spacecraft component and the SBC.

11 Configurations

The LRO is characterised by a modular structure, with subsystems grouped in separated modules that include plumbing, thermal control and wiring connecting each internal element. This solution allows independent assembly and proof testing, with the need to only design the interfaces. Then, the spacecraft is assembled according to the needs of each module.

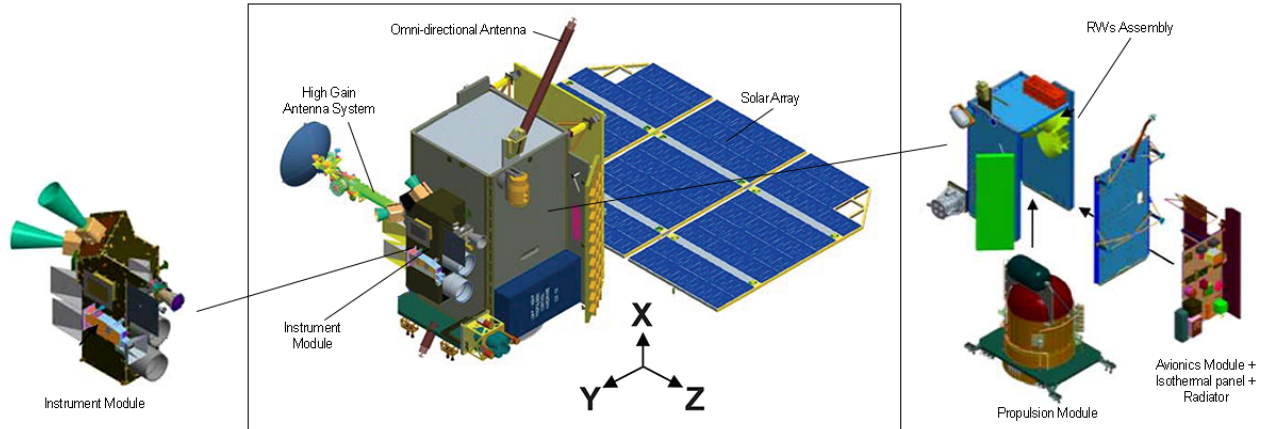


Figure 20: LRO design overview showing modular construction [1]

11.1 Launch Configuration

As it can be seen in Figure 21, the stowed Lunar Reconnaissance Orbiter (LRO) in launch configuration is placed above the Lunar Crater Observation and Sensing Satellite (LCROSS), with the interface between the two spacecrafts located at the -X face of the former. The LCROSS is then linked to the spacecraft through an adapter. The LRO position supports the Lunar Orbit Insertion (LOI) manoeuvres to be performed.

In order to achieve the stowed configuration, the SA and the HGA are retracted through the use of different gimbals, which are located along the arm of the antenna and between the faces of the solar panel; these are also used to move and point the components during the whole mission.

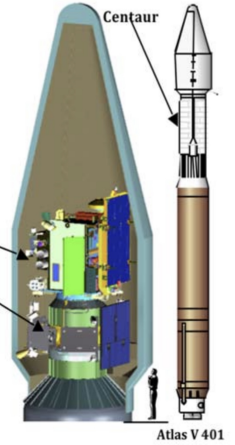


Figure 21: LRO Launch configuration

11.2 Propulsion System (PS)

The PS assembly is placed at the core of the spacecraft, accommodating as much hardware as possible in a compact configuration through a stacked tank structure. The location of the main components is explained hereafter:

- 8 ACS Thruster (AT) are located at the four corners of the spacecraft's aft face (-X face) and are tilted of 15° towards the symmetry axis of the spacecraft, increasing the thrusters' moment arm about the centre of mass.
- 4 Insertion Thruster (NT) are positioned in a diamond configuration on the same face of AT and arranged to minimise the torsional motion generated during orbit insertion manoeuvres.
- Two Hydrazine tanks are placed one over the other at the centre of the spacecraft's aft deck to reduce the effects of the propellant on the inertia properties of the orbiter. A Helium tank is then situated above them for the same rationale, slightly shifted towards the +Y face for the sensor installation on the Avionics Panel.

11.3 Tracking, Telemetry and Telecommand (TTMTC)

The TTMTC location is highly dependant on the variable orientation between Earth and the space-craft, with the need to both transmit high amount of data during nominal operations and vital information during Sun Safe mode. This led to the following arrangement:

- An High Gain Antenna (HGA) is placed on the -Z face, opposite with respect to the instruments FOV, with a deployable arm able to accurately face Earth despite the continuous nadir-pointing operations. The component is independent in terms of thermal control, capable to dissipate its own internal heat, and is located in such a way to not shadow the solar panel.
- Two Omni-Directional Antennas (ODAs) are positioned in such a way to not have their field of view limited by the on-board instruments and sensors, since they're needed in critical situations and characterised by mild power. They are integrated in the Propulsion Module because of the its central position.
- A Laser Ranging Telescope (LRT), in charge of precise orbit determination and tracking, is mounted on the HGA because of the continuous Earth pointing of the assembly.
- A Traveling Wave Tube Amplifier (TWTA) is placed in the proximity of the HGA in order to minimize cable losses and noise.

11.4 Attitude and Orbit Control System (AOCS)

The AOCS is composed by different sensors and actuators, each with specific requirements:

- The 2 Autonomous-Star Trackers (A-STRs) are the most critical sensors to be located since they must be protected from high energy sources. Hence, they are placed on the Instrument Module on the +Y face, the opposite side with respect to the solar panel, pointing outwards and aligned 60° apart to provide a measure even when one of the two is occulted by Earth, Sun or the Moon.
- 10 Coarse Sun Sensors (CSSs) are scattered in every corner of the spacecraft and on the solar panel in order to provide the correct orientation of the latter with respect to the Sun and to guarantee the measurement of at least 3 sensors to estimate the Sun relative position. Moreover, their information are used to shield the A-STRs in case of high energy source pointing.
- An Inertial Measurement Unit (IMU) is mounted on the LRO Avionics Panel on the -Y face, the closest to the centre of mass to provide more accurate measurement of the accelerations.
- Four Reaction Wheels (RWs) are arranged in a pyramid configuration (with the apex aligned with the +X body axis of the spacecraft) and attached to the Avionics Panel too, to provide very quiet, smooth changes in the spacecraft pointing thanks to the proximity of the centre of mass. The assembly is concentrated in one point also to perform an easier thermal regulation.
- A Propulsion-Deploy Electronics (PDE) is placed on the Avionics Panel in a central position due to its numerous functionalities that involve different subsystems: this component commands the thrusters firings and the opening of the pressurization tank, orders the deployment of the SA and HGA and prevents RF transmitters from functioning until launch vehicle fairing separation. Due to its importance it was designed with four identical electronic boards.

11.5 Thermal Control System (TCS)

The TCS is widely distributed inside the spacecraft in order to maintain the temperatures of each component within allowable limits through heaters and heat pipes, and transfer the heat produced through precise thermal paths. In detail:

- A radiator assembly is integrated on the zenith face of the orbiter (-Z face) to provide the minimal exposure to the lunar environment and enhance exchange with the deep space. Dedicated heat pipes transport heat from the Instrument Module, the battery pack and the Avionics Module to each radiator.

- Multiple layers of MLI are extensively used around and/or inside the spacecraft (e.g. the PS is wrapped in the insulator) in order to prevent strong heat dissipation towards the deep space.
- The Avionics Module and the RWs are wrapped around the propulsion system to minimize temperature variations during an orbit, exploiting the heating of the latter that has to prevent the freezing of the propellant.
- Each deployable device (HGA and SA) is designed with dedicated heaters and radiators to be independent from the main spacecraft in terms of thermal control, avoiding heat paths passing close to instruments and sensors.

11.6 Electric Power System (EPS)

The EPS is arranged in order to gather the maximum electrical power from the Sun with the minimum cable losses possible.

- A Solar Array (SA), primary energy source of the LRO, is attached to the -Y face through gimbals in order to constantly maintain the correct pointing towards the Sun along an orbit. In addition, the panel presents cut edges not to interfere with LROC FOV.
- A Li-Ion battery, secondary energy source, is placed on the Avionics Module (the -Y face) to minimize the distance from the solar panel and the sensors to which it has to provide power during eclipses, thus minimizing cable losses.

11.7 Command and Data Handling (C&DH)

The C&DH is the heart of the control and processing data of the spacecraft, hence its components are spread in every corner of the LRO to collect and send information:

- The C&DH enclosure is placed on the Avionics Module (-Y face), close to energy sources, due to its high power, heat production and dissipation requirements and close to the centre of mass, due to its high weight.
- A SpaceWire (SpW) network is established between the SBC and LROC, Mini-RF, the HK/IO card and the Communication cards to allow and manage high speed and high volume data transfers, granting the use of standardised interfaces.

11.8 Scientific Payload

The instruments LOLA, LROC, LAMP are located on a separated optical bench on the +Y face (the Instrument Module), which allows independent testing. Different rationales led this accommodation:

- Very high accuracy alignment required, so an independent panel has been developed.
- The FOV of each instrument, both nadir and inertial pointing, is clear of any impingement.
- Sun avoidance to protect optical instruments is satisfied, being the +Y face opposite to the Sun direction.
- The mechanical structure that supports the bench is built in aluminum honeycomb panels with *M55J* (High Modulus Carbon Fiber) skin, which allows to withstand the most extreme thermal environment without losing too much in pointing accuracy and to decouple the instruments from the rest of the structure.
- Thermally isolated instruments are guaranteed of a view factor towards deep space for their radiators, while thermally coupled ones can be located close to each other.

The remaining instruments, CRaTER, DLRE, Mini-RF and LEND, are mounted on the main Orbiter structure on the +Z and on the +Y faces. This choice is made due to lower accuracy required, although independent thermal control through radiators and heaters could be achieved.

11.9 Mass Budget

Table 39 reports the mass budget of the LRO spacecraft, divided into the main subsystems.

subsystem	component	Data [kg]	Computed [kg]	notes
PS	AT	4.72	-	
	NT	4.8	-	
	PDE	14	-	
	Tank He	12.7	-	
	Tank N2H4	70	7.78	computed (min. req.)
	Prop hardware	16	-	
	Lines and fittings	7.2	13.3	10% of PS mass
	subsystem total	129.4	n/a	
TTMTC	% of dry mass	12.7%	13%	*
	HGA assembly	38.2	-	
	Ka comm	6.2	6.5	from Fig.13-15 [21]
	S comm	10.7	-	
	laser ranging	1.2	-	
	other	10	-	
	subsystem total	66.3	n/a	
	% of dry mass	6.5%	6%	*
AOCS	A-STR	6	-	
	IMU	4.5	-	
	RW	48	-	
	Sun Sensors	0.12	-	
	other	26	-	
	subsystem total	84.6	n/a	
	% of dry mass	8.3%	9%	*
	thermal	22.8	-	
TCS	other	15	-	
	subsystem total	37.8	n/a	
	% of dry mass	3.7%	3%	*
EPS	PSE	16.1	-	
	SA Assembly	75.8	48.79	cells and frame masses only
	Battery	30	35.98	computed
	other	75	-	
	subsystem total	196.9	n/a	
	% of dry mass	19.3%	19%	*
C&DH	C&DH	21.2	-	
	other (plus cabling)	104	-	
	subsystem total	125.2	n/a	
	% of dry mass	12.3%	13%	*
P/L	CRaTER	5.6	-	
	Diviner	10	-	
	LAMP	5	-	
	LEND	23.7	-	
	LOLA	10.7	-	
	LROC	14.4	-	
	Mini-RF	10.5	-	
	other	29	-	
	subsystem total	108.9	n/a	
	% of dry mass	10.7%	11%	*
STRUCT	Harness	36	-	
	Bus structure	232.9	-	
	subsystem total	268.9	n/a	
	% of dry mass	26.4%	26%	*
TOTAL MASS		1018.0	n/a	
TOTAL %		100.0%	100%	

Table 39: Dry mass budget comparison between theoretical/computed and real data [14][1]. * the % of dry mass was retrieved from statistical data of satellites with similar mission to LRO

12 References

- [1] Craig R. Tooley et al. “Lunar Reconnaissance Orbiter Mission and Spacecraft Design”. In: *Space Science Reviews* 150.1 (Jan. 2010), pp. 23–62. ISSN: 1572-9672. DOI: 10.1007/s11214-009-9624-4. URL: <https://doi.org/10.1007/s11214-009-9624-4>.
- [2] NASA. *The Vision for Space Exploration*. URL: https://www.nasa.gov/pdf/55583main_vision_space_exploration2.pdf. (accessed: 2023.04.01).
- [3] Stewart Nozette et al. “The Lunar Reconnaissance Orbiter Miniature Radio Frequency (Mini-RF) Technology Demonstration”. In: *Space Science Reviews* 150 (Jan. 2010), pp. 285–302. DOI: 10.1007/s11214-009-9607-5.
- [4] eoPortal. *LRO (Lunar Reconnaissance Orbiter)*. URL: <https://www.eoportal.org/satellite-missions/lro>. (accessed: 2023.03.23).
- [5] Gordon Chin et al. “Lunar Reconnaissance Orbiter Overview: The Instrument Suite and Mission”. In: *Space Science Reviews* 129.4 (Apr. 2007), pp. 391–419. ISSN: 1572-9672. DOI: 10.1007/s11214-007-9153-y. URL: <https://doi.org/10.1007/s11214-007-9153-y>.
- [6] NASA. *LRO Operations Concept*. URL: <https://player.slideplayer.com/24/7115894/>. (accessed: 2023.04.06).
- [7] NASA. *LRO Mission Concept of Operations Summary*. URL: <https://slideplayer.com/slide/8105754/>. (accessed: 2023.04.07).
- [8] United Launch Alliance. *Atlas V Launch Services User’s Guide*. URL: <https://www.ulalaunch.com/docs/default-source/rockets/atlasvusersguide2010.pdf>. (accessed: 2023.04.05).
- [9] Martin B Houghton, Craig R Tooley, and Richard S Saylor Jr. “Mission design and operations considerations for NASA’s Lunar Reconnaissance Orbiter”. In: *58th International Astronautical Congress, Hyderabad, India*. 2007, pp. 24–28. URL: https://lunar.gsfc.nasa.gov/library/IAC-07-C1_7_06.pdf.
- [10] Michael Mesarch et al. “Maneuver Operations Results from the Lunar Reconnaissance Orbiter (LRO) Mission”. In: *SpaceOps 2010 Conference* (2010). DOI: 10.2514/6.2010-1985. URL: <https://arc.aiaa.org/doi/abs/10.2514/6.2010-1985>.
- [11] Mark Beckman. “Mission Design for the Lunar Reconnaissance Orbiter”. In: *29th ANNUAL AAS GUIDANCE AND CONTROL CONFERENCE*. Feb. 2006. URL: https://lunar.gsfc.nasa.gov/library/LRO_AAS_Paper_07-057.pdf.
- [12] J. Kreitzman et al. “Mission opportunities to trans-neptunian objects - Part III, orbital capture, low-thrust trajectories and vehicle radiation environment during jovian flyby”. In: *2013 Astrodynamics Specialists Conference*. Vol. 150. Aug. 2013, pp. 1487–1506. URL: https://www.researchgate.net/publication/293081475_Mission_opportunities_to_trans-neptunian_objects_-_Part_III_orbital_capture_low-thrust_trajectories_and_vehicle_radiation_environment_during_jovian_flyby.
- [13] Mark Fiebig and Charles Zakrzewski. “LRO Propulsion System Design & On-Orbit Operations”. In: *48th AIAA/ASME/SAE/ASEE Joint Propulsion Conference & Exhibit*. Sept. 2012. DOI: 10.2514/6.2012-4330. URL: <https://arc.aiaa.org/doi/pdf/10.2514/6.2012-4330>.
- [14] NASA. *LRO Preliminary Design Review Payload Systems Overview*. URL: <https://studylib.net/doc/25389652/day-2>. (accessed: 2023.04.10).
- [15] Moog Inc. *MONARC-90LT*. URL: <https://satsearch.co/products/moog-monarc-90lt>. (accessed: 2023.04.15).
- [16] Aerojet Rocketdyne. *MR-106L 22N*. URL: <https://www.satcatalog.com/component/mr-106l-22n/>. (accessed: 2023.04.15).

- [17] Yinan Qiu et al. “Experimental investigation on the temperature and pressure characteristics of supercritical helium for liquid hydrogen pressurisation”. In: *Journal of Energy Storage* 46 (2022). ISSN: 2352-152X. DOI: <https://doi.org/10.1016/j.est.2021.103895>. URL: <https://www.sciencedirect.com/science/article/pii/S2352152X21015607>.
- [18] NASA. “Lunar Reconnaissance Orbiter (LRO): Leading NASA’s Way Back to the Moon”. In: *LRO/LCROSS press conference* (2009), pp. 5–25. URL: https://www.nasa.gov/pdf/360020main_LRO_LCROSS_presskit2.pdf.
- [19] ESA. *Margin philosophy for science assessment studies*. URL: https://sci.esa.int/documents/34375/36249/1567260131067-Margin_philosophy_for_science_assessment_studies_1.3.pdf. (accessed: 2023.04.28).
- [20] Northrop Grumman. *Diaphragm Tanks Data Sheets – Sorted by Part Number*. URL: <https://www.northropgrumman.com/space/diaphragm-tanks-data-sheets-sorted-by-part-number/>. (accessed: 2023.04.29).
- [21] James R. Wertz and Wiley J. Larson. *Space Mission Engineering: The New SMAD*. 3rd ed. Space Technology Library, 2011. ISBN: 9781881883159.
- [22] Steve Currier et al. “NASA Ground Network Support of the Lunar Reconnaissance Orbiter Mission”. In: *SpaceOps 2006 Conference*. DOI: 10.2514/6.2006-5819. URL: <https://arc.aiaa.org/doi/abs/10.2514/6.2006-5819>.
- [23] *Low-Earth Orbit (LEO) 26 GHz K-band Study Group Final Report*. Tech. rep. May 2013. URL: https://www.ioag.org/Public%20Documents/2019-02-22_LE026SG_Report_Final.pdf.
- [24] Neerav Shah et al. *Launch and Commissioning of the Lunar Reconnaissance Orbiter (LRO)*. Tech. rep. 20100014880. NASA, Feb. 2010. URL: <https://ntrs.nasa.gov/citations/20100014880>.
- [25] Philip C. Calhoun and Joseph C. Garrick. *Observing Mode Attitude Controller for the Lunar Reconnaissance Orbiter*. Tech. rep. 20080012716. NASA, Sept. 2007. URL: <https://ntrs.nasa.gov/citations/20080012716>.
- [26] Roland Burton et al. “State of the Art in Guidance, Navigation and Control: A Survey of Small Satellite GNC Components”. In: Feb. 2016.
- [27] Russell R. DeHart. *Prediction of Lunar Reconnaissance Orbiter Reaction Wheel Assembly Angular Momentum Using Regression Analysis*. Tech. rep. 20180002084. NASA, Jan. 2017. URL: <https://ntrs.nasa.gov/citations/20180002084>.
- [28] Erik Stalcup. *Lunar Thermal Environment - NASA*. URL: https://www.nasa.gov/sites/default/files/atoms/files/ericstalcup_lunar_thermal_environment_v2.pdf. (accessed: 2023.05.15).
- [29] Che-Shing Kang. “Multilayer Insulation for Spacecraft Applications”. In: *Microsatellites as Research Tools*. Ed. by Fei-Bin Hsiao. Vol. 10. COSPAR Colloquia Series. Pergamon, 1999, pp. 175–179. DOI: [https://doi.org/10.1016/S0964-2749\(99\)80023-7](https://doi.org/10.1016/S0964-2749(99)80023-7). URL: <https://www.sciencedirect.com/science/article/pii/S0964274999800237>.
- [30] J. H. Henninger. *Solar absorptance and thermal emittance of some common spacecraft thermal-control coatings*. URL: <https://ntrs.nasa.gov/citations/19840015630>.
- [31] K.P. Sibin et al. “Optical and electrical properties of ITO thin films sputtered on flexible FEP substrate as passive thermal control system for space applications”. In: *Solar Energy Materials and Solar Cells* 145 (2016), pp. 314–322. ISSN: 0927-0248. DOI: <https://doi.org/10.1016/j.solmat.2015.10.035>. URL: <https://www.sciencedirect.com/science/article/pii/S0927024815005462>.
- [32] NASA. *Technical Resource Allocations Specification*. URL: <https://studylib.net/doc/15969064/>. (accessed: 2023.05.26).

- [33] C.L. Baker et al. *General Thermal Subsystem Specification*. URL: <https://studylib.net/doc/15969055/>. (accessed: 2023.05.31).
- [34] T. Spitzer, M. Pryzby, and C. Tooley. *Electrical Power Subsystem Specification*. URL: https://snebulos.mit.edu/projects/crater/file_cabinet/0/02002/02002_02_r-m.pdf. (accessed: 2023.05.31).
- [35] EnerSys Advanced Systems - ABSL Space Products. *Product Data Sheet Li-ion Rechargeable Battery ABSL 8s84p 28V 126Ah*. URL: https://www.enersys.com/493bb4/globalassets/documents/product-documentation/absl/amer/am-absl-8s84p-f1-aa_0320.pdf. (accessed: 2023.05.27).
- [36] Daniel C. Law et al. “Lightweight, Flexible, High-Efficiency III-V Multijunction Cells”. In: *2006 IEEE 4th World Conference on Photovoltaic Energy Conference*. Vol. 2. 2006, pp. 1879–1882. DOI: 10.1109/WCPEC.2006.279862.
- [37] Quang Nguyen et al. “A High Performance Command and Data Handling System For NASA’s Lunar Reconnaissance Orbiter”. In: *AIAA SPACE 2008 Conference & Exposition*. DOI: 10.2514/6.2008-7926. URL: <https://arc.aiaa.org/doi/abs/10.2514/6.2008-7926>.
- [38] BAE Systems. *RAD750 6U CompactPCI extended single-board computer*. URL: <https://www.baesystems.com/en-media/uploadFile/20210404051009/1434555675344.pdf>. (accessed: 2023.06.01).
- [39] BAE Systems. *RAD750 radiation-hardened PowerPC microprocessor*. URL: <https://www.baesystems.com/en-media/uploadFile/20210404045936/1434555668211.pdf>. (accessed: 2023.06.01).
- [40] BAE Systems. *RAD750 SpaceWire Enabled Flight Computer for Lunar Reconnaissance Orbiter*. URL: <http://2007.spacewire-conference.org/proceedings/Presentations/Onboard%20Equipment%20and%20Software/berger.pdf>. (accessed: 2023.06.03).

13 Appendix

13.1 Mission Profile Overview

13.1.1 Launch

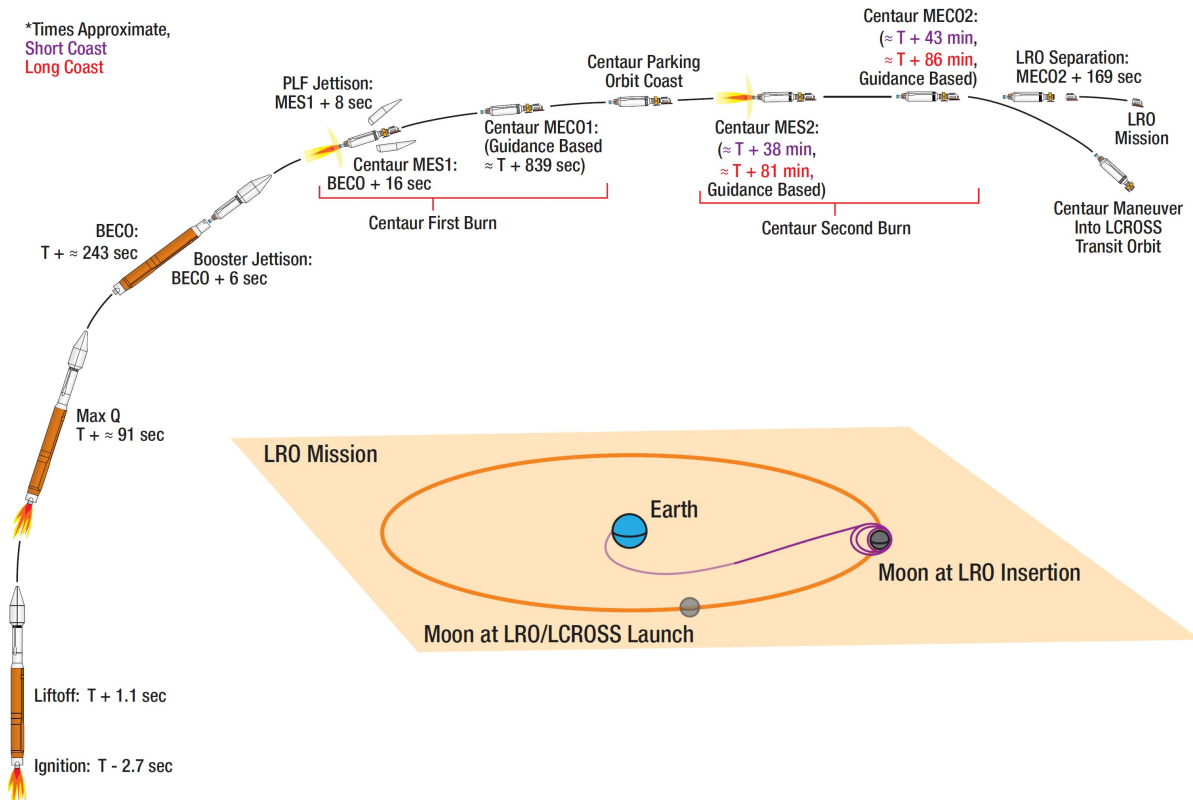


Figure 22: Mission Profile

Table 40 presents a preliminary analysis of the Δv produced by the launcher.

Δv budget	Δv [m/s]
Provided by launcher	12 919.0
To achieve a circular 185 km orbit	7500.0
To reach 35000 x 185 parking orbit	2447.8
To insert into lunar transfer	2550.8
Remaining	420.6

Table 40: Δv computed through Tsiolkovsky equation knowing the masses of the launcher. All Δv are retrieved for a worst case scenario. [8]

13.1.2 Lunar Orbit Insertion

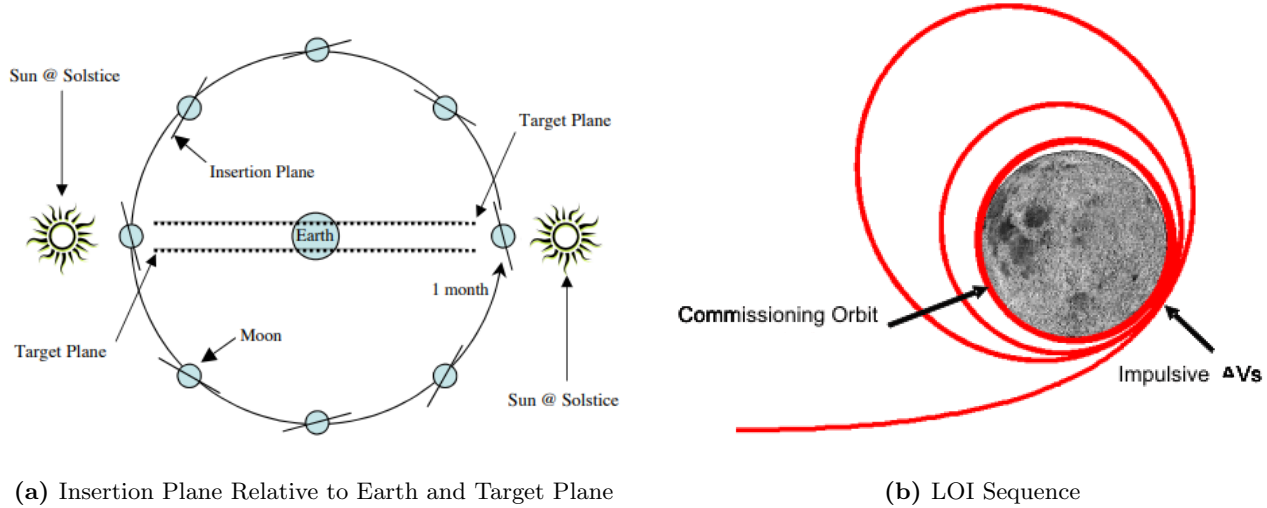


Figure 23: LRO Lunar Orbit Insertion

13.1.3 Station Keeping Manoeuvre

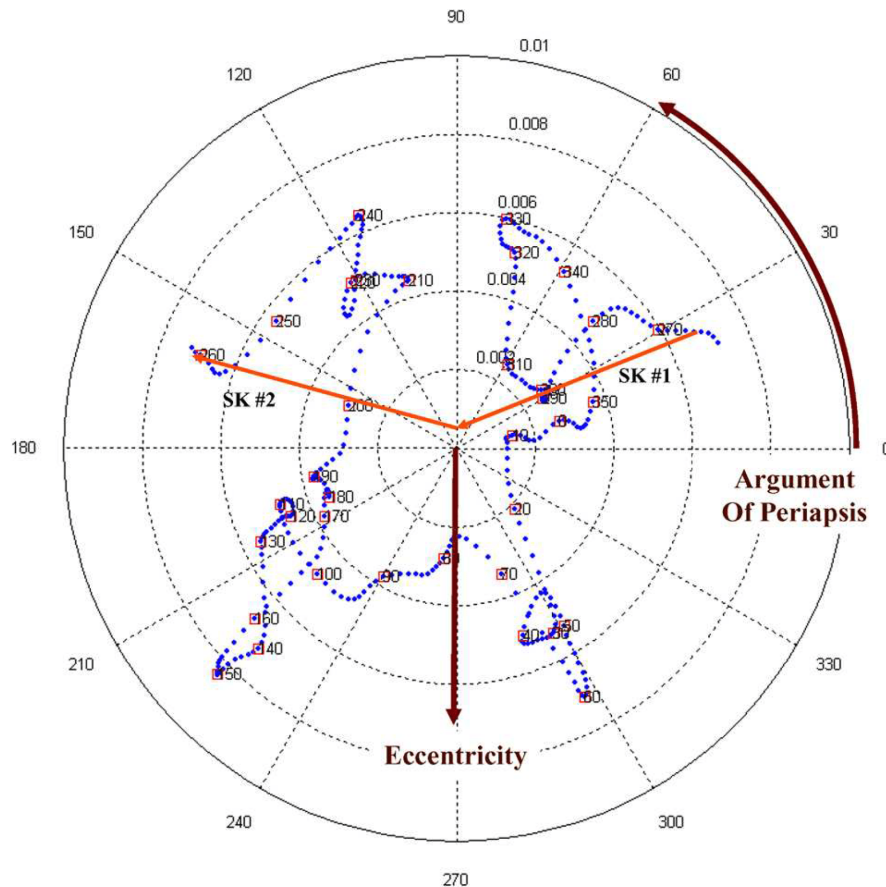


Figure 24: Effects of perturbations on Mission Orbit [9]

13.2 Spacecraft Overview

13.3 Tracking, Telemetry and Telecommand System

13.3.1 Scientific Data Volume

Data Source	Data per Orbit [Gbits]	Data per Day [Gbits]
CRaTER	0.61020	7.78
DLRE	0.18052	2.30
LAMP	0.16822	2.14
LEND	0.02052	0.26
LOLA	0.22629	2.88
LROC	34.65916	441.67
House-Keeping	0.37965	4.84
Total [Gbits]	36.24	461.87

Table 41: Breakdown of LRO's daily data volume (source: [1])

13.3.2 Ka-band down-link usage

As it can be noticed, while the first two passes are almost fully exploited to transmit the majority of the data stored on-board, only a small portion of the other windows are used. Indeed, only a small amount of data was still inside the memory after the first two passes, and the amount of data accumulated by the instruments during a single visibility window was quite small.

Passes	2	3	4	5	6
Number	Pass utilization in minutes				
1	45.0	45.0	45.0	45.0	45.0
2	40.1	33.4	26.7	20.0	13.3
3	-	6.7	6.7	6.7	6.7
4	-	-	6.7	6.7	6.7
5	-	-	-	6.7	6.7
6	-	-	-	-	6.7
Used [%]	96.4	63.0	43.7	37.8	31.5

Table 42: Ka-band down-link utilization

13.3.3 WS1 Ground Station Antenna Characteristics

Characteristics	Ka-band	S-band (telemetry)	S-band (command)
Frequency [GHz]	25.5—27	2.2—2.3	2.025—2.120
Gain [dB]	70.5	50	49
Beamwidth [deg]	0.04	0.5	0.56
G/T [dB/K]	46.98 (10° elevation)*	29.6 (minimum at 5° elevation)*	n/a
Max. EIRP [dBW]	n/a	n/a	79

* Clear sky

Table 43: WS1 characteristics

13.3.4 System Integration

Figure 25 shows the integration of the TTMTC system, particularly the position of the ODAs, the HGA and the on-board avionics panel.

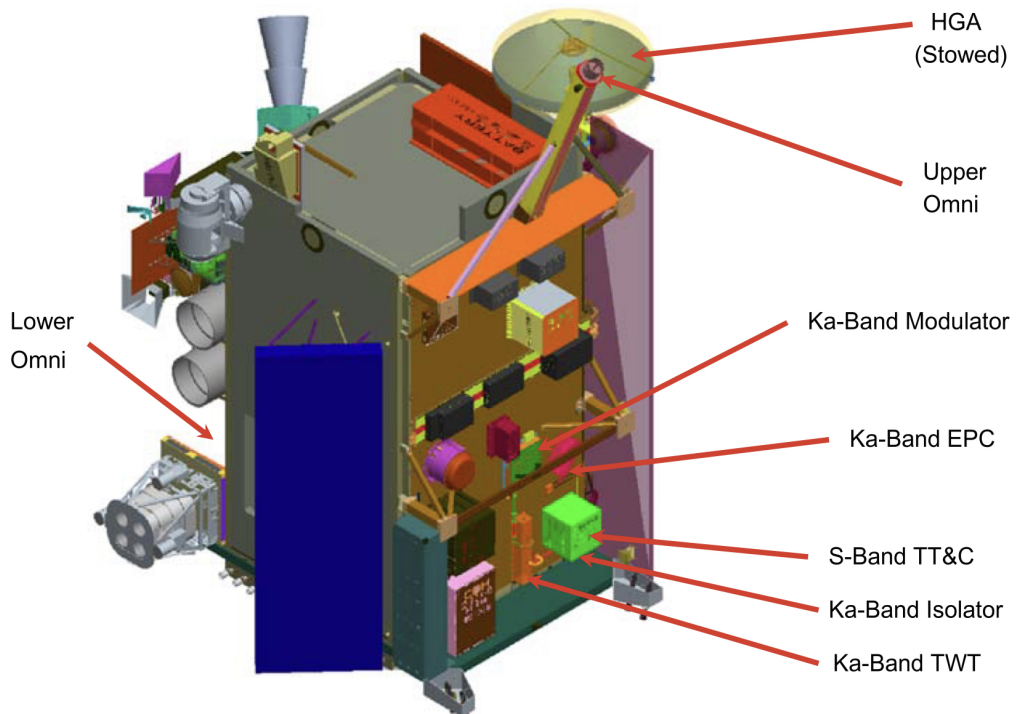
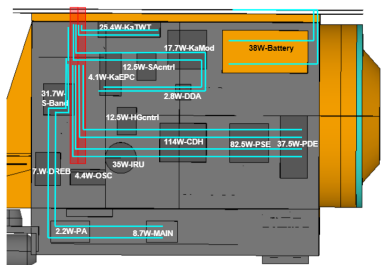
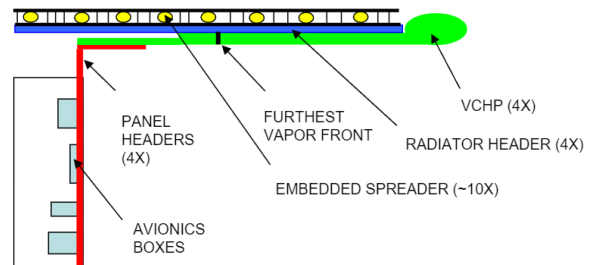


Figure 25: Lunar Reconnaissance Orbiter

13.3.5 Thermal Control System



(a) Avionics Panel Heat Pipe Network



(b) Avionics Radiator

Figure 26: Avionics TCS (source: [14])



Figure 27: LRO MLI

13.4 Electric Power System

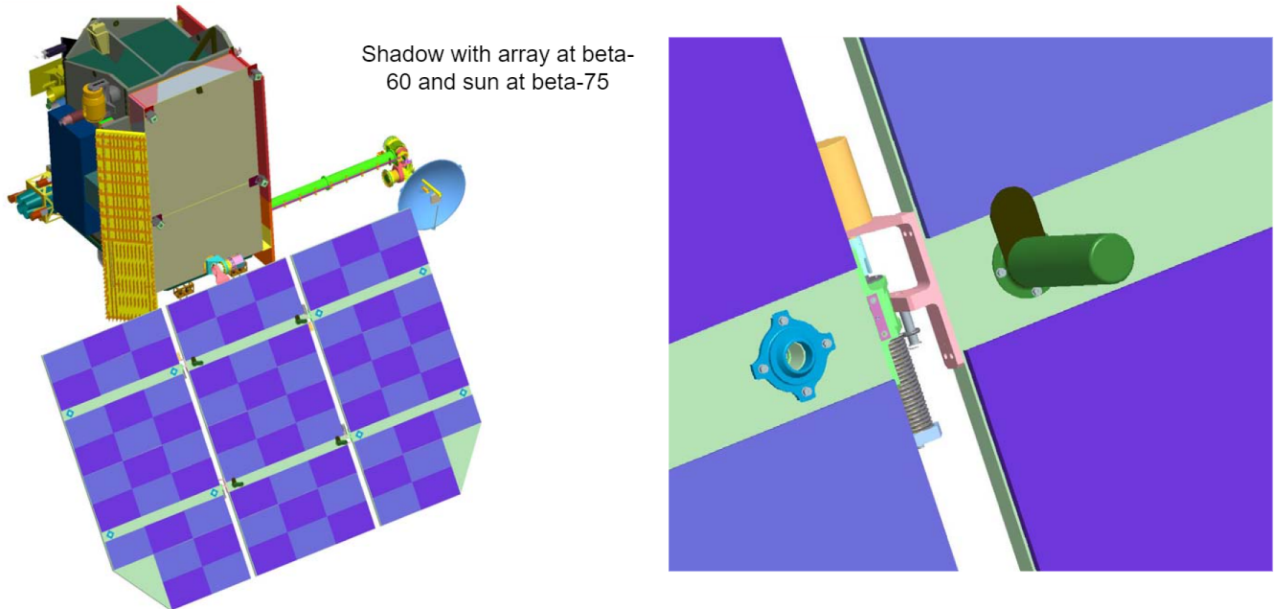


Figure 28: SA containment canisters for the restraint bolts, shadowing 4 solar cells [14]

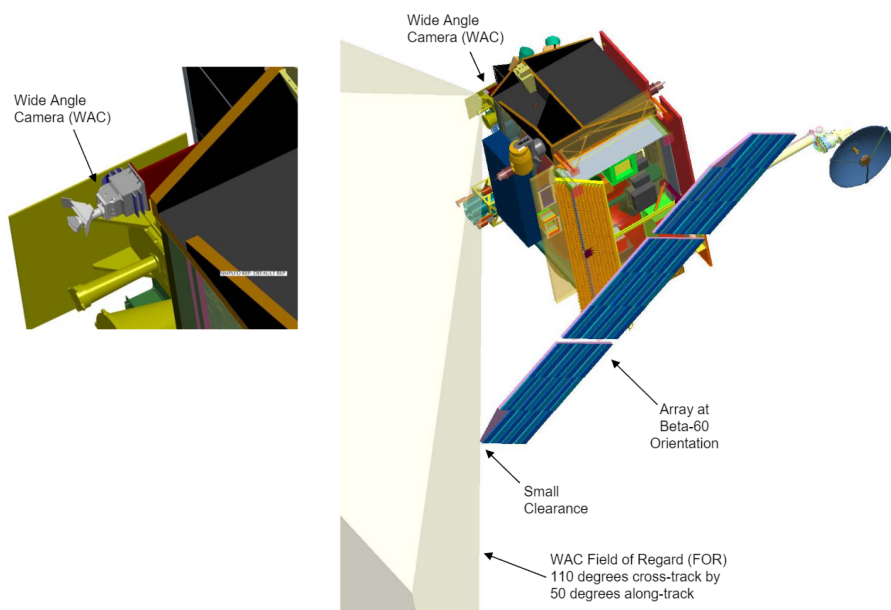


Figure 29: SA issue with LROC FOV[14]

13.5 Command and Data Handling

Tables 44 and 45 present the data used for C&DH sizing.

OBDH Throughput Computation								
System	Components	qty	Code [words]	Data [words]	Typical kIPS	Typical Frequency [Hz]	Acquisition Frequency [Hz]	kIPS
ADCS	Reaction Wheels Control	4	1000	300	5	2	100	250
	Thruster Control	12	600	400	1.2	2	10	6
	Star Tracker	2	3000	15000	2	0.01	10	2000
	IMU	1	800	500	9	10	100	90
	Coarse Sun Sensors	10	500	100	1	1	10	10
	Attitude Determination	1	15000	3500	150	10	10	150
	Attitude Control	1	25000	4200	60	10	10	60
	Kinematic Integration	1	2000	200	15	10	10	15
	Error Determination	1	1000	100	12	10	10	12
	Complex Ephemerides	1	4500	2500	4	0.5	1	8
	Kalman Filter	1	10000	1000	80	0.01	0.01	80
	Orbit Propagation	1	13000	4000	20	1	1	20
	Tot		93500	53000	-	-	-	5607
PS	Latch valve	19	800	1500	3	0.1	1	30
	Pressure regulator	2	800	1500	3	0.1	1	30
	AT	8	1200	1500	5	0.1	10	500
	NT	4	1200	1500	5	0.1	1	50
	PDE	1	600	400	1.2	2	2	1.2
	Pressure Transducer	2	800	1500	3	0.1	1	30
EPS	Tot		33400	52900	-	-	-	4891.2
	Power Monitor Card	1	1200	500	5	1	1	5
	Power Subsystem Electronics	1	1200	500	5	1	1	5
	SA Gimbal	2	1000	2000	15	5	10	30
TCS	Tot		4400	5000	-	-	-	70
	Heater (Thermal Control)	20	800	1500	3	0.1	0.1	3
TTMTC	Tot		16000	30000	-	-	-	60
	Transponder	1	1000	4000	7	10	10	7
	Uplink Card	1	2000	4000	7	10	10	7
	Dowlink Card	1	2000	4000	7	10	10	7
	HGA Gimbal	2	1000	2000	15	5	10	30
System	Tot		7000	16000	-	-	-	81
	Complex Autonomy	1	15000	10000	20	10	10	20
	Fault Detection	10	4000	1000	15	5	10	30
	Fault Correction	10	2000	10000	5	5	10	10
	Executive	2	3500	2000	60	10	100	600
	Run Time Kernel	1	8000	4000	60	10	100	600
	Math Utilities	1	1200	200	0.5	0.1	10	50
	Test and Diagnostic	4	800	400	0.5	0.1	10	50
Payload	I/O Device Handlers	10	2000	7000	50	5	10	100
	Tot		114400	199800	-	-	-	3470
	CRaTER	1	1500	11255.8	n/a	n/a	n/a	n/a
Payload	Diviner	1	1500	3327.5	n/a	n/a	n/a	n/a
	LAMP	1	1500	3096.1	n/a	n/a	n/a	n/a
	LEND	1	1500	376.2	n/a	n/a	n/a	n/a
	LOLA	1	1500	4166.7	n/a	n/a	n/a	n/a
	LROC	1	1500	638990.2	n/a	n/a	n/a	n/a
	Mini-RF	1	1500	0.03	n/a	n/a	n/a	n/a
	HK data collection	1	500	7002.31	50	5	10	100
	Data Handling and Storage	10	100	4000.0	50	5	10	100
	Tot		12000	708214.7	-	-	-	1100

Table 44: OBDH Throughput Computation

Memory Sizing								
Mode	Subsystem	On/Off	Throughput [kIPS]	Margined	Code [words]	Margined	Data [words]	Margined
Observing	ADCS	1	5607	22428	93500	374000	53000	212000
	PS	0	0	0	0	0	0	0
	EPS	1	70	280	4400	17600	5000	20000
	TCS	1	60	240	16000	64000	30000	120000
	TTMTC	1	81	324	7000	28000	16000	64000
	System	1	3470	13880	114400	457600	199800	799200
	Payload	1	1100	4400	12000	48000	708214.7	2832858.9
	Tot		10388	41552	247300	989200	1012014.7	4048058.9
Sun Safe	ADCS	1	5607	22428	93500	374000	53000	212000
	PS	0	0	0	0	0	0	0
	EPS	1	70	280	4400	17600	5000	20000
	TCS	1	60	240	16000	64000	30000	120000
	TTMTC	1	81	324	7000	28000	16000	64000
	System	1	3470	13880	114400	457600	199800	799200
	Payload	0	0	0	0	0	0	0
	Tot		9288	37152	235300	941200	303800	1215200
Delta V	ADCS	1	5607	22428	93500	374000	53000	212000
	PS	1	4891.2	19564.8	33400	133600	52900	211600
	EPS	1	70	280	4400	17600	5000	20000
	TCS	1	60	240	16000	64000	30000	120000
	TTMTC	0	0	0	0	0	0	0
	System	1	3470	13880	114400	457600	199800	799200
	Payload	0	0	0	0	0	0	0
	Tot		14098.2	56392.8	261700	1046800	340700	1362800
Delta H	ADCS	1	5607	22428	93500	374000	53000	212000
	PS	1	4891.2	19564.8	33400	133600	52900	211600
	EPS	1	70	280	4400	17600	5000	20000
	TCS	1	60	240	16000	64000	30000	120000
	TTMTC	0	0	0	0	0	0	0
	System	1	3470	13880	114400	457600	199800	799200
	Payload	0	0	0	0	0	0	0
	Tot		14098.2	56392.8	261700	1046800	340700	1362800

Table 45: OBDH Memory Budget Computation (margined values use 400% margin)

Figure 30 represents the schematic of the C&DH System.

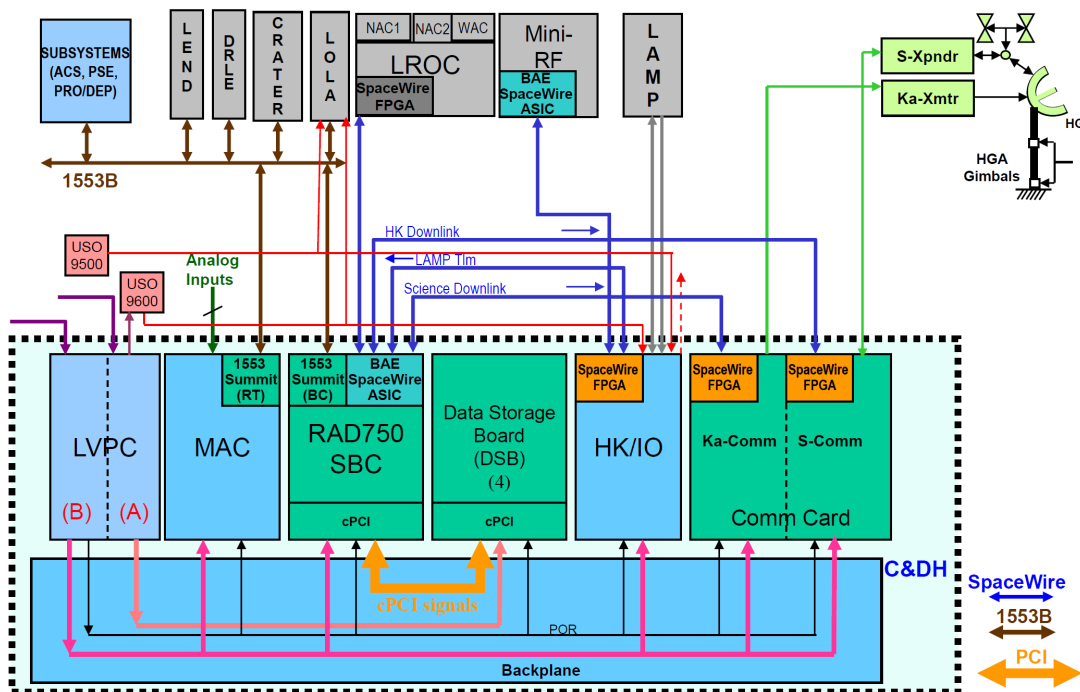


Figure 30: C&DH schematic

13.6 Configurations

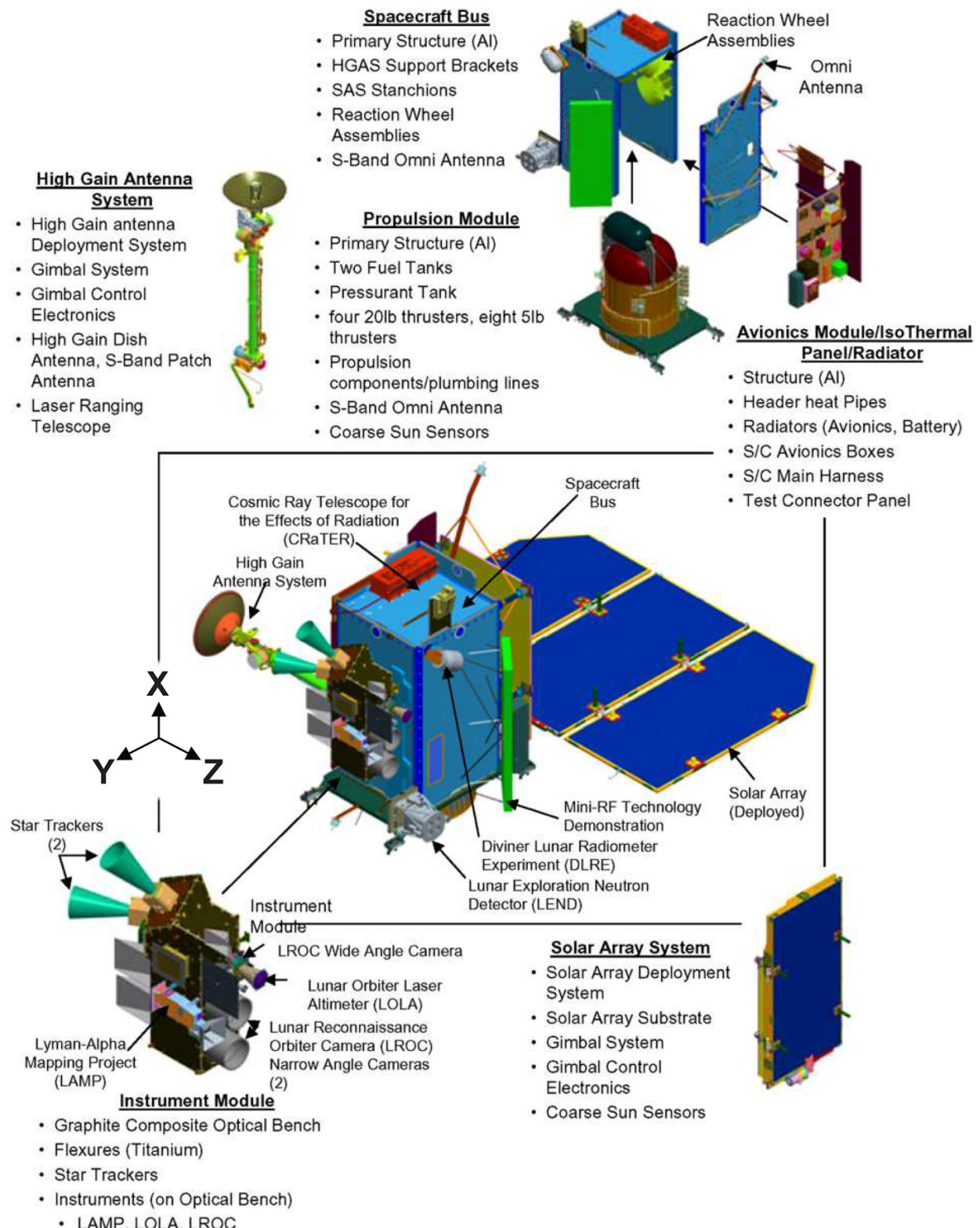


Figure 31: LRO design overview showing modular construction [1]